Unione Europea
Fondo Sociale Europeo

Ministero dell'Università e della Ricerca Scientifica e Tecnologica

Università degli Studi di Palermo

Tesi cofinanziata dal Fondo Sociale Europeo

PROGRAMMA OPERATIVO NAZIONALE 2000/2006

"Ricerca Scientifica, Sviluppo Tecnologico, Alta Formazione"
Misura III.4. "Formazione Superiore e Universitaria"

Istituto Nazionale di Geofisica e Vulcanologia

Soil CO_2 Flux Measurements in Volcanic and Seismic Areas: Laboratory Experiments and Field Applications

PhD thesis by:
Marco Camarda

Tutor:
Prof. Mariano Valenza

Co-Tutor:
Dr. Sergio Gurrieri

REVIEWERS

Prof. Luigi Marini
Dipartimento per lo Studio del Territorio e delle sue Risorse (DIP.TE.RIS.).
Università di Genova, Italy.

Dr. B. Mack Kennnedy
Earth Sciences Division, E.O.
Lawrence Berkeley National Laboratory
Berkeley
CA 94720, USA

Dottorato di Ricerca in Geochimica XVI ciclo (Luglio 2001-Giugno 2004)

Dipartimento di Chimica e Fisica della Terra ed Applicazioni alle Georisorse ed ai Rischi Naturali (CFTA)

Table of contents

ABSTRACT

The measurement of the CO_2 flux exhaled from the soils is a delicate operation because of unavoidable errors caused by the measuring apparatus that disturbs both the soil and the gases circulation. Several methods have been developed in order to perform accurate measurements of soil CO_2 flux. The methods used most widely to measure the emission of CO_2 from the soil to the atmosphere in volcanic and geothermal areas are the dynamic method (Gurrieri & Valenza 1988) and the accumulation chamber method (Baubron et al., 1990; Tonani and Miele., 1991). The flux measurements performed using the dynamic method can be influenced by soil permeability and by the rate of the sampling pump. The accumulation chamber measurements can also be affected by several problems such as wind speed, pumping flux, valuation of tangent at $t = 0$ of the $[CO_2] \rightarrow t$ plot, etc. A laboratory apparatus able to simulate different flux regimens, under known conditions, has been developed and was used to test the performance and reliability of these two methods. The investigated fluxes fell within the range of values close to soil respiration up to those normally measured in active volcanic and geothermal areas. The correct functioning of the laboratory apparatus was checked by comparing the experimental steady state concentration profiles with those predicted by the advective-diffusion model. As can be inferred from the data obtained, the flux measurements performed using the dynamic method are significantly influenced by soil permeability especially if the measurements are taken at high pumping flux. An empirical equation for performing careful soil CO_2 flux measurements as a function of the soil permeability was obtained by fitting experimental data to a model that explained the functioning of the system. In order to measure *in situ* soil permeability, a new method based on the theory of radial gas advection through an isotropic porous medium was developed. The method was tested in the laboratory and at several locations on the island of Vulcano (Aeolian Islands, Italy).

Tests performed on the accumulation chamber method have highlighted several sources of errors in measuring CO_2 flux with this method. The magnitude and sign of the obtained errors depend on the imposed flux, on soil permeability and on the rate used to induce air circulation in the close loop of the system.

Permeability measurements were performed with the radial gas advection method over a large sector of the island of Vulcano (Aeolian Islands, Italy) and the results compared with soil CO_2 fluxes measured at the same sites using the dynamic method. Based on the results, the influence of soil permeability on the flux measurements and on their spatial distribution

was assessed. Finally, the dynamic method was also applied to a seismic area of Sicily (Capo Calavà) in order to study the relationships between soil degassing and tectonics.

Chapter 1

Introduction

Measuring of gaseous emissions from the soil to the atmosphere has been widely effected in many branches of science e.g., agriculture, ecology, volcanic and seismic geochemistry. During quiescent periods, active volcanoes release large amounts of fluids as both visible emissions (fumaroles and hot springs) and non-visible emissions (diffuse soil gas emissions). Changes in the amount of fluids discharged in volcanic areas can be related to the level of volcanic activity and the movement of magma beneath the volcanic edifice (Allard et al., 1987, 1991; Badalamenti et al., 1988, 1991; Baubron et al., 1990; Chiodini et al., 1995; Gerlach et al., 2001; Giammanco et al., 1998; Carapezza and Federico, 2000; Chiodini and Frondini, 2001; Hernández et al., 2001; Toshiya et al., 2001; Diliberto et al., 2002).

Furthermore, soil gas are widely used in other several research fields such as earthquakes forecasting, gas hazard and geochemical explorations of active faults (Badalamenti et al., 1988; Ciotoli et al., 1998; Giammanco et al., 1998; Guerra and Lombardi, 2001; Rogie at al., 2001; Spicák and Horálek, 2001). A soil degassing map of the carbon dioxide of central and southern Italy has recently been presented (Chiodini et al; 2000, 2004). This map indicates the presence, in western Italy (close to the Tyrrhenian Sea), of two extensive anomalous areas bound to the east by the highly seismic zone of the Apennine Chain. As shown by Irwin and Barnes (1980), the spatial association of areas characterized by anomalous degassing and zones of seismicity and of high tectonic stress is not casual. In fact, fluids often play an important role in fault mechanisms and in the triggering of earthquakes (Wakita, 1996; Noorishad and Witherspoon, 1984/85, Spicák and Horálek, 2001; Salazar et al., 2002). Over-pressurized fluids stored in deep reservoirs can cause additional stress to host rocks and trigger seismicity (Zhao et al., 1996).

The study of diffuse soil gas emissions in geothermal and volcanic areas has focused on CO_2 because it is usually the most abundant volatile species in magma after water and it is the first species that exsolves (Symonds et al., 1994; Giggenbach, 1996). CO_2 flux measurements can be performed utilizing both indirect and direct methods. The first comprise measuring the concentration of CO_2 at different depths in the soil (Baubron et al. 1990). In this case the flux values are calculated in accordance with a one-dimensional steady state model of gas transport through a homogeneous porous medium. The employment of these methods is actually very limited because the measurement of soil CO_2 concentration is neither fast nor simple and moreover these methods also require the accurate measurement of soil properties (i.e., air filled porosity, tortuosity and permeability). Therefore, several indirect

methods have been developed to perform more accurate and rapid flux measurements. Some of these methods are based on the absorption of CO_2 in a caustic solution (alkali adsorption methods, Witkamp, 1966; Kirita, 1971; Anderson, 1973). Other methods are based on the measurement of the difference in CO_2 concentrations between inlet and outlet air in a closed chamber (open flow infra-red gas analysis, Witkamp and Frank, 1969; Nakaday et al., 1993). Actually, the methods most used to measure soil CO_2 fluxes in volcanic and geothermal areas are those of the accumulation chamber (Tonani and Miele, 1991**;** Bekku et al., 1995; Norman et al., 1992; Chiodini et al., 1998) and the dynamic method (Gurrieri and Valenza, 1988). The first is based on a theoretical relationship between soil CO_2 flux and the rate of increase in the CO_2 concentration inside an inverted chamber placed on the surface of the soil. The second is based on CO_2 content in a mixture of air and soil gas (*dynamic concentration*, C_d) sampled using a special probe inserted in the soil up to the depth of 50 cm (see Figure 4.1). As deducted by Gurrieri and Valenza (1988) this concentration is proportional to the soil CO_2 flux through an empirical relationship found experimentally in a laboratory for a flux range of 441-9,159 g m^{-2} day^{-1} (**=** $2.6 \cdot 10^{-6}$- $5.4 \cdot 10^{-5}$ m^3 m^{-2} s^{-1}) and a soil with a permeability of 24 darcys.

The error in the flux measurements referred to conditions different from those used in the laboratory, such as different soil permeability, was not known. Starting from these considerations, a new apparatus intended to simulate a natural degassing system under known conditions was developed in the laboratory. We utilized this apparatus to clarify the influence of soil permeability on the relationship used to calculate soil CO_2 flux with the dynamic method. The investigated range of soil CO_2 flux (97–22,050 g m^{-2} day^{-1}) was wider than that investigated on the past while it covers the range of fluxes normally encountered in volcanic and geothermal areas. Furthermore, the permeability of the media utilized in the laboratory experiences was varied by about three orders of magnitude (0.36-125 darcys), from low, to high permeability Also some important characteristics of measurement system (as the pumping flux) were systematically changed during these laboratory experiments, in order to define the best operating conditions to measure CO_2 flux from the soil with the dynamic method and to deduce a new empirical relationship for making accurate measurement of soil CO_2 flux as function of dynamic concentration and of the soil permeability. As consequence, a new method to measure *in situ* soil permeability based on the theory of the radial gas advection through homogeneous porous media, was developed and tested in the field.

The laboratory apparatus developed in this thesis was also used to asses the performance and reliability of soil CO_2 flux measurements taken using accumulation chamber method (Norman et al., 1992; Chiodini et al., 1998).

Finally, the dynamic concentration method was applied in an active volcanic area (island of Vulcano) and in a seismic area of Sicily (Capo Calavà) to evaluate the influence of soil permeability on flux measurement and to study the relationships between soil degassing and tectonics.

Chapter 2

Gas transport in porous media

Knowledge of the physical processes governing the transport of gas through a porous medium is crucial to the study and development of a method aimed to measure gas fluxes from soils. In this Chapter, several equations that describe gas flux through a homogeneous porous medium will be derived and discussed. These equations will later be used to ascertain the relationships between various parameters that can be measured in the laboratory.

2.1 Gas transport

Gas transport through porous media can occur by means of two different processes: diffusion and advection. Molecular diffusion is the process where matter is transported from a region of high concentration to a region of low concentration, as the result of random molecular movement. Advection (or "convection", or "mass transport", or "viscous flow", as called by different authors) is the process where matter is transported in response to a pressure gradient. Generally, in a natural context, gas transport occurs due to the combination of these two different mechanisms.

2.2 Diffusion

Gas diffusion processes are governed by Fick's first law, which highlights the relationships between diffusive flux for unit of area section, J_d ($M \cdot L^{-2} \cdot T^{-1}$), and the concentration gradient ∇C ($M \cdot L^{-4}$):

$$J_d = -D_m \nabla C \tag{2.1}$$

where D_m is the molecular diffusion coefficient ($L^2 \cdot T^{-1}$) that reflects the mobility of the diffusing gas in the host fluid, which can be either another gas, as in our case, or a liquid. If diffusion through a porous media is considered, the volume where the gas can diffuse is reduced, but this depends on the porosity of the medium. Moreover, the real gas path is not linear but tortuous. To take in account these characteristics, the molecular diffusion coefficient D_m in Fick's first law must be substituted by the "bulk" diffusion coefficient D**,** which is expressed by the following relationship:

$$D = \frac{D_m \cdot n}{\tau} \tag{2.2}$$

where n is the air-filled porosity which take into account the space effectively available for diffusion and τ is the tortuosity factor. This can be thought as the average distance a gas

molecule must travel through the network of pores in order to move of an unit distance through the porous media (Kutilek and Nielsen, 1994). Therefore, τ is always higher than 1, because the tortuous path is always greater than the linear path. For a wet, porous medium such as a soil, the n/τ ratio can be estimated from (Fang and Moncrieff, 1999):

$$\frac{n}{\tau} = n^{2a}\left(\frac{n}{n_t}\right)^2 \tag{2.3}$$

where n_t is the total porosity of the medium (air and water filled porosity) and a is an empirical coefficient determined from the relation (Millington and Shearer, 1971):

$$n^{2a} + (1-n)^a = 1 \tag{2.4}$$

2.3 Advection

Advective gas transport through a homogeneous porous medium is governed by the Darcy's law, which highlights the relationship between the rate of gas transfer per unit of area section, v ($L \cdot T^{-1}$) and the pressure gradient, ∇P ($M \cdot L^{-2} \cdot T^{-2}$):

$$v = -\frac{k}{\mu}\nabla P \tag{2.5}$$

where μ ($M \cdot L^{-1} \cdot T^{-1}$) is the gas viscosity and k (L^2) is the intrinsic permeability, which is only a function of the properties of the soil, such as air-filled porosity and tortuosity. Soil permeability indicates the soil's capacity to be crossed by a fluid. The dependence of the intrinsic permeability on the main physical properties of the soil is expressed by the Kozeny–Carman equation (Bear, 1972):

$$k = \frac{c_0 n^3 \tau}{s^2}$$

where c_0 is the pore shape factor, which has been widely used for relating permeability with the morphology of the solid, and s is the surface area of the solid per unit volume of sample.

2.4 Simultaneous advection and diffusion

When pressure and concentration gradients coexist, gas transport is due to a combination of advection and diffusion processes, and the flux J_i of a generic gas species can be expressed as the sum of its advective and diffusive contributions:

$$J_i = J_{d,i} + J_{ad,i} = -D\nabla C_i + C_i v \tag{2.6}$$

where C_i (M·L^{-3}), ∇C_i (M·L^{-4}) and $J_{d,i}$ (M·L^{-2}·T^{-1}), are the concentration, the gradient and the diffusive flux of the considered gas species, respectively, while $J_{ad,i}$ (M·L^{-2}·T^{-1}) is the advective flux of the gas species.

2.5 The advective-diffusion model

In order to quantitatively describe a system where diffusion and advection occur simultaneously, the mass conservation law must be taken in due consideration:

$$div(J_i) + \frac{\partial C_i}{\partial t} = 0 \tag{2.7}$$

This equation shows that the temporal change in the concentration ($\partial C_i/\partial t$) of a gas species is equal to the spatial change of the total flux ($div(J_i)$).

By combining equations (2.6) and (2.7) and assuming that J_{ad} and D are constants, the well-known *advective-diffusion equation* is obtained:

$$v\nabla C_i - D\nabla^2 C_i = \frac{\partial C_i}{\partial t} \tag{2.8}$$

Equation (2.8) is the basic equation for all problems where simultaneous diffusion and advection occur.

The one-dimensional form of equation (2.8), along the z-axis, is:

$$v\frac{\partial C_i}{\partial z} - D\frac{\partial^2 C_i}{\partial z^2} = \frac{\partial C_i}{\partial t} \tag{2.9}$$

2.6 Concentration profiles

In this thesis we will focus our attention on the solution to the problem of one-dimensional gas flow through homogeneous porous media. In particular, a simple equation, that describes the profiles of CO_2 concentration at steady state as a function of soil properties and of imposed CO_2 flux, will be derived and discussed.

In Appendix A, a solution to the advective-diffusion equation is provided to describe theoretical CO_2 concentration in soils as a function of depth (z):

$$C_i(z) = C_0 + \frac{(C_L - C_0)}{\left(e^{\frac{v}{D}L} - 1\right)}\left(e^{\frac{v}{D}z} - 1\right) \tag{2.10}$$

Equation (2.10) shows the change in the soil CO_2 concentration as a function of depth through two generic sufaces at depths *0* and L respectively. C_L and C_0 are respectively the concentration of gas at depths *0* and L. The steady-state concentration profile is a function of

the advective rate of gas transfer, v. In particular, the form of the concentration profile depends on the vL/D term shown in equation (2.10). In literature, this term is known as the Peclet number (Pe) (Sahimi, 1995) and is used to measure the competition between advection and diffusion. As shown in Figure 2.1, when this number is significantly lower than 1 the diffusion process prevails and the concentration profile is linear. However, when Pe is higher than 1 advection prevails and the resulting concentration profile is a curved line.

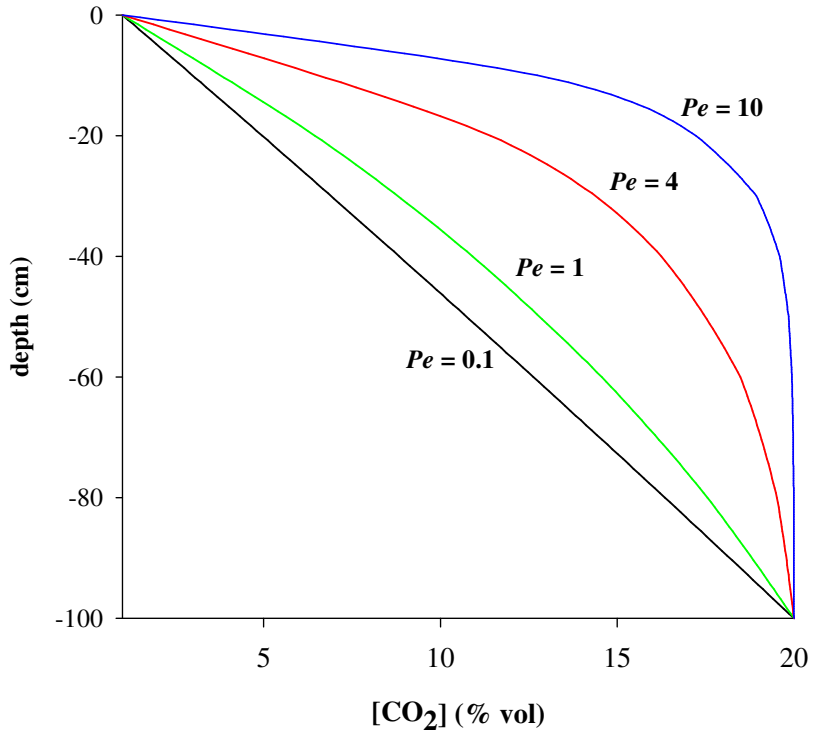

Figure 2.1 Theoretical CO_2 concentration profiles at different values of the Peclet number ($v \cdot L/D$).

2.7 Total flux

The total flux of gas through a generic surface at depth z is given by equation (2.6):

$$J_i(z) = C_i(z)v - D\frac{\partial C_i}{\partial z} \tag{2.11}$$

therefore, calculating $\left(\partial C_i / \partial z\right)$ by equation (2.10), we obtain:

$$J_i(z) = vC_i(z) - v\frac{(C_L - C_0)}{\left(e^{\frac{v}{D}L} - 1\right)}e^{\frac{v}{D}z} \tag{2.12}$$

where $vC_i(z)$ term is the advective contribution, while, $-v(C_L - C_0)e^{\frac{v}{D}z}\left(e^{\frac{v}{D}L} - 1\right)^{-1}$ is the diffusive contribution.

Equation (2.12) can be further semplified by espressing the term $C_i(z)$ by means of equation (2.10):

$$J_i(z) = v\left(C_0 - \frac{(C_L - C_0)}{e^{\frac{v}{D}L} - 1}\right) \tag{2.13}$$

According to equation (2.13), the total flux of a generic gaseous species does not depend on depth but is merely a function of the gas concentration, at depths *0* and *L*, of the advective rate of gas transfer and of the soil and gas properties. Equation (2.13) suggests that the sum of the diffusive and advective flux is constant at each depth, while equation (2.12) shows that the prevalent gas transport modality changes, moving from the gas source towards the surface. As shown in Figure 2.1, the theoretical concentration gradient is higher when close to the surface than when close to the gas reservoir and therefore the diffusive flux increases moving from the gas reservoir towards the soil-air interface.

Chapter 3

Simulations of gas transport

A special apparatus able to simulate a natural degassing system was developed in the laboratory to perform tests on the *dynamic method* with the aim of measuring CO_2 fluxes from the soil. For each simulation, soil CO_2 concentration profiles were measured in a steady-flow state and compared with theoretical profiles predicted in keeping with the advective-diffusion model. Thereby, the theoretical coherence of all the measured data was verified and a rigorous check of the efficiency of our laboratory apparatus was performed.

3.1 Laboratory apparatus

The device used to test the dynamic method (Figure 3.1) is similar to that described by Gurrieri and Valenza (1988). It consists of 700 kg of soil stored in a cylindrical vessel, 58 cm in diameter. Below the soil layer (100cm high) a free space lung (10cm high), equipped with a special gas diffuser, simulates a homogenous CO_2 gas source. Furthermore, eight sampling steel capillary tubes are inserted at different depths in the soil through which the CO_2 concentrations can be measured.

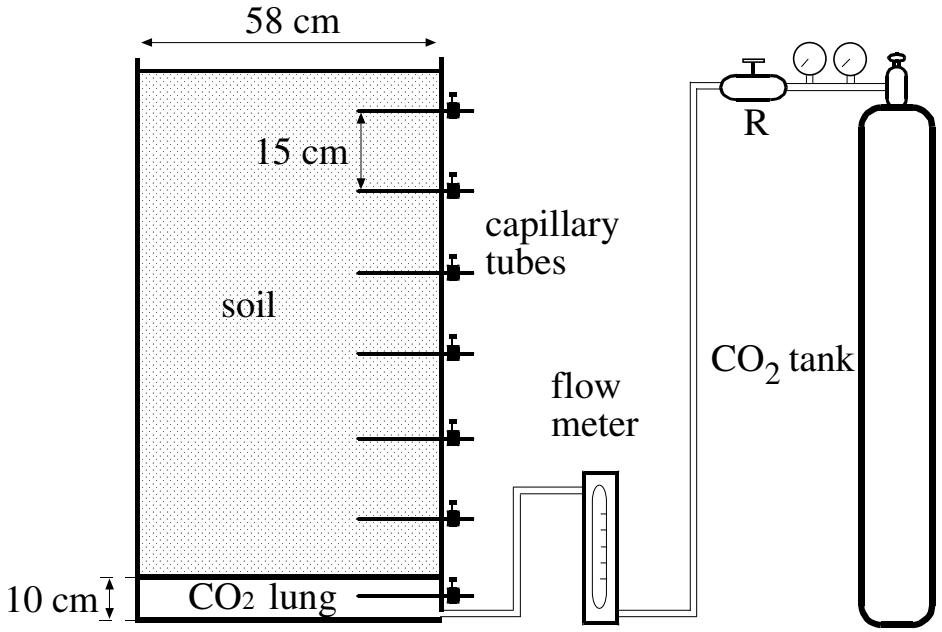

Figure. 3.1. Schematic illustration of the apparatus used in the laboratory. This consists of: a cylindrical metallic container, 58 cm in diameter, fed by a known flux of CO_2 at the bottom. Sampling capillary steel tubes are inserted at different depths in soil. The capillaries are placed 15 cm from each other and they are closed hermetically from the outside, by spherical valves. The rate of the CO_2 admitted into the lung is measured by a flow meter interposed between the lung and a CO_2 tank.

Four different soil samples (S_1, S_2, S_3 and S_4) where used for the laboratory tests. Their principal physical properties are shown in Table 3.1.

The gas permeability values (K) of the soil samples were obtained by measuring the pressure gradient in the soil generated by different air fluxes (v) according to the one-dimensional form of Darcy's law (Scheidegger, 1974, page 93):

$$v = -\frac{k}{\mu}\frac{P_L^2 - P_0^2}{2LP_L}$$

where μ is the CO_2 viscosity, k *is* the intrinsic gas permeability, L is the thickness of the soil layer, P_L and P_0 are, respectively, the gas pressure measured at *0* and L depths (in this case the soil surface in contact with the gas source was assumed as *0* depth). The P_L and P_O pressure measurements were carried out by a digital differential manometer (accuracy = 0.01 mbar) connected to the capillary tubes of the cylindrical vessel (Figure 3).

soil sample	k (darcys)	porosity (%)	tortuosity factor	D (cm^2s^{-1})
S_1	125 ± 7	39	1.38	$4.5 \cdot 10^{-2}$
S_2	36 ± 2	38	1.39	$4.4 \cdot 10^{-2}$
S_3	5.60 ± 0.7	34	1.41	$3.8 \cdot 10^{-2}$
S_4	0.36 ± 0.02	28	1.46	$3.0 \cdot 10^{-2}$

Table 3.1. Main physical characteristics of the investigated soil samples. The tortuosity factor (τ) relative to each soil samples are calculated by the porosity values, according to the relation (2.3) (Fang and Moncrieff, 1999).

Soil samples S_1 and S_2 were obtained by grain size separation of pyroclastic sand collected close to the isthmus of the island of Vulcano (Figure 7.1). The grain size of sample S_1 ranges between 1 and 0.5 mm while that of sample S_2 is smaller than 0.5 mm. According to the Wentworth classification (1922), S_1 sample is coarse sand while S_2 is fine sand. Sample S_4 is a limestone powder produced by industrial processing of marble. Finally, sample S_3 was obtained in the laboratory by mixing 7 parts of soil S_1 with 3 parts of S_4. The four samples supply a wide range of permeability and porosity that can normally be encountered in field soil gas measurements.

3.2 Laboratory experiments

To simulate a real soil gas regimen, pure CO_2 gas was let into the lung at a constant, known flux. The range of explored fluxes was between 97 – 22050 g m^{-2} day^{-1} ($5.7 \cdot 10^{-7}$ - $1.3 \cdot 10^{-4}$ $m^3m^{-2}s^{-1}$) (ϕ_{CO_2} values were calculated dividing the CO_2 flux from the tank by the

surface of the metallic container (2,642 cm^2)). At the beginning of each test, the soil gas in each layer consisted exclusively of air at atmospheric pressure. Subsequently, as CO_2 was let in, the CO_2 concentrations at different depths increased at varying rates until the steady state was reached. For each test, these variations were monitored by sampling the soil gas at different depths by the capillary tubes and measuring the relative CO_2 concentrations with an infrared gas analyzer. Figure 3.2 shows the CO_2 concentration at various depths versus time for the experiment in which J_{CO_2} = 340 g m^{-2} day^{-1} (= $2 \cdot 10^{-5}$ $m^3 m^{-2} s^{-1}$) and k = 125 darcys.

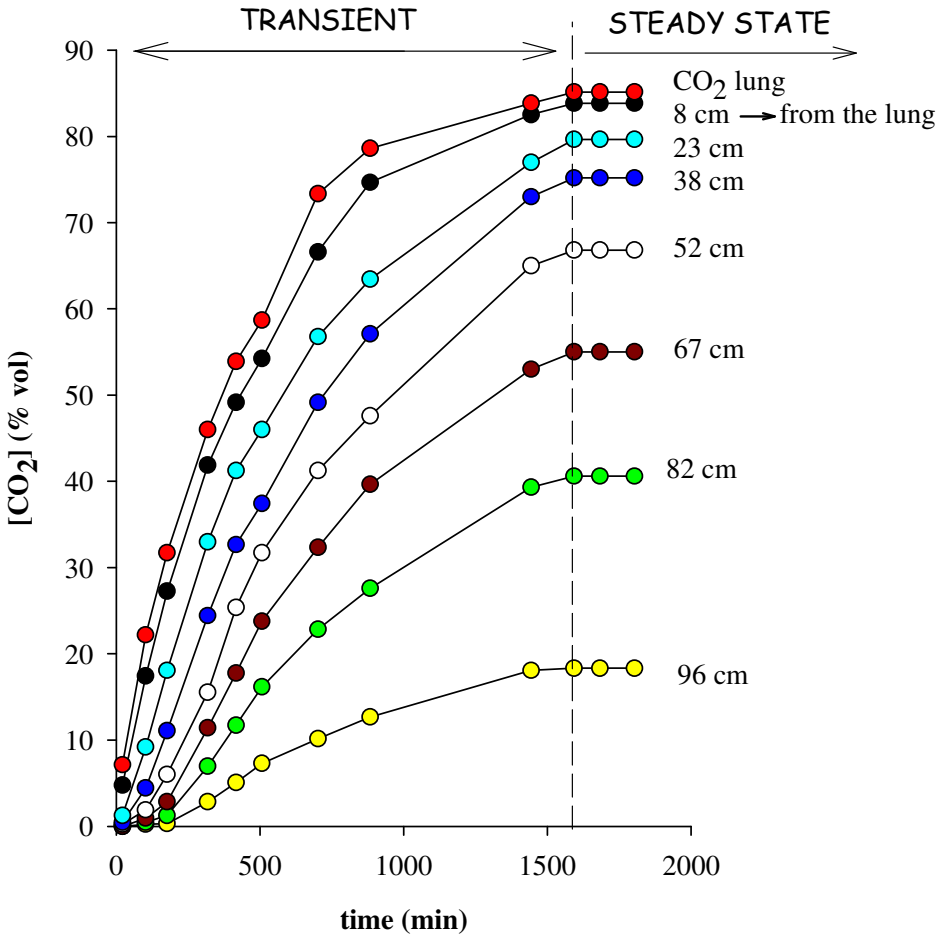

Figure. 3.2. An example of temporal variation of soil CO_2 concentrations at different depths (k = 125 darcys and J_{CO_2} = 340 g m^{-2} day^{-1}).

Before the steady state was reached, the CO_2 flux admitted at the base of the soil layer was higher than the CO_2 flux released by the system into the atmosphere. The difference between these two quantities of CO_2 is stored inside the soil and it determines an increase in the concentration of CO_2 at various depths. Only when the steady state was reached did the CO_2 flux inlet equal the CO_2 flux outlet. The steady state, for these specific boundary conditions, was reached after about 28 hours (mass inlet = mass outlet).

Thirteen different CO_2 fluxes ranging between 97 g m^{-2} day^{-1} and 22050 g m^{-2} day^{-1} were investigated. In this range of explored fluxes the modality of CO_2 transport changes from conditions dominated by diffusion to conditions dominated by advection. The imposed fluxes are from one to four orders of magnitude higher than those normally measured in soil respiration studies (3.6-14 g m^{-2} day^{-1}, Monteith et al. 1964; 3.4-56 g m^{-2} day^{-1}, Lunderghard, 1927) but they are within the range of CO_2 fluxes normally encountered in active volcanic areas (Badalamenti et al., 1988, 1991; Chiodini et al., 1998; Gerlach et al., 2001; Giammanco et al., 1998; Carapezza and Federico, 2000; Chiodini and Frondini, 2001; Diliberto et al. 2002; Finizola et al., 2002, 2004; Carapezza and Granieri, 2004). The experimental values of CO_2 concentrations measured at steady state for each investigated soil sample are reported in Tables 3.2, 3.3, 3.4 and 3.5 (Appendix B).

Moreover, Figure 3.3 shows some examples of these experimental concentration profiles obtained for each soil sample. As predicted by the theory, the shape of the experimental concentration profiles change as a function of J_{CO_2}. The CO_2 profiles are linear at low J_{CO_2} when the Peclet number (*Pe*, see Chapter 2) is lower than 1, but they curve progressively at higher fluxes.

In Figure 3.3 the theoretical CO_2 profiles calculated in accordance with equation (2.10) are compared with the relative experimental profiles. As shown by this figure, a good agreement can be observed between experimental and teoretical data. The *D* values utilized to carry out these simulations were calculated according to relation (2.2):

$$D = \left(D_m \cdot n\right) / \tau$$

where D_m = 0.15972 $cm^2 s^{-1}$ at 298 °K (Marrero and Mason, 1972). The *n* values were experimentally measured to evaluate the amount of water necessary to saturate a known volume of soil (Table 3.1). The tortuosity factor (τ) relative to each soil sample was calculated using the porosity values, in accordance with relation (2.3) (Fang and Moncrieff, 1999).

As shown in Table 3.1, τ values increase as a function of porosity. Moreover, the total diffusion coefficient calculated by equation (2.2) is very similar for soil samples S_1 and S_2 while it is lower for the other samples (S_3 and S_4). Therefore, the Peclet number for each soil sample calculated at the same advective rate of gas transfer (v) is higher for soil samples S_3 and S_4 than the others. In other words under the same J_{CO_2} the advective component in the total flux is higher for sample S_4 than the others. This was confirmed by the laboratory experiences reported in Figure 3.4 where some examples of the experimental profiles obtained

at the same J_{CO_2} are shown for each investigated soil permeability. Similar CO_2 profiles were obtained in samples S_1 and S_2, which are characterized by similar D values (see Table 3.1). On the contrary, different, curved profiles were obtained for soil samples S_3 and S_4, which are characterized by lower D values than the S_1 and S_2 samples.

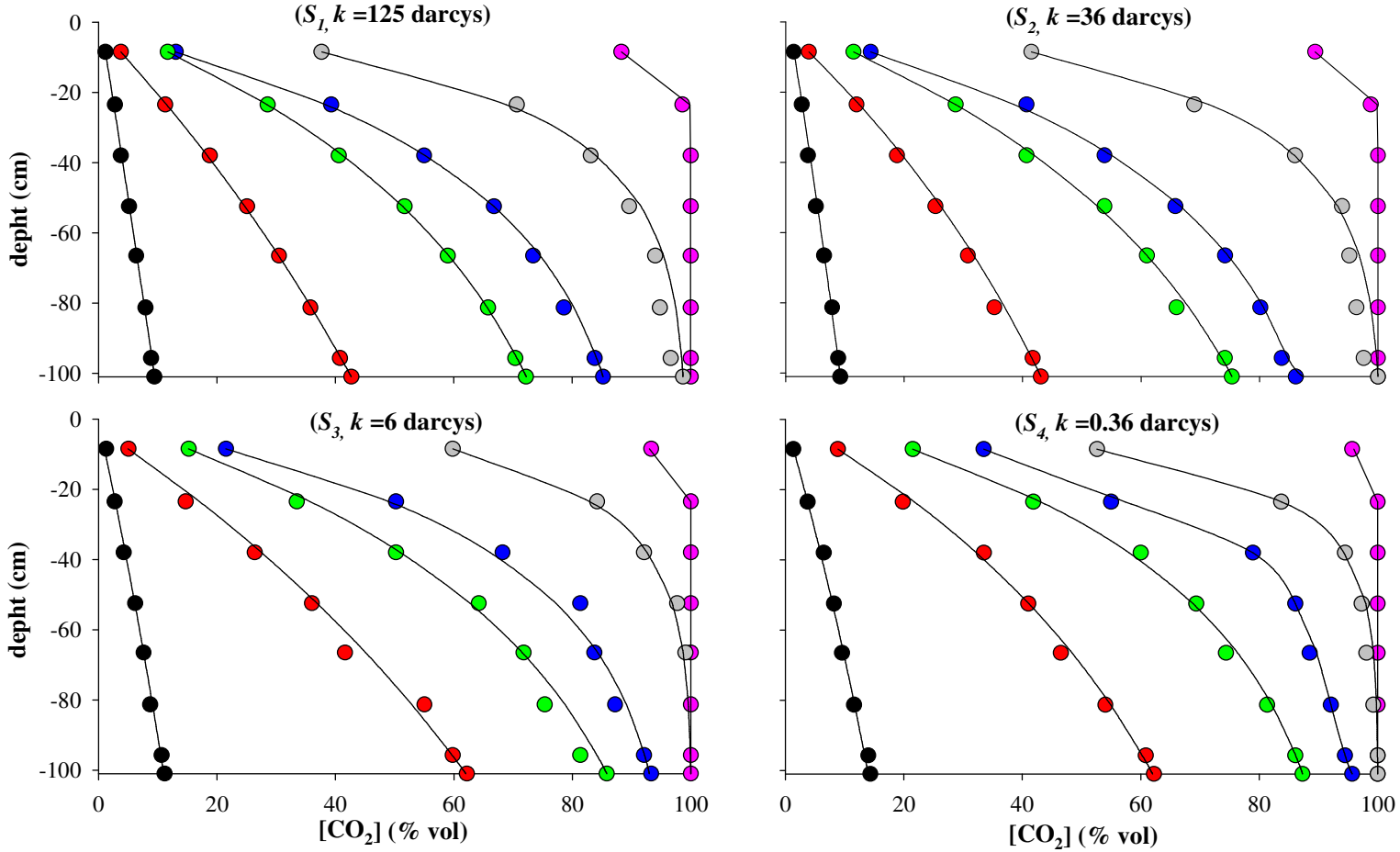

Figure 3.3. Experimental (filled circles) and theoretical (lines) profiles of CO_2 concentration at six different J_{CO2} for each investigated soil sample (S_1, S_2, S_3 and S_4): black circles, J_{CO2} = 96 g m^{-2} day^{-1}; red circles, J_{CO2} = 504 g m^{-2} day^{-1}; green circles, J_{CO2} = 1210 g m^{-2} day^{-1}; blue circles, J_{CO2} = 2352 g m^{-2} day^{-1}; grey circles, J_{CO2} = 3529 g m^{-2} day^{-1}; pink circles, J_{CO2} = 21849 g m^{-2} day^{-1}.

14

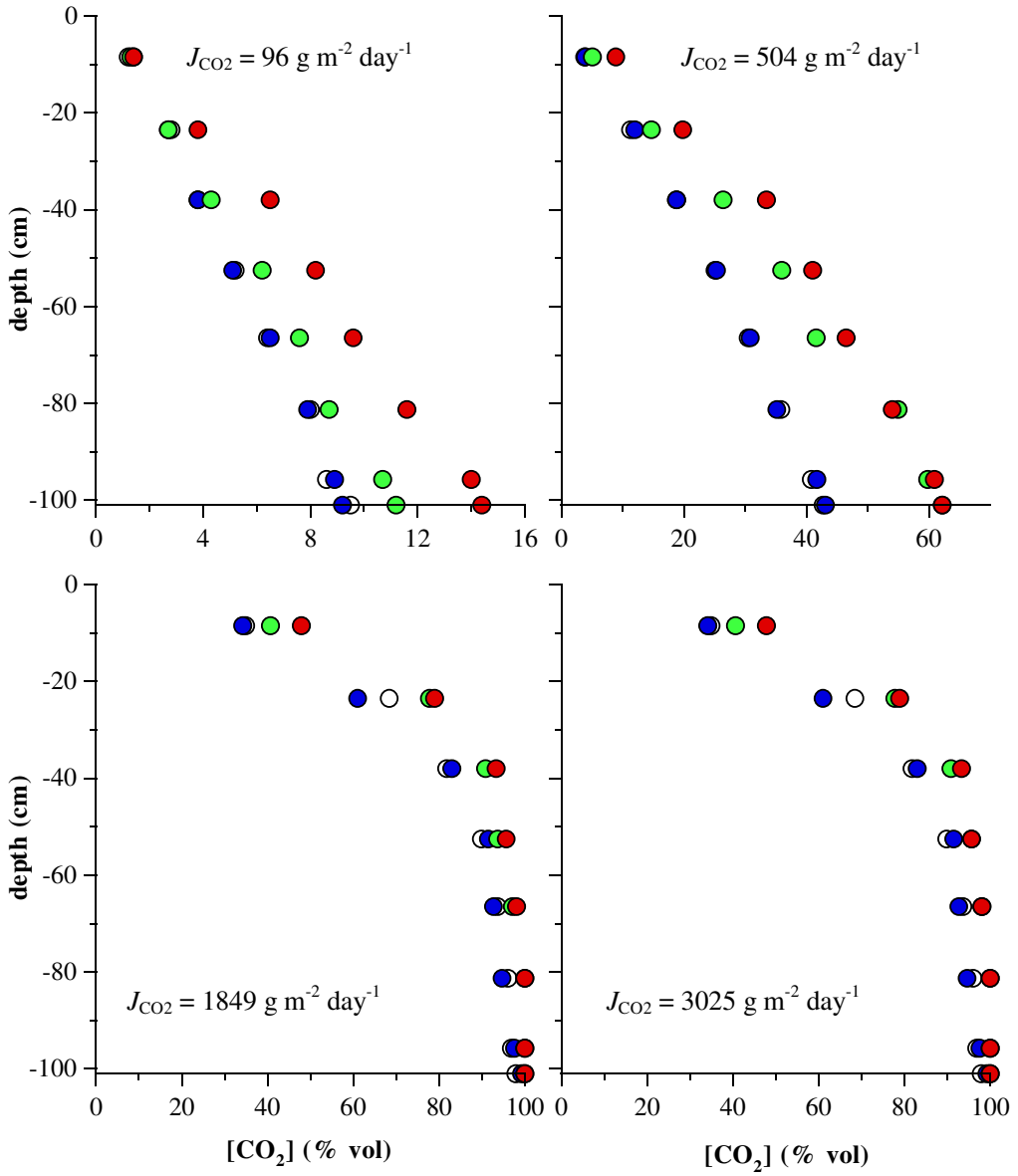

Figure 3.4. Different soil CO_2 concentration profiles for some of the investigated soil samples under different CO_2 fluxes. Blue circles = S_1 soil; white circles = S_2 soil; green circles = S_3 soil; red circles = S_4 soil.

Chapter 4

The dynamic method for measuring CO_2 flux from the soil

In this Chapter we will discuss the results of several tests performed in the laboratory using the dynamic method for measuring CO_2 flux from the soil. Initially, the theoretical basis of the method will be shown and subsequently we will examine the influence of soil permeability and pumping rate on flux measurements performed using this method. Finally we will discuss the results of several CO_2 flux measurements performed in a selected area of the island of Vulcano in order to evaluate the reproducibility of the method.

4.1 Theoretical principles of the dynamic concentration method

The system used to measure CO_2 flux from soils is shown schematically in Figure 4.1.

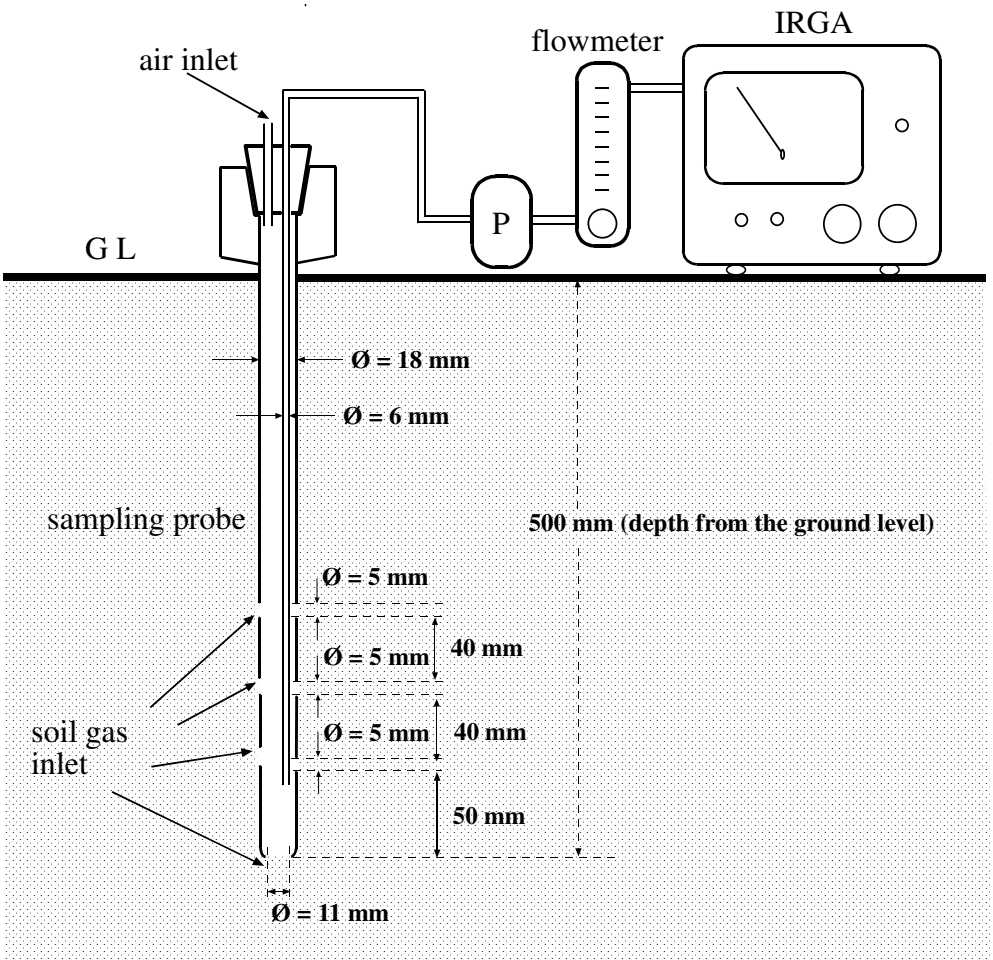

Figure 4.1. Schematic illustration of the system used to measure soil CO_2 flux. P = sampling pump; GL = ground level; IRGA = Infra Red Gas Analyzer.

The main components are an Infra Red Gas Analyzer (Riken 550 A), a constant flux sampling pump and a specially designed probe which is inserted into the soil at a depth of 50 cm. This probe allows soil gas to drain through some openings located on its lower part and air to be admitted through a calibrated tube on the top of the same probe (see the Figure 4.1). By pumping at constant flux, an air and soil gas mixture is obtained inside the probe. After a given time, depending on the pumping flux and probe geometry, the gas mixture reaches a constant composition. Gurrieri & Valenza (1988) defined *dynamic* the concentration values (C_d) obtained by this method to distinguish them from the *static* gas concentrations in soils, generally measured to determine the concentration gradients. The same authors observed that the *dynamic* concentration of CO_2 is mainly a function of soil CO_2 flux (J_{CO_2}) in accordance with the following relationship:

$$J_{CO_2} = M \cdot C_d \tag{4.1}$$

where M is a constant that depends on the characteristics of the device (geometry of probe, soil insertion depth and pump suction flux, soil permeability) and C_d is the *dynamic concentration* of CO_2.

To understand the physical concept of *dynamic* concentration, the mass balance between the CO_2 inlet and outlet of the probe must be taken into consideration.

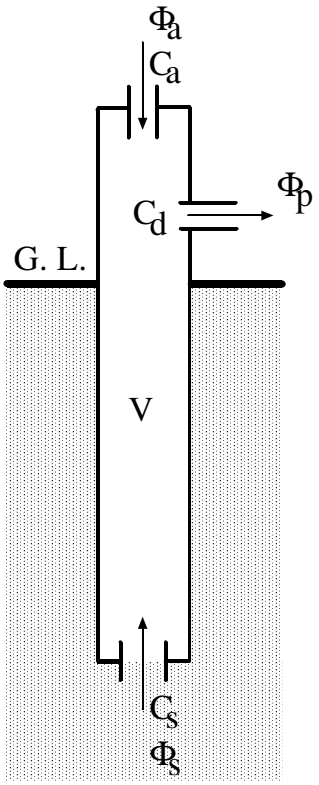

Figure 4.2 Simplified diagram of the probe used to measure soil CO_2 flux. V is the inner volume of the probe; C_d is the CO_2 concentration of the gas-air mixture; ϕ_a and C_a are the volumetric flux and CO_2 concentration in the inlet air, respectively; ϕ_s and C_s are the volumetric flux and CO_2 concentration (called static concentration) in the sucked soil gas, respectively; ϕ_p is the volumetric pumping flux.

Fig. 4.2 shows a scheme of the probe, where all the lower openings of the sampling probe are assimilated to a single opening. The CO_2 mass change within the probe ($dM_{CO_2}(t)$) ($M \cdot L^{-3} \cdot T^{-1}$) can be expressed as the difference between the CO_2 going into the probe (from the soil and from the atmosphere) and the CO_2 issuing from the probe (to the Infra Red Gas Analyzer):

$$dM_{CO_2}(t) = VdC_d(t) = \phi_a C_a dt + \phi_s C_s(t)dt - \phi_p C_d(t)dt \tag{4.2}$$

where:

- V (L^3) is the inner volume of the probe;
- $C_d(t)$ ($M \cdot L^{-3}$) is the CO_2 concentration of the gas mixture inside the probe;
- ϕ_a ($L^3 \cdot T^{-1}$) and C_a ($M \cdot L^{-3}$) are respectively the volumetric flux and the CO_2 concentration of the air entering into the probe;
- ϕ_s ($L^3 \cdot T^{-1}$) and $C_s(t)$ ($M \cdot L^{-3}$) are respectively the volumetric flux and CO_2 concentration of the soil gas entering into the probe;
- ϕ_p ($L^3 \cdot T^{-1}$) is the volumetric pumping flux;

Assuming that $C_a = 0$ and that C_s remains constant during the time necessary to reach the steady state ($C_s(t) = C_s$), a first-order homogeneous differential equation for $C_d(t)$ can be obtained:

$$\frac{dC_d(t)}{dt} + \frac{\phi_p}{V} C_d(t) = \frac{\phi_s C_s}{V},$$

As shown in Appendix C, the general solution to this equation is:

$$C_d(t) = \frac{\phi_s}{\phi_p} C_s \left(1 - a \cdot e^{-\frac{\phi_p}{V}t}\right), \tag{4.3}$$

where a is a constant that can be calculated assuming that the concentration of CO_2 inside the probe at $t = 0$ is equal to concentration of the soil gas entering into the probe:

$$C_d(0) = C_s \ .$$

According to the specified boundary conditions, equation (4.3) becomes:

$$C_d(t) = \frac{\phi_s}{\phi_p} C_s \left(1 - \frac{\phi_s - \phi_p}{\phi_s} e^{-\frac{\phi_p}{V}t}\right) \tag{4.4}$$

which shows the time variation of the CO_2 concentration of the gas mixture generated inside the probe by pumping at constant flux. At the steady state ($t \rightarrow \infty$), the concentration of each gas species in the gas mixture becomes constant and is expressed by:

$$C_d = \frac{\phi_s}{\phi_p} C_s . \tag{4.5}$$

For ϕ_p constant, C_d (the dynamic concentration) is a function of C_s and ϕ_s. It does not depend on the inner volume of the probe (V), but is a function of the pumping flux (ϕ_p) and of the flux and CO_2 concentration of the soil gas going into the probe (ϕ_s and C_s).

The relationship between C_d and J_{CO_2} is a very complex function which involves both the geometry of the probe and the properties of the soil. To investigate this relationship, several C_d measurements were performed in the laboratory by simulating different soil gas regimens using the special device (Figure 3.1) discussed in the previous Chapter.

Equation (4.4) suggests that the time necessary to reach the steady state inside the probe depends on the ratio between ϕ_p and V: in particular, it decreases when the ϕ_p / V ratio increases. Figure 4.3 shows the theoretical $C_d(t)$ values versus time at different values of pumping flux calculated by equation (4.4). In this simulation we have imposed a value of C_s equal to 82% and a value of ϕ_s equal to 1 l min^{-1} and a value of V equal to the real inner volume of the probe (equal to 226 cm^3).

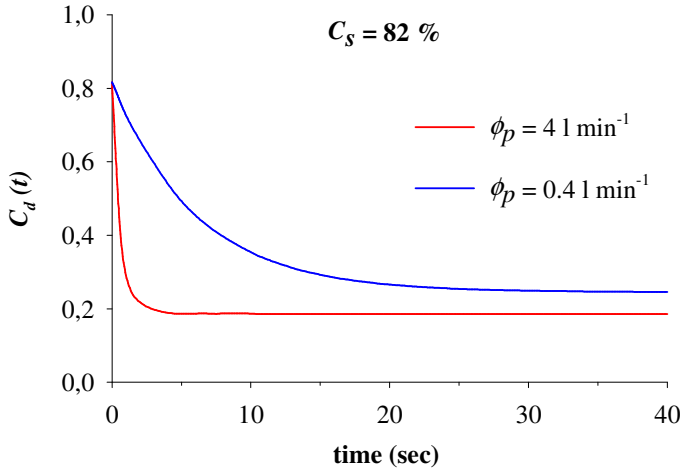

Figure 4.3. Theoretical variation of the gas mixture concentration $C_d(t)$, versus time, for two different values of pumping flux (4 and 0.4 l·min^{-1}). $C_d(t)$ is expressed in terms of molar fraction,

In each case, the gas mixture concentration decreases with time from C_s to C_d. The time necessary to reach a steady state ranges between 5 seconds, for high values of pumping flux (4 l·min^{-1}), to 25 seconds for lower flux values (0.4 l·min^{-1}). As confirmed by experimental observations, the theoretical values represent the minimum time necessary to carry out the C_d measurements. The model does not take into consideration some geometrical aspects such as the length of the tube between the probe and the Infra Red Gas Analyzer or the volume of the spectrophotometer measurement cell which appreciably increase the time necessary to reach a steady state. The discrepancies can range between 5 s (for a ϕ_p = 4 l·min^{-1}) and 60 s (ϕ_p = 0.4 l·min^{-1}).

4.2 Generality on laboratory tests

To investigate the relationship between J_{CO_2} and C_d, several C_d measurements, at different imposed CO_2 fluxes, were carried out using the experimental apparatus described in the previous Chapter (see Figure 3.1). In each flux simulation, the C_d value was measured when the steady state had been reached.

Several C_d measurements where carried out for very different experimental conditions: J_{CO_2} = 97–22050 g m^{-2} day^{-1} (= 5.6·10^{-7}-1.3·10^{-4} m^{3}m^{-2}s^{-1}), k = 0.36 - 125 darcys. Moreover, also the pumping flux with which air and soil gas mixture is carried out from the measurement probe (Figure 4.1), was changed from 0.4 to 4 l·min^{-1}. Only the probe geometry and insertion depth in the soil of the measurement probe were not varied (see Figure 4.1). The probe employed in these experiments was characterized by a greater number of openings than the probe used by Gurrieri & Valenza (1988). This solution was preferred because it increases sensitivity at the lowest soil CO_2 fluxes. Indeed, at the same soil flux, a greater CO_2 inlet surface determines a higher amount of soil gas in the gas mixture and, consequently, provides higher C_d values.

4.3 Experimental data

4.3.1 Constant soil permeability and pumping flux

The first set of measurements was performed on soil sample S_1 (K = 125 darcys) at a constant pumping flux of 4 l min^{-1} (Table 4.1 in the Appendix *D*).

Figure 4.4 shows the relationship between the C_d values (expressed as molar fraction) and the relative imposed fluxes (J_{CO_2}). As a first consideration, the C_d values seem to increase, giving different slopes, as a linear function of J_{CO_2} at low and high imposed fluxes (J_{CO_2} <3500 g m^{-2} day^{-1} and J_{CO_2} > 7000 g m^{-2} day^{-1}). This general behaviour characterizes all the measurement sets and essentially reflects the mechanism of gas transfer prevailing at specific soil degassing conditions.

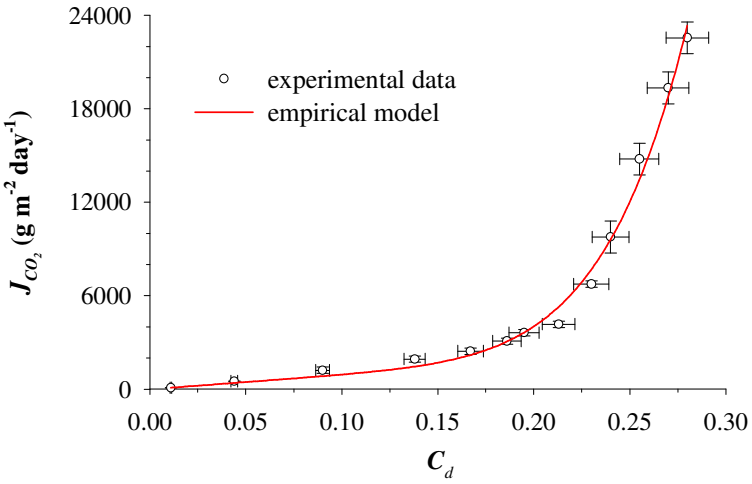

Figure 4.4. Experimental relationship between C_d and J_{CO2} for soil sample S_1 at constant ϕ_p = 4 l·min^{-1}. Solid line shows best fitting curve calculated according to equation 4.8. C_d values are expressed in terms molar fraction.

In order to explain this particular behaviour, the theoretical expression of the dynamic concentration (equation 4.5) must be considered:

$$C_d = \frac{\phi_s}{\phi_p} C_s$$

In the case of Figure 4.4, the pumping flux is constant (4 l·min^{-1}). Therefore, in accordance to equation (4.5), the change of C_d as function of J_{CO_2} can be only explained as the result of the variation in the flux and in the CO_2 concentration of the soil gas entering into the measurement probe (ϕ_s and C_s, respectively). A value able to describe the CO_2 concentration of gas sucked out from the soil can be given by calculating the mean value of the CO_2 concentration measured at the different depths where soil gas enters in to the probe (equal to 39 cm, 41 cm, 46 cm and 50 cm, respectively (see Figure 4.1)):

$$C_s = (C_a + C_b + C_c + C_d)/4, \qquad (4.5)$$

where C_a, C_b, C_c and C_d are the CO_2 concentration measured in the soil gas sampled at depths of 50, 46, 41 and 39 cm, respectively. Table 4.5 (pag. 25) reports the C_s values calculated, for each soil, according to equation (4.5). As shown in this table, the CO_2 concentration of gas sucked out from the soil depends on the soil properties and on the imposed CO_2 flux. Figure 4.5 shows the variation of C_s as function of J_{CO_2} for soil sample S_1. By comparing the figures 4.4 and 4.5, it can be seen that at low J_{CO_2} values, an increase of J_{CO_2} determines a linear increase in C_s and, harmoniously, an increase in the C_d values.

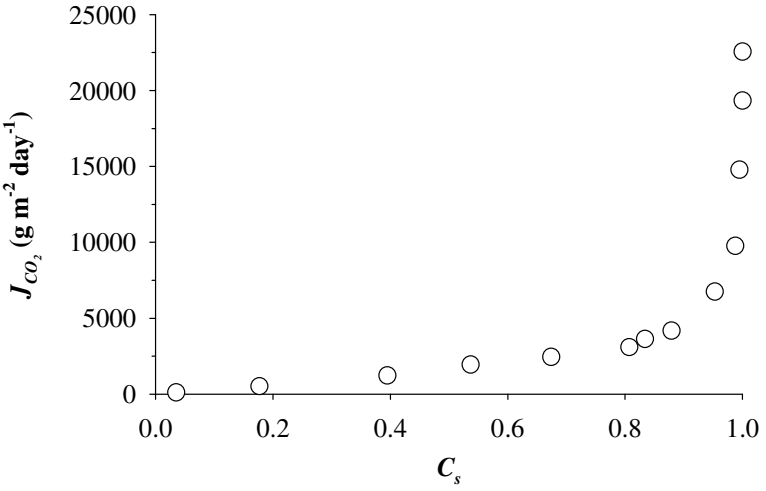

Figure 4.5. Plot of CO_2 concentration of the sucked-soil gas (C_s) measured in sample S_1 as a function of J_{CO2}. C_s values are expressed as molar fraction.

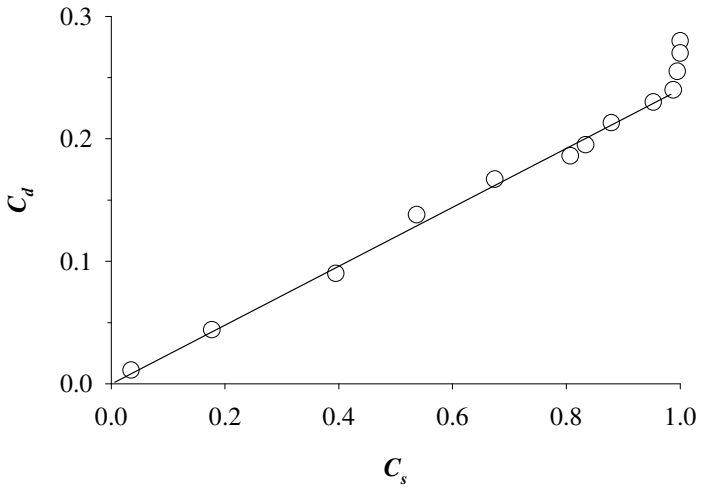

Figure 4.6. Experimental relationship between C_d and C_s obtained for soil sample S_1. A good correlation is found between these two parameters for φ_{CO2}< 7000 g m^{-2} day^{-1} (R = 0.99). C_d and C_s values are expressed as molar fraction.

By plotting C_d versus C_s (Figure 4.6), a good correlation between these two parameters can be recognized for J_{CO_2} < 7000 g m^{-2} day^{-1}. For high J_{CO_2} (> 7000 g m^{-2} day^{-1}), the CO_2 concentration of the soil gas entering into the probe remains constantly equal to 100% and C_d continues to increase as function of the imposed CO_2 flux (see Figure 4.4) with a rate lower than that observed for lower imposed fluxes. In this case, ϕ_p and C_s terms of equation (4.5) are constant, and the mechanism responsible of the C_d variations is only the increase, as function of J_{CO_2}, of the flux of soil gas entering into the probe (ϕ_s). In fact this flux, which is caused by a difference in pressure between the soil and the inside of the probe, increases as function of the pressure gradient in the soil and therefore on the imposed CO_2 flux.

The results shown here suggest that the variation in the dynamic concentration can be caused by two different mechanisms which occur simultaneously. One of these is the change as function of J_{CO_2} in the CO_2 concentration of the gas sucked out from the soil. The second mechanism is the variation as function of J_{CO_2} of the amount of gas having a high concentration of CO_2 sucked out from the soil (ϕ_s). As shown by Figure 4.6, the first factor is the prevailing cause of the change in C_d at low flux values, while the second is the only cause of change in C_d at flux values higher than those where the CO_2 concentration of the sucked soil gas is constant and equal to 100%.

The experimental relationship between J_{CO_2} and C_d can be described by combining two different functions: a power (equation 4.6) and a linear function (equation 4.7):

$$J_{CO_2} = a \cdot C_d^{\,b} \tag{4.6}$$

$$J_{CO_2} = c \cdot C_d \tag{4.7}$$

The first function describes the relationship between C_d and J_{CO_2} for J_{CO_2} < 7000 g m^{-2} day^{-1}, where the variation in C_d strongly depends on the values of C_s (which change as function of J_{CO_2} in accord to a power law); the second function describes the relationship between C_d and J_{CO_2} for J_{CO_2} > 7000 g m^{-2} day^{-1}. Therefore, to describe the relationship between C_d and J_{CO_2} in the whole J_{CO_2} range, a linear combination of equations (4.6) and (4.7) should be considered:

$$J_{CO_2} = c \cdot C_d + a \cdot C_d^{\,b} \tag{4.8}$$

By fitting this model to the experimental data (Figure 4.4) a good accord can be recognized (R = 0.996). The values of a, b and c coefficients of equation (4.8) are function of the soil permeability and on the pumping flux (see next, paragraph # 4.4).

4.3.2 Influence of soil permeability

In order to evaluate the effects of soil permeability on the relationship between C_d and J_{CO_2}, several measurements of C_d were performed at the same imposed CO_2 fluxes with different permeable soils. In particular we used soils S_2 (k = 36 darcys), S_3 (k = 6 darcys) and S_4 (k = 0.36 darcys) whose main characteristics have been reported in Table 3.1 (Chapter 3). The results of these investigations are reported in Tables 4.1, 4.2, 4.3 and 4.4 (Appendix *D*).

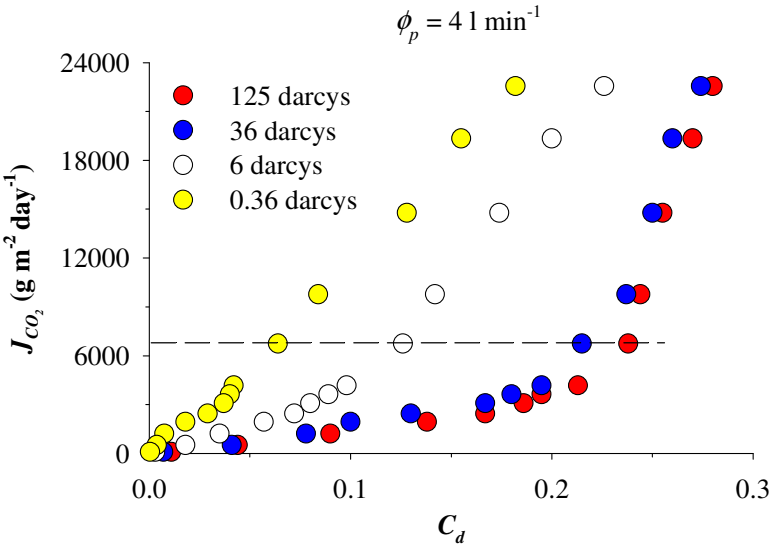

Figure 4.7. Comparison between the experimental J_{CO2} - C_d relationships found for each investigated soil sample at a constant pumping flux of 4 l·min^{-1}. C_d values are expressed as molar fraction.

Figure 4.7 shows the experimental relationships between the values of C_d and the relative J_{CO_2} observed for each investigated soil permeability and for a constant pump flux of 4 l min^{-1}. Several considerations can be made regarding the influence of soil permeability on the C_d measurements. At constant value of J_{CO_2}, the measured C_d values increase with soil permeability. As shown in Table 4.5 (next page) this result contrasts with the general trend shown by the experimental concentration values of soil gas entering into the measurement probe (C_s) which generally shows a little decrease as a function of soil permeability. On the

contrary, the increase in C_d as function of soil permeability reflects the differences in flux of soil gas entering into the measurement probe (ϕ_s) which depends on the soil permeability. Thus, for a constant imposed CO_2 flux and a constant pumping flux, the volume of gas which can be sucked out from the soil depends only on its permeability, which represents the ease with which a fluid can pass through a soil. In the case of highly permeable soils, a higher volume of gas with a high CO_2 content can easily be extracted from the soil and the resulting gas mixture is richer in CO_2.

J_{CO2} (g m^{-2} day^{-1})	C_s (% vol) (k = 125 darcys)	C_s (% vol) (k = 36 darcys)	C_s (% vol) (k = 6 darcys)	C_s (% vol) (k = 0.36 darcys)
22558	100	100	100	100
19335	100	100	100	100
14773	99.5	100	100	100
9769	98.8	99.2	99.6	100
6750	95.3	95.8	98.4	98.4
4172	87.9	89.2	94.4	96.8
3630	83.4	83.7	93.4	94.3
3087	80.7	82.4	90.8	91.8
2442	67.4	69.2	79.6	86.2
1934	53.7	54.2	67.1	72.4
1219	39.5	39.8	48.1	57.3
514	17.7	18.0	24.6	30.7
96	3.5	3.7	4.0	5.9

Table 4.5. Variation of static concentration, C_s, as a function of J_{CO2} for each investigated soil sample.

4.3.3 Influence of the pumping flux on C_d measurements

Another aim of this study was to evaluate the influence of the pumping flux on the relationship between J_{CO_2} and C_d. This parameter determines the proportions of gas sucked out from the soil and from the atmosphere and, of course, it influences C_d values. Several C_d measurements were repeated at different values of pumping flux, from 4 to 0.4 l·min^{-1} (Table 4.1, 4.2, 4.3 and 4.4 (Appendix *D*)).

Figure 4.8 shows the relationship between C_d and ϕ_{CO_2} for each investigated value of pumping flux and for a constant soil permeability of 125 darcys. The dashed area indicates the range of the C_d and J_{CO_2} values normally encountered in volcanic and geothermal areas ($C_d <$ 200,000 ppm and $J_{CO_2} <$ 5000 g m^{-2} day^{-1}). In this range, most of the C_d and CO_2 fluxes

measured in volcanic and geothermal areas are included (Badalamenti et al. 1988, 1991; 1990; Chiodini et al., 1998; Gerlach et al., 2001; Giammanco et al., 1998; Chiodini and Frondini, 2001; Diliberto et al. 2002; Carapezza and Granieri, 2004; this thesis).

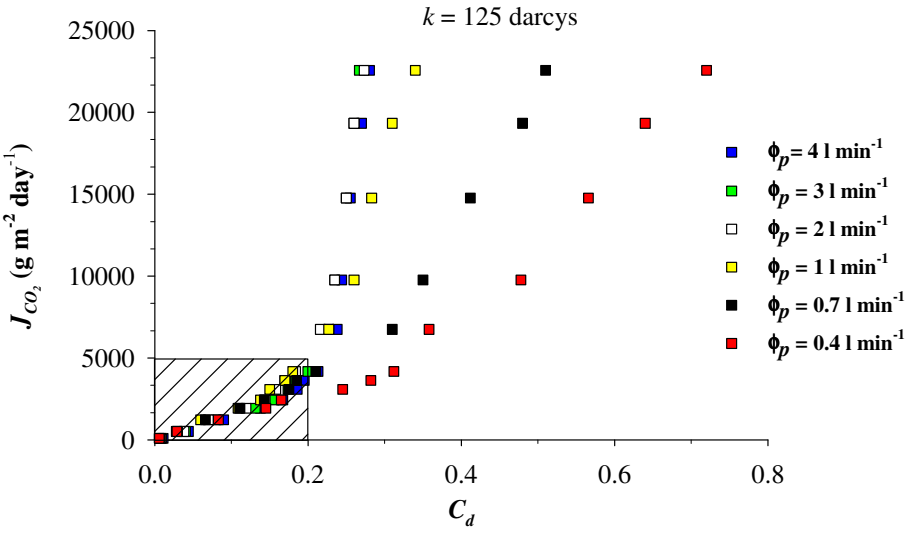

Figure 4.8. Relationships between C_d and J_{CO2} for each investigated pumping flux and for a constant soil permeability of 125 darcys. C_d values are expressed as molar fraction. The dashed area indicates the J_{CO2} and C_d values normally encountered in the field.

As shown in this figure, the influence of the pumping flux on the relationship between C_d and J_{CO_2} is low within the range of values generally measured in the field. On the contrary, more significant differences can be observed at higher J_{CO_2}.

As previously shown (Figure 4.7), for a constant pumping flux of 4 l min^{-1}, significant differences were observed among C_d values measured in soils characterized by different permeability values. The graphs in Figure 4.9 show the experimental relationships between J_{CO_2} and C_d found for different values of the pumping flux and for each investigated soil permeability. By decreasing the pumping flux from 4 to 0.4 l min^{-1} the discrepancies among the relationships between J_{CO_2} and C_d observed in relation to the different investigated soil permeability, are reduced. In particular, for a pumping flux of 0.8 and 0.4 l min^{-1}, low discrepancies can be observed within the range of C_d and J_{CO_2} values that are normally encountered in the field (indicated in Figure 4.9 by the dashed area). Therefore, to decrease the influence of soil permeability in flux measurements, it is necessary to perform the C_d measurements at low values of pumping flux. However, as previously discussed (4.1 section), the time necessary to perform a flux measurement with the dynamic method increases at low

values of pumping flux (see 4.1 section). A good compromise between speed of measurement and influence of soil permeability can be reached by performing the flux measurements at a pumping flux of 0.8 l·min^{-1}. In fact, in these conditions only small discrepancies were observed among the experimental C_d - J_{CO_2} relationships obtained in soils characterized by different permeability values. Furthermore, the soil flux measurements were performed in a relatively short time.

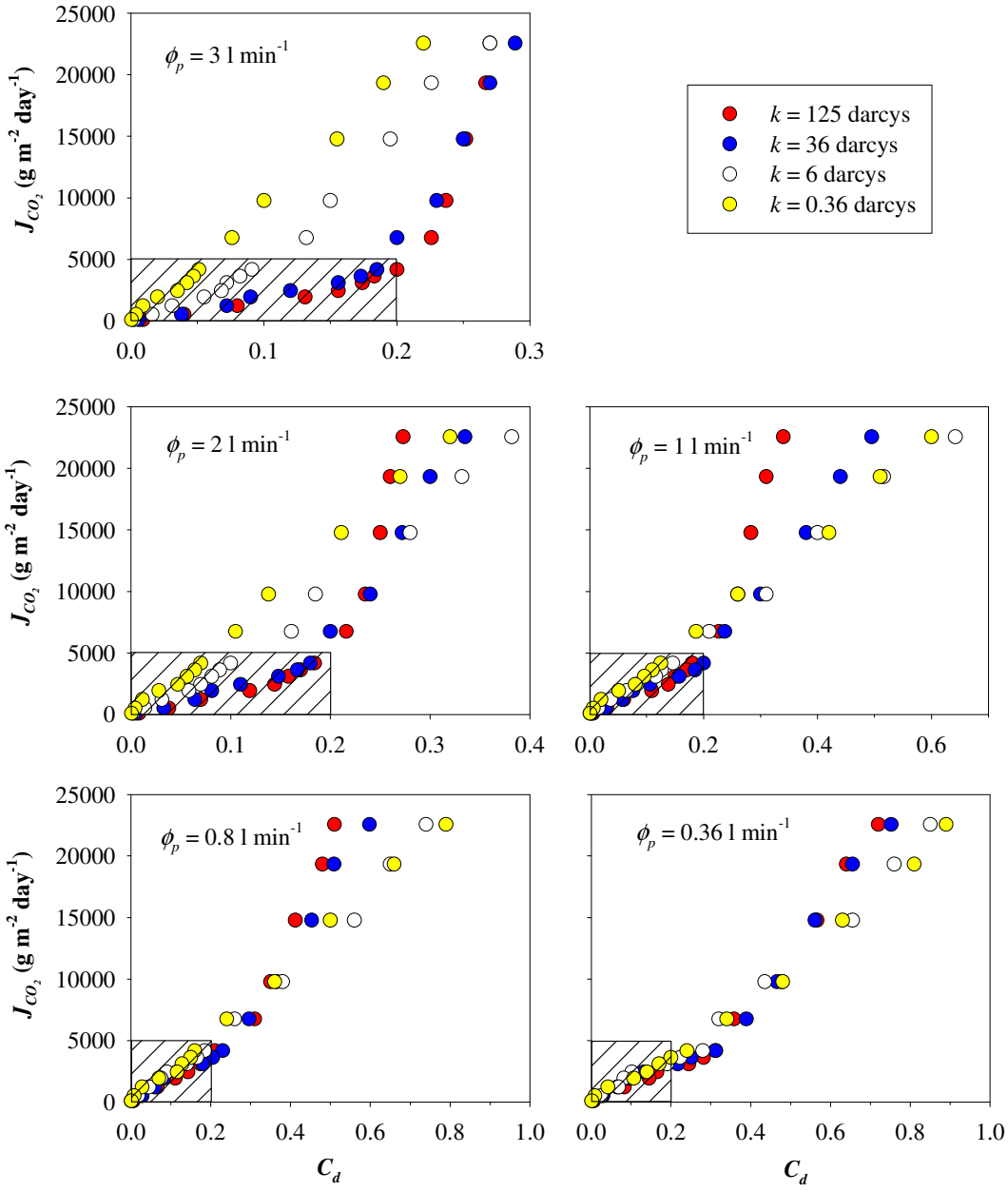

Figure 4.9. Relationship between C_d and J_{CO2} relative to each investigated permeability and for each pumping flux. The discrepancies among the relationships between C_d and J_{CO2} obtained at different permeability, decrease when C_d measurements were performed at low values of pumping flux. C_d values are expressed as molar fraction.

4.4 Empirical relationship for measuring J_{CO_2} as a function of C_d and k

As previously discussed in section 4.3.1, the relationship between the experimental values of C_d and J_{CO_2} obtained at constant soil permeability and at constant pumping flux, are well explained by the empirical model expressed by the equation (4.8) (see Figure 4.4):

$$J_{CO_2} = c \cdot C_d + a \cdot C_d^{\,b}, \tag{4.8}$$

where the coefficients *a, b* and *c* depend on the value of soil permeability and pumping flux. In this section we would express these coefficients as a function of soil permeability, in order to deduce an equation able to calculate J_{CO_2} as a function of C_d and *k,* when C_d measurements are taken at a constant pumping flux of 0.8 l·min^{-1}.

***k* (darcys)**	***a* (g m^{-2} day^{-1})**	***b* (g m^{-2} day^{-1})**	***c* (g m^{-2} day^{-1})**
125	$1.158 \cdot 10^5$	3.021	$1.410 \cdot 10^4$
36	$5.961 \cdot 10^4$	2.949	$1.873 \cdot 10^4$
6	$1.321 \cdot 10^4$	3.083	$2.339 \cdot 10^4$
0.36	$2.385 \cdot 10^3$	3.044	$2.758 \cdot 10^4$

Table 4.6. Values of *a*, *b* and *c* coefficients found for each investigated permeability fitting equation (4.8) to experimental C_d and J_{CO_2} data for a constant value of pumping flux of 0.8 l·min^{-1}.

Table 4.6 reports the values of *a*, *b* AND *c* coefficients found for each permeability and for a constant pumping flux of 0.8 l·min^{-1}.

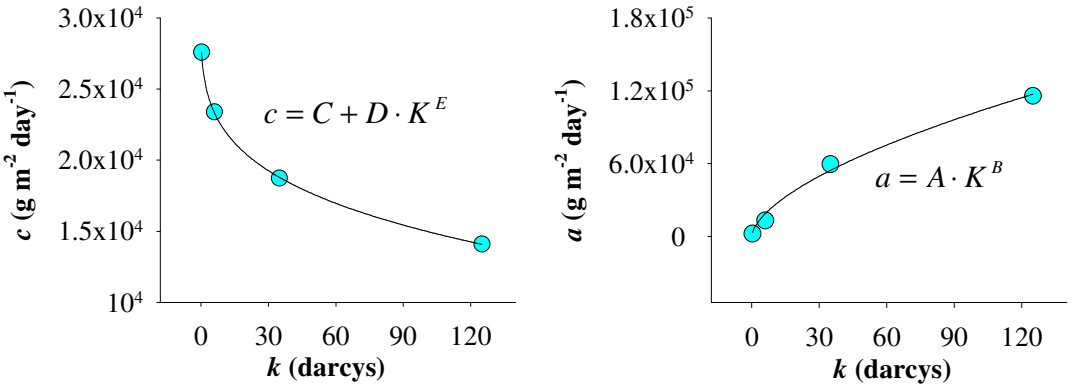

Figure 4.10. Variation of constants *a* and *c* of equation (4.8) as a function of soil permeability at a constant pumping flux of 0.8 L·min^{-1}.

As shown in Figure 4.10, the values of coefficients *a* and *c* of equation (4.8) change as a function of soil permeability in keeping with a power function, while the values of *b* seem to be constant for this value of pumping flux (0.8 l·min^{-1}) and equal to 3 (see Table 4.6). Therefore, equation (4.8) can express as a function of the soil permeability as follows:

$$J_{CO_2} = (C + D \cdot K^E) \cdot C_d + (A \cdot K^B) \cdot C_d{}^3$$

By fitting this model to C_d, k and J_{CO_2} experimental data achieved for a constant pumping flux of 0.8 l·min^{-1}, the following equation is obtained:

$$J_{CO_2} = (3.2 \cdot 10^4 - 5.7 \cdot 10^3 k^{0.24}) \cdot C_d + 6.5 \cdot 10^3 \cdot k^{0.6} \cdot C_d{}^3 \qquad (4.9)$$

The *R* value of the fitting is equal to 0.982.

As shown in Figure 4.11, equation (4.9) is a complex three-dimensional surface whose intersection with the constant permeability planes are curves expressed by equation (4.8). Equation (4.9) can be used to perform accurate measurements of soil CO_2 flux by measuring C_d and soil permeability.

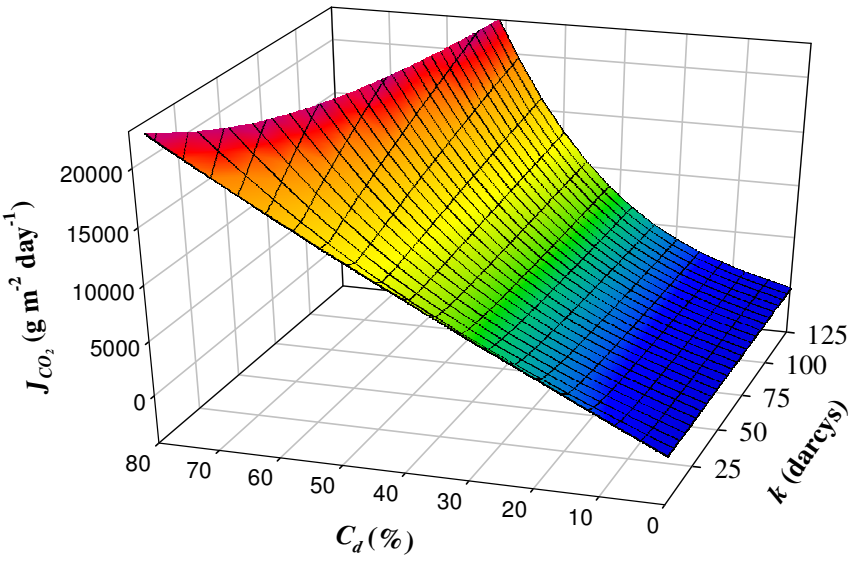

Figure 4.11. Relationship between C_d, k and J_{CO_2} calculated from equation (4.9).

4.7 Reproducibility of the method

In order to verify the reproducibility of the flux measurements performed with this method, several measurements of soil CO_2 flux were performed in a selected area of Vulcano (Aeolian Islands, Italy) close to Grotta dei Palizzi. In one hour, soil CO_2 flux measurements

were repeated ten times at four sites: A, B, C and D. The results of these flux measurements are reported in Table 4.7, which also gives the main statistical parameters.

Sites	A	B	C	D
CO_2 flux measurements ($g\ m^{-2}\ day^{-1}$)	139	30	458	797
	132	27	475	814
	139	27	475	814
	132	27	475	814
	139	30	458	831
	139	27	475	797
	136	30	458	831
	139	27	458	831
	132	27	475	831
	136	27	475	814
Mean	136	28	468	817
Standard deviation	3	1	9	13
CV	2%	5%	2%	2%

Tabella 4.7. Results of the CO_2 flux measurements ($g\ m^{-2}\ day^{-1}$) repeated at sites A, B, C and D. Main statistical parameters are also reported.

The reproducibility of this method was estimated using the coefficient of variation (CV), which is the standard deviation for the repeated measurements divided by their average value and expressed as a percentage. As shown in Table 4.7, the CV values obtained for each site were lower than 5%, which indicates that the flux measurements performed with this method are characterized by good reproducibility. This feature is very important if we want to employ the method in the continuous monitoring of volcanic activity.

Chapter 5

The Radial Gas Advection Method for measuring *In situ* Soil Permeability

In the last Chapter we have shown that one important parameter which must be known to perform accurate measurements of soil CO_2 flux with the dynamic method is soil permeability. Starting from this consideration we have developed a new method for measuring *in situ* soil permeability, based on the theory of radial gas advection through an isotropic porous medium. In this Chapter we will describe the theory on which this method is based, and subsequently we will discuss the results of the several tests performed in the field (Vulcano Islands, Italy) and in the laboratory in order to verify the performance reliability of the developed method.

5.1 Generalities on soil permeability measurements

As discussed in Chapter 2, soil gas permeability is the main parameter that influences the advective gas transport through porous media. This parameter depends on the properties and the specific conditions of the soil such as porosity, structure, tortuosity, specific surface, air saturation, etc. (Moldrup et al., 1998). Soil permeability can be defined as the easy with which a fluid can pass through the soil. Laboratory methods, employed in measuring soil gas permeability, consist of special filtration devices in which the soil samples are traversed in one direction by a gas flux. Generally, treatment of soil samples with these methods (sample collection, transport and insertion inside the measuring device) profoundly modify all soil properties and the resulting permeability values could be affected by serious errors (Evans and Kirkham, 1949). In order to solve this problem, various empirical methods have been developed to measure soil permeability directly in the field (Evans and Kirkham, 1949; Grover, 1955; Fish and Koppi, 1994). The devices employed consist of an inverted chamber placed on the soil and connected to a gas tank. The gas pressure reached in the chamber is proportional to gas flux and soil permeability, according to an empirical model of gas advection through a homogenous porous medium.

A new method for measuring shallow soil permeability *in situ* is presented and discussed in this Chapter. This new method is based on the theory of radial gas advection through an isotropic porous medium. The model describes the relationship between the permeability of the medium and the pressure gradients induced by a radial and continuous gas source.

5.2 Generalities on fluid advection

As discussed in Chapter 2, the advective fluid transport in a natural porous medium is governed by the Darcy's law. This highlights the relationship between velocity (v) of the fluid and the pressure gradient (∇P):

$$v = -\frac{k}{\mu}\nabla\left(P + \rho g z\right)$$

where g is the acceleration gravity constant, ρ and μ are the density and the viscosity of the fluid respectively, and k is the *intrinsic permeability* of the soil. Regarding these fluids, the term $\rho g z$ in the following calculations will be ignored because it is three orders of magnitude less than the P term. Theoretically, *intrinsic permeability* only depends on the properties of the porous medium and not on the permeating fluid (Carman, 1956). This assumption is generally true when fluids do not interact with soil. In other cases (especially water and other liquids), the fluid can interact with soil, thereby changing its properties. *Intrinsic permeability* could, thereby, strongly depend on the characteristics of the fluid (Fish and Koppi, 1994; Michaels and Linn, 1954). In this work we shall consider the advection of air and CO_2 through a porous medium. k is the *intrinsic permeability* of the medium for these gases which we call *gas permeability*, as suggested by several authors (Moldrup et al., 1998; McCarthy and Brown, 1992).

Combining Darcy's law with the continuity equation [$div(\rho v)+n\partial\rho/\partial t = 0$], in which n is the porosity of the porous medium, the fundamental equation for gas transfer through porous media is obtained (Scheidegger, 1974):

$$div\left(\rho\frac{k}{\mu}\nabla P\right) = n\frac{\partial\rho}{\partial t}$$

or

$$\nabla^2 \rho P = 0 \qquad (5.1)$$

if the system is under steady state conditions, at constant temperature (μ = constant) and the porous medium is homogeneous (k = constant). Moreover, assuming ideal behaviour regarding the gas involved in the transfer process and constant temperature:

$$\rho = cP$$

where $c = M/RT$, M is the molecular weight of a generic gas, R is the universal gas constant and T is the absolute temperature. Substituting this expression in equation (5.1), Laplace's equation is obtained:

$$\nabla^2 \chi = 0 \qquad (5.2)$$

where $\chi = cP^2$. Equation (5.2) can be used to determine the gas pressure spatial variation for any gas advection model.

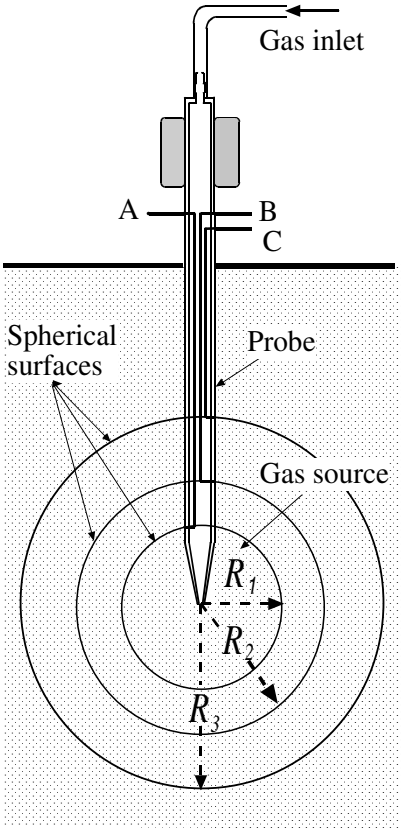

Figure 5.1. Schematic representation of the probe used in making soil permeability measurements and graphical representation of the isobar surfaces produced from the soil; A, B, C are tubes which measure the pressure and R_1, R_2, R_3 are the radii of the spherical shells. The tubes are connected to external pressure sensors (see Figure 5.2).

Modeling a radial gas pressure distribution through a porous medium (Figure 5.1), it was useful to express Laplace's equation using the polar spherical coordinates *r*, θ and γ:

$$\frac{\partial}{\partial r}\left(r^2 \frac{\partial \chi}{\partial r}\right) = 0$$

in which we do not consider the terms θ and γ, in light of a hypothesis of a homogeneous porous medium. The solution of this differential equation is:

$$\chi = a + b/r \tag{5.3}$$

where *a* and *b* depend on boundary conditions. Considering two spherical shells with radii R_1 and R_2, which are concentric with the gas source and assuming that the pressure of these two shells is equal to P_1 and P_2 respectively, the expression of the constant *a* and *b* can be easily found:

$$a = cP_1^2 - \frac{b}{R_1} \qquad \text{and} \qquad b = \frac{c(P_2^2 - P_1^2)R_1R_2}{R_1 - R_2}$$

Substituting *a* and *b* terms into equation (5.3) and solving for the pressure, we obtain the following equation:

$$P = \sqrt{P_1^2 - \frac{\left(P_2^2 - P_1^2\right)R_2}{R_1 - R_2}\left(\frac{R_1}{r} - 1\right)} \tag{5.4}$$

which shows the variation of the gas pressure (*P*) as a function of the radius (*r*), generated by a radial gas source inside a homogeneous porous medium. Substituting the first derivative of the equation (5.4) at $r = R_1$ in Darcy's law, the equation for the volumetric gas flux across a spherical shell of radius R_1 is obtained:

$$\varphi_{r=R_1} = \frac{2k\pi}{\mu}\frac{R_1 R_2}{R_1 - R_2}\frac{\left(P_2^2 - P_1^2\right)}{P_1} \tag{5.5}$$

Equation (5.5) predicts the gas flux crossing a spherical shell of radius R_1, when a radial gas source is generated in a homogeneous porous medium of permeability *k* and the gas pressure at R_1 and R_2 shells is equal to P_1 and P_2, respectively.

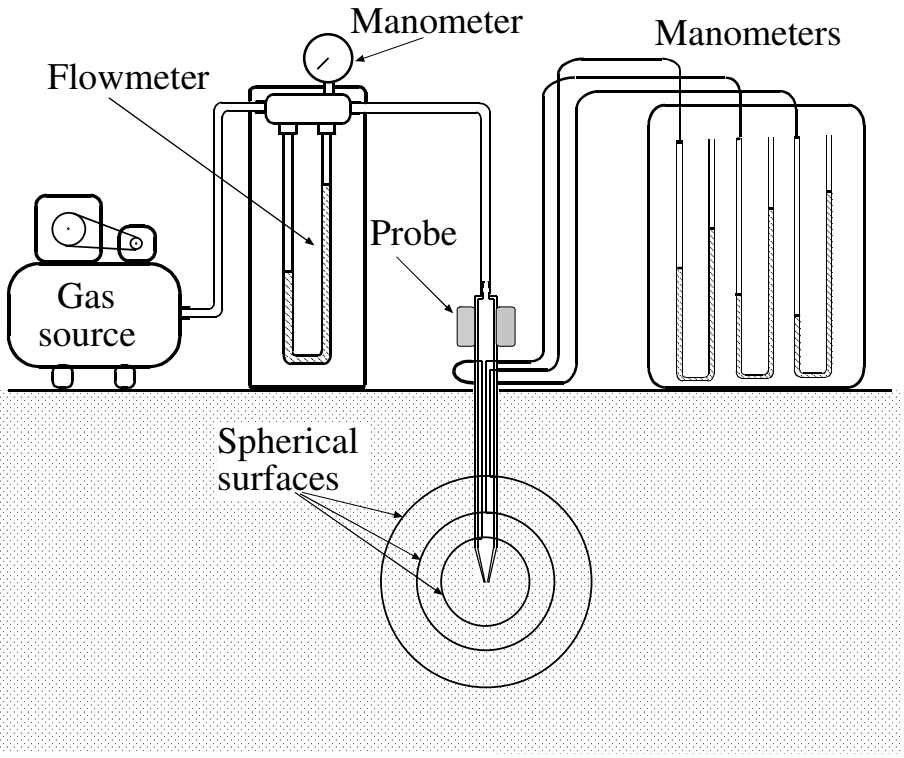

Figure 5.2. Permeability equipment used for field measurements, as discussed in this thesis. The apparatus consists of: an external pump, a flux meter, a probe with which to supply gas to the soil, three water manometers for reading the soil gas pressure at different depths.

5.3 Laboratory and field tests

The permeability values, discussed in this Chapter, were calculated according to equation (5.5) and the measurements of gas pressure for different concentric spherical shells. The radial gas source was generated by using the probe shown in Figure 5.1 (diameter = 2 cm, length = 75 cm), which was inserted in the soil at a depth of 50 cm. The gas pressure gradients are measured by three thin tubes, externally connected to water manometers and located inside the probe; the tubes were opened at depths of 35, 40 and 45 cm (Figure 5.1, A, B and C). Figure 5.2 shows the equipment used for measuring soil permeability. The gas flow was generated by a membrane pump connected with a flowmeter and both the flux and pressure measurements were carried out at steady state (reached in a few minutes). The method was tested in the field (the island of Vulcano) and in the laboratory.

Site	Volumetric Flux (cm^3s^{-1})	$k_{1,2}$ (darcys)	$k_{2,3}$ (darcys)	$k_{1,3}$ (darcys)	$\delta(k_{1,2}-k_{1,3})$
$\mathbf{1_a}$	260	14.6 ± 0.8	13 ± 2	13.9 ± 0.6	7
$\mathbf{1_b}$	230	12.3 ± 0.6	16 ± 3	12.6 ± 0.5	1
101	230	18 ± 1	19 ± 2	18 ± 1	0
$\mathbf{4_a}$	280	50 ± 5	47 ± 12	48 ± 3	4
$\mathbf{4_b}$	178	48 ± 6	45 ± 15	46 ± 3	4
$\mathbf{4_c}$	230	43 ± 5	27 ± 10	37 ± 3	15
$\mathbf{30_a}$	60	10 ± 2	10 ± 5	10 ± 2	0
$\mathbf{30_b}$	185	7.5 ± 0.3	12 ± 2	7.9 ± 0.3	5
$\mathbf{30_c}$	255	6.4 ± 0.2	5.5 ± 0.3	5.9 ± 0.2	8
6	275	63 ± 6	70 ± 23	62 ± 4	2
$\mathbf{43_a}$	260	6.6 ± 0.2	8.6 ± 0.8	6.5 ± 0.2	2
$\mathbf{43_b}$	265	7.1 ± 0.2	7.0 ± 0.8	6.9 ± 0.2	3
41	275	34 ± 3	28 ± 7	31 ± 2	9
$\mathbf{8_a}$	305	35 ± 3	31 ± 8	33 ± 3	6
$\mathbf{8_b}$	310	33 ± 2	31 ± 6	32 ± 1	3
$\mathbf{12_a}$	275	9.7 ± 0.3	17 ± 4	10.5 ± 0.3	8
$\mathbf{12_b}$	295	6.8 ± 0.2	16 ± 3	7.0 ± 0.2	3
$\mathbf{40_a}$	290	9.5 ± 0.3	11 ± 1	9.5 ± 0.3	0
$\mathbf{40_b}$	265	10.9 ± 0.4	13 ± 2	10.9 ± 0.4	0

Table 5.1. Soil permeability measurements and the relative confidence interval relative to different soil portions and different air fluxes. The location of the measurement sites are shown in the Figure 5.3. The sites with the same number and different subscripts refer to permeability measurements carried out a few meter one another. Discrepancy values $\delta(k_{1,2} - k_{1,3})$ expressed in % between the $k_{1,2}$ and $k_{1,3}$ permeability values are also shown. The permeability $k_{1,2}$ and $k_{1,3}$ are very similar and confirms the assumption that the porous medium can be considered quite homogeneous. The air flux values reported here was corrected by the output air pressure values.

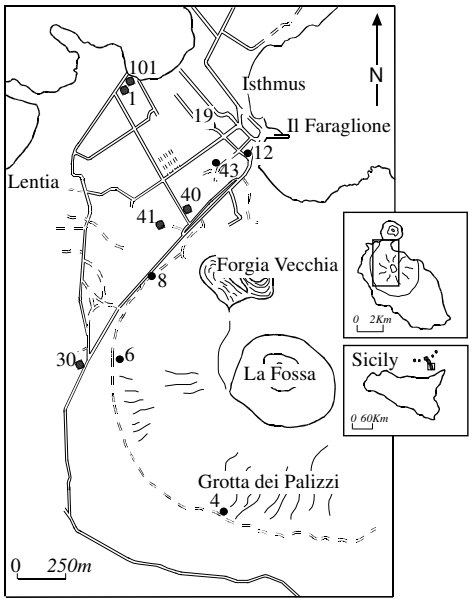

Figure 5.3. Location of the measurement sites where the new method to measure *in situ* soil permeability was tested.

The permeability values measured in the field, together with relative confidence intervals, have been reproduced in Table 5.1. Three permeability values, $k_{1,2}$, $k_{2,3}$ *and* $k_{1,3}$ were measured for each site, each value referring to different spherical soil shells with inner and outer radii of $R_1 - R_2$, $R_2 - R_3$ and $R_1 - R_3$ respectively. The confidence interval was obtained by applying the rule of error propagation (Taylor, 2000) to equation (5.5). According to the field equipment, the uncertainty regarding the pressure and flux measurements is equal to ± 1 mmH_2O (≅0.1 *mbar*) and ± 4 cm^3s^{-1} respectively. The absolute error in the permeability measurements depends on the pressure difference relative to the spherical shells under consideration.

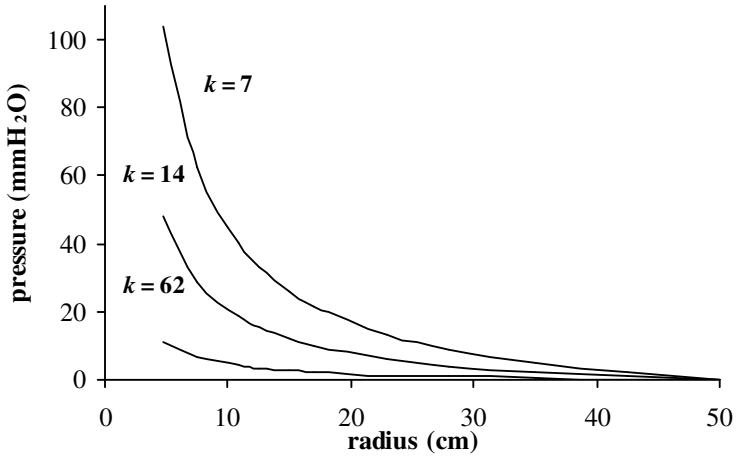

Figure 5.4. Theoretical variation (solid lines) in gas pressure as a function of the radius for three different permeability values (7, 14 and 62 darcys respectively). The pressure produced in the soil significantly decreases with increasing distance from the gas source (0 cm).

According to equation (5.5), soil gas pressure rapidly decreases with increasing distance from the gas source (Figure 5.4). Therefore, the most distant shells were characterized as possessing the lowest difference in pressure. Considering the uncertainty regarding the water manometer, any error in the pressure difference measured between the R_2 and R_3 shells is significantly higher than the other shells (Table 5.1).

Gas flux values and soil permeability also influence the error made in taking soil permeability measurements. Low flux and high soil permeability yield small differences in gas pressure and, as a consequence, permeability measurements will be affected by larger errors.

Table 5.1 also reports discrepancies $\delta(k_{1,2} - k_{1,3})$, expressed as percentages between the permeability values measured, considering the spherical shells of soil with inner and outer radii of $R_1 - R_2$ and $R_1 - R_3$. The calculated permeability produced very similar results with a discrepancy of less than 10%, except in one case (15% for the site 4). The agreement between the permeability values $k_{1,2}$ *and* $k_{1,3}$ calculated for the same sites confirms our assumption that the porous medium can be considered relatively homogeneous.

Finally, the method was also tested comparing the *in situ* measurements with the values determined by using standard laboratory procedures. Several soil samples were collected in sites where soil permeability had been previously measured with the method described in this chapter. The four selected sites (1, 4, 6 and 8) were characterized by presence of no-cohesive soils with different permeability values (15-90 darcys). The soil samples were collected with a shovel from a hole approximately 50cm deep; in many cases the extracted soils were disturbed. The permeability of the soil samples was measured in the laboratory by a gas permeameter (Loosveldt et al., 2002) and the values compared with the *in situ* measurements (Table 5.2).

Sample	***k* (darcys) (laboratory)**	***k* (darcys) (in situ)**	**δ (%)**
4	48.5	45.3	7
6	85.5	62.5	31
1	16.9	13.5	22
8	41.2	33.3	21

Table 5.2. Comparison between laboratory and in situ soil permeability values. The discrepancies between these values are also shown. The in situ data are the mean values of the permeability measurements reported for each sites in Table 5.1.

The laboratory results were always higher than the *in situ* measurements with a discrepancy ranging from 7 to 31% (Table 5.2). These results can be explained by considering that the sample procedure and laboratory treatments destroyed the original soil structure and caused an increase in porosity. Moreover, during the waiting period prior to taking the measurements, samples were subjected to a continuous decrease in soil moisture content which resulted in a further increase in gas permeability.

In conclusion, applying a physical model to gas radial advection through porous media, a new method has been developed to determine *in situ* soil permeability by taking simple measurements of gas pressure at different depths.

Chapter 6
Tests on the accumulation chamber method

The apparatus employed to simulate a natural degassing system described in Chapter 3 was also used to perform several tests on the accumulation chamber method. The results obtained are discussed in this Chapter. Subsequently we will discuss the comparison between the *dynamic* method and the accumulation method performed at Vulcano by Carapezza and Granieri (2004).

6.1 Generalities on the accumulation chamber methods

The accumulation chamber methods are well known in literature. They have been used extensively in the agricultural and ecological fields to measure the emission of gases such as CO_2, N_2O, and CH_4 from soils to the atmosphere (Kanemasu et al., 1974; Denmead, 1979; Matthias et al., 1980; Cicerone and Shetter, 1981; Moore and Roulet, 1991; Fukui and Doskey, 1996). These methods are based on the accumulation of soil gas in a cylindrical chamber of known volume placed on the surface of the soil. As shown by Tonani and Miele (1991), the basic idea of measuring soil CO_2 flux with an accumulation method is that the rate of variation in the concentration of CO_2 inside the chamber ($[CO_2]$) is directly proportional to soil CO_2 flux:

$$d[CO_2]/dt \propto J_{CO_2}$$

In general, the accumulation chamber methods include discontinuously-monitored flux chambers (DM) (also called static or passive chambers) and continuously-monitored (CM) flux chambers. In the first case, the temporal variation in the concentration of CO_2 inside the chamber is monitored by sampling a small volume of gas from a rubber septum placed in the chamber. CO_2 concentration in the sampled gas is measured by a portable infrared gas analyzer. In the case of the CM method, the CO_2 concentration inside the chamber is monitored continuously by an infrared gas analyzer linked via a close loop to the chamber (Figure 6.1). These later methods have been widely used in the last decade to measure CO_2 flux from the soil in volcanic and geothermal areas (Chiodini et al., 1998 and 2001; Evans et al., 2001; Rogie et al., 2001; Bergfeld et al., 2001; Gerlach et al., 2001).

To understand the assumptions on which the measurement of soil CO_2 flux with a continuous-monitored accumulation chamber method is based, we must make a mass balance of the CO_2 within the volume of the chamber (see Figure 6.1). Moreover, in the formulation of the CO_2 mass balance, we would take also into account that a constant flux of the inner

chamber atmosphere (ϕ_{exc}) can be lost through the pressure equilibration tube, which is placed on top of the chamber usually employed in the field (see for example the West System's chambers and Licor's chambers)**.** Under these considerations, the CO_2 mass balance is given by:

$$VdC_c(t) = A \cdot J_{CO_2}dt + C_c(t)\phi_{in}dt - C_c(t)\phi_{out}dt - C_c(t)\phi_{exc}dt \qquad (6.1)$$

where:

- A and V are the cross section area and the inner volume of the chamber, respectively;
- $C_c(t)$ is the CO_2 concentration of the gas inside the chamber;
- ϕ_{in} and ϕ_{out} are the fluxes of gas entering and leaving the chamber, respectively.
- ϕ_{exc} is the volumetric flux of gas leaving the chamber through the pressure equilibration tube placed on top of the chamber (Figure 6.1)

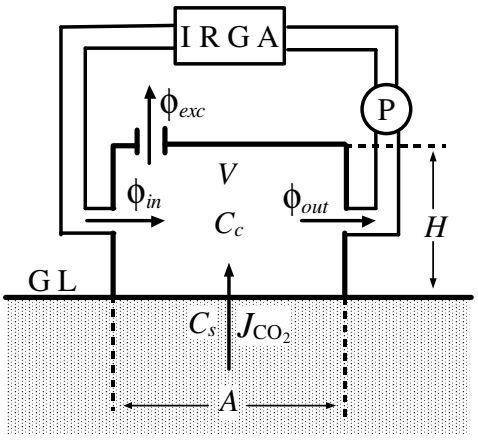

Figure 6.1. Schematic illustration of a generic continuously-monitored chamber system. P = sampling pump; G L = ground level; IRGA = Infra Red Gas Analyzer. For the other symbols see the text.

If no pressure difference exists between the inside and the outside of the chamber and no flux is forced through the soil, the J_{CO_2} term in equation (6.1) can be expressed as the sum of the advective and diffusive fluxes:

$$J_{CO_2} = -\frac{D}{h}(C_c(t) - C_s(t)) + C_s(t)\phi_{ad}\,, \qquad (6.2)$$

where ϕ_{ad} is its advective flux, h is an infinitesimal thickness of soil close to the chamber atmosphere and $C_s(t)$ is the CO_2 concentration in soil gas at this depth. Combining equation (6.1) with equation (6.2), we obtain:

$$VdC_c(t) = A \cdot \left(-\frac{D}{h}(C_c(t) - C_s(t)) + C_s(t)\phi_{ad} \right) dt + C_c(t)\phi_{in}dt - C_c(t)\phi_{out}dt - C_c(t)\phi_{exc}dt$$

$$\Downarrow$$

$$VdC_c(t) = A \cdot \left(\frac{D}{h}(C_s(t) - C_c(t)) + C_s(t)\phi_{ad} \right) dt + C_c(t)\phi_{in}dt - C_c(t)\phi_{out}dt - C_c(t)\phi_{exc}dt$$

and assuming that $\phi_{in} = \phi_{out}$ we can obtain:

$$dC_c(t) = \frac{A}{V}\frac{D}{h}(C_s(t) - C_c(t))dt + \frac{A}{V}C_s(t)\phi_{ad}dt - C_c(t)\frac{\phi_{exc}}{V}dt$$

Noting that $V/A = H$ for our dynamic chamber:

$$\frac{dC_c(t)}{dt} = \frac{D}{hH}(C_s(t) - C_c(t)) + \frac{C_s(t)\phi_{ad}}{H} - C_c(t)\frac{\phi_{exc}}{V}$$

$$\Downarrow$$

$$\frac{dC_c(t)}{dt} + \left(\frac{D}{hH} + \frac{\phi_{exc}}{V} \right) C_c(t) = \frac{D}{hH}C_s(t) + \frac{C_s(t)\phi_{ad}}{H}$$

Assuming that $C_s(t)$ is a constant during the time necessary to perform the flux measurement a first-order differential equation for $C_c(t)$ is obtained:

$$\frac{dC_c(t)}{dt} + \left(\frac{D}{hH} + \frac{\phi_{exc}}{V} \right) C_c(t) = \frac{C_s}{H}\left(\frac{D}{h} + \phi_{ad} \right)$$

The last equation has the following general solution:

$$C_c(t) = VC_s \frac{D + h \cdot \phi_{ad}}{VD + hH\phi_{exc}} \left(1 - a \cdot e^{-\left(\frac{D}{hH} + \frac{\phi_{exc}}{V} \right) t} \right) \tag{6.4}$$

where a is a constant that can be calculated by the initial conditions. Assuming that the CO_2 concentration of gas inside the chamber at $t = 0$ is equal to zero ($C_c(0) = 0$), the equation (6.4) becomes:

$$C_c(t) = VC_s \frac{D + h \cdot \phi_{ad}}{VD + hH\phi_{exc}} \left(1 - e^{-\left(\frac{D}{hH} + \frac{\phi_{exc}}{V} \right) t} \right) \tag{6.5}$$

Equation (6.5) shows the variation of the CO_2 concentration inside the chamber as a function of time. Calculating the first derivative of the equation (6.5) at $t = 0$ we obtain:

$$\left(\frac{\partial C_c(t)}{\partial t} \right)_{t=0} = V \frac{D + h \cdot \phi_{ad}}{VD + hH\phi_{exc}} \frac{VD + hH\phi_{exc}}{hHV}$$

$$\Downarrow$$

$$\left(\frac{\partial C_c(t)}{\partial t}\right)_{t=0} = \frac{D + h \cdot \phi_{ad}}{hH}$$

$$\Downarrow$$

$$\left(\frac{\partial C_c(t)}{\partial t}\right)_{t=0} = \frac{1}{H}\left(\frac{D}{h} C_s + C_s \phi_{ad}\right) \tag{6.6}$$

According to the specified initial condition $C_c(0) = 0$, equations (6.2) and (6.6) become, respectively:

$$J_{CO_2} = \frac{D}{h} C_s + C_s \phi_{ad}$$

$$\Downarrow$$

$$J_{CO_2} = H\left(\frac{\partial C_c(t)}{\partial t}\right)_{t=0} \tag{6.7}$$

which is the relationship used to calculate J_{CO_2} as a function of the slope of the CO_2-*t* line at *t* = 0. As discussed by Chiodini et al., (1998) the assessment of the tangent at *t* = 0 can be difficult in real cases and this can cause some errors in the flux measurements which are however lower than 5% (Chiodini et al., 1989).

As we will show in the following paragraph, new and more significant sources of error are likely to be introduced.

6.2 Laboratory experiments

In order to asses the performance and the reliability of the accumulation chamber system, several CO_2 flux measurements at different imposed CO_2 fluxes were carried out utilizing the experimental system described in Chapter 3 (see Figure 3.1).

The accumulation system utilized in our investigations is composed of an inverted cylindrical chamber, 10 cm high, and a portable "Drager Polytron IR CO_2" (accuracy 3% of reading for $[CO_2]$ > 350 ppm) linked by a close loop to the chamber (see Figure 6.1). Therefore, our system chamber is a continuously-monitored (CM) flux chambers. The spectrophotometer is connected to a portable computer that records the temporal variations in the concentration of CO_2 inside the chamber and finds the slope of the $[CO_2]$-*t* line, extrapolated at *t* = 0. The ambient temperature (*T*), and pressure (*P*) of the gas inside the chamber. For each investigated J_{CO_2}, when the steady state had been reached, flux measurements were performed according to the following equation (Werner et al., 2000):

$$J_{CO_2} = k\left(\frac{P}{P^0}\right)\left(\frac{T^0}{T}\right)H\left(\frac{\partial C_{CO_2}}{\partial t}\right)_{t=0} \tag{6.7}$$

where k = 169.34 m^3 converts ppm·sec^{-1} in g·day^{-1}, P is the measured pressure (atm), T is the measured temperature (K). T^0 and P^0 normalize the flux to STP (298 K and 1 atm). The last equation differs from equation (6.6) in that it converts the ppm·sec^{-1} values obtained by the portable computer in g·day^{-1}, so that the CO_2 flux is denoted in units of g m^{-2} day^{-1}.

The results of the accumulation chamber measurements performed on soil samples S_2, S_3 and S_4 (see Chapter 3, Table 3.1) are reported in Table 6.1. The deviations of each measured flux from the imposed CO_2 fluxes (% Dev) are expressed in percentage and are also reported in the same table. In Figure 6.2 the accumulation chamber measurements performed on sample S_4 (k = 0.36 darcys) are compared with the imposed fluxes (solid line).

***k* = 36 darcys**			***k* = 6 darcys**			***k* = 0.36 darcys**		
J_{CO_2} (g $m^{-2}day^{-1}$)	$J_{CO_2\ meas.}$ (g $m^{-2}day^{-1}$)	% Dev	J_{CO_2} (g $m^{-2}day^{-1}$)	$J_{CO_2\ meas.}$ (g $m^{-2}day^{-1}$)	% Dev	J_{CO_2} (g $m^{-2}day^{-1}$)	$J_{CO_2\ meas.}$ (g $m^{-2}day^{-1}$)	% Dev
573	385	-39	95	82	-15	318	233	-31
573	394	-37	95	76	-22	318	205	-43
1145	763	-40	95	70	-30	318	215	-39
1145	769	-39	95	65	-38	795	633	-23
1145	736	-44	95	105	10	1909	1806	-6
1591	1348	-17	1145	965	-17	1909	1745	-9
1909	1670	-13	1145	981	-15	1909	1699	-12
2100	1774	-17	1145	975	-16	3055	2983	-2
2100	1772	-17	1145	987	-15	3055	2729	-11
2100	1875	-11	3055	3670	18	3055	2989	-2
2800	2841	1	3055	3805	22	3055	2986	-2
3309	3361	2	3055	3630	17	3055	2705	-12
3309	3483	5	3564	3890	9	4136	3892	-6
3309	3356	1	3564	3801	6	4136	4027	-3
4582	4807	5	3564	3920	10	4136	4016	-3
5473	5832	6	3564	3905	9	5282	4652	-13
5473	5870	7	3564	3920	10	5282	4698	-12
5473	5585	2	4136	4607	11			
5473	5780	5	4136	4728	13			
			4136	4893	17			
			9673	9982	3			
			9673	10181	5			
			9673	9906	2			
			14828	16812	13			
			14828	15616	5			
			14828	15530	5			

Table 6.1. Dynamic chamber measurements performed at different imposed CO_2 fluxes (J_{CO2}) at each investigated soil permeability. The deviation of each measurement from the imposed flux, expressed in percentage, is also shown.

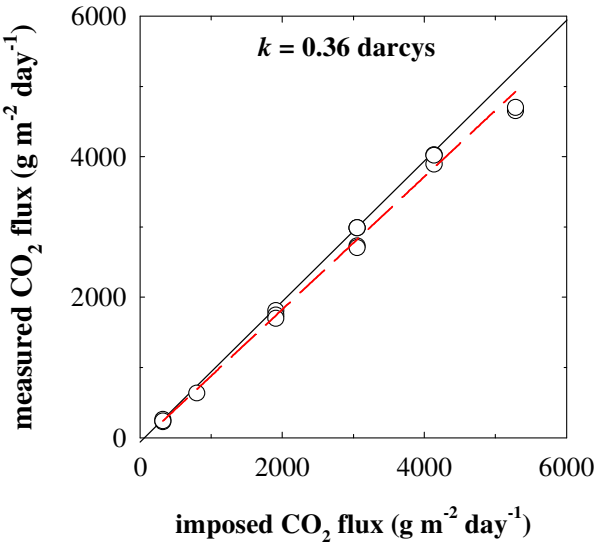

Figure 6.2. Comparison between imposed and measured CO_2 fluxes. The dashed line is the best fitting line of the measured data. Soil permeability, k = 0.36 darcys.

The dashed regression line shown in this figure indicates that the measured values are in reasonable agreement with the imposed fluxes, although they show a negative bias. All the measured fluxes are lower than the imposed fluxes with a mean difference of -16 %. This result is very similar to the value (-12.5 %) found by Evans et al., (2001).

The comparison between measured and imposed CO_2 fluxes for k = 6 darcys (Figure 6.3) shows a negative bias for $J_{CO_2} < 3000$ g m^{-2} day^{-1} and a positive bias for $J_{CO_2} > 3000$ g m^{-2} day^{-1} with a mean difference of 13%.

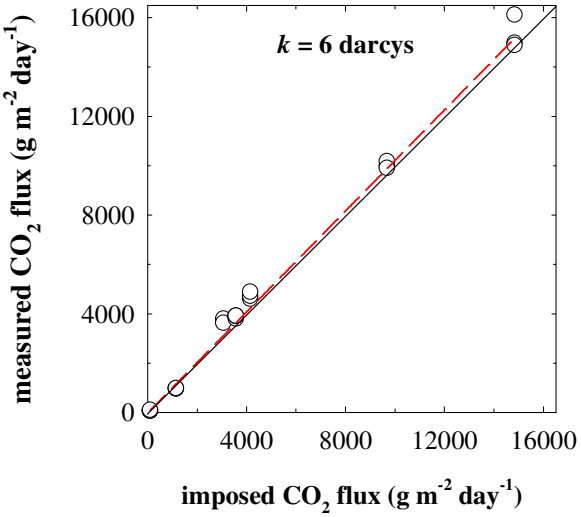

Figure 6.3. Comparison between imposed and measured CO_2 fluxes. The dashed line is the best fitting line of the measured data. Soil permeability, k = 6 darcys.

A similar result can also be observed for the experiment performed on soil sample S_2 (k = 36 darcys) (Figure 6.4).

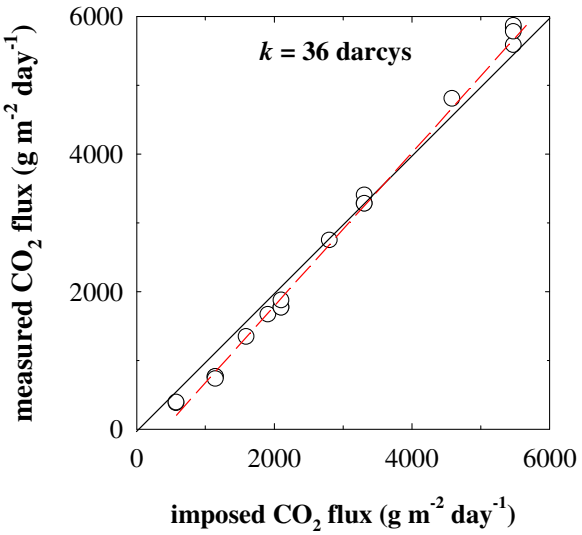

Figure 6.4. Comparison between imposed and measured CO_2 fluxes. The dashed line is the best fitting line of the measured data. Soil permeability, k = 36 darcys.

The underestimation shown by the chamber measurement data at low permeability (0.36 darcys) and at low fluxes could be the result of different factors. A constant underestimation can be attribute to the presence of a systematic error committed in the valuation of the real volume of the system in equation (6.8). In the case of a continuously-monitored chamber, the real volume of the system is equal to the sum of the inner volume of the chamber plus that of the close loop (tubes and filters) and the measurement cell of the infrared gas analyzer (see Figure 6.1). In other words, the volume is increased by the volume of the loop and that of the spectrophotometer cell. We calculated that for the system employed in our investigations this volume is about 4% in respect of the inner volume of the chamber (2923 cm^3) and this causes a constant error in the flux measurements equal to -4%.

The negative bias in the flux measurements could also be caused by some characteristics of the system, such as pumping flux and CO_2 detector speed that are not able to keep up the variation of the CO_2 concentration in the chamber. In order to investigate the influence of the pump flux on the dynamic chamber measurements, we performed some measurements of soil CO_2 flux by changing the pumping flux from 1 to 0.2 $l \cdot min^{-1}$. The results of these investigations are reported in Table 6.2 along with the discrepancy expressed in percentage between the measured and imposed fluxes.

Pumping flux ($l \cdot min^{-1}$)	J_{CO_2} = 702 ($g\ m^{-2} day^{-1}$)		J_{CO_2} = 970 ($g\ m^{-2} day^{-1}$)		J_{CO_2} = 1688 ($g\ m^{-2} day^{-1}$)		J_{CO_2} = 2140 ($g\ m^{-2} day^{-1}$)	
	measured J_{CO_2} ($g\ m^{-2}\ day^{-1}$)	% Dev	measured J_{CO_2} ($g\ m^{-2}\ day^{-1}$)	% Dev	measured J_{CO_2} ($g\ m^{-2}\ day^{-1}$)	% Dev	measured J_{CO_2} ($g\ m^{-2}\ day^{-1}$)	% Dev
1	645	-8	928	-4	1665	-1	2286	6
0.8	595	-15	810	-17	1542	-9	2222	3
0.6	557	-21	725	-25	1560	-8	2002	-7
0.4	451	-36	607	-37	1402	-17	1772	-18
0.2	380	-46	506	-48	1087	-36	1485	-31

Table 6.2. Accumulation chamber measurements performed at different pump fluxes and for four constant imposed fluxes. Soil permeability = 6 darcys.

As shown in this table, the measured CO_2 fluxes are strongly dependent on the pumping flux. Very high underestimations, i.e., up to 48 %, were obtained at the lowest pumping flux (0.2 l min^{-1}) suggesting that in these conditions the circulation rate of air in the system is not enough able to keep up the variation of CO_2 concentration in the chamber. On the contrary, when the pumping rate is increased from 0.2 to 1 $l \cdot min^{-1}$ the difference between the imposed and measured CO_2 flux decreases and a slight overestimation appears for the highest imposed fluxes (see also Figure 6.3 and 6.4). As discussed in several papers (Conen and Smith, 1998; Fang et al., 1998) the overestimation can be explained as an effect of air circulation in the chamber. This may create a pressure deficit within the chamber inducing an additional advective CO_2 flow from the covered soil matrix to the chamber. Following Fang and Scott, (1998) the pressure difference (ΔP) between a generic layer of soil below the enclosed area and the chamber atmosphere (Figure 6.5) can be expressed using Bernulli's equation:

$$\Delta P = P_h - P_c - \frac{1}{2}\rho_a v^2$$

where P_h is the pressure at one generic depth $z = h$ in the soil; P_c is the pressure at the enclosed soil surface; ρ_a is the air density and v is the velocity of air circulating inside the chamber close to the soil-air surface.

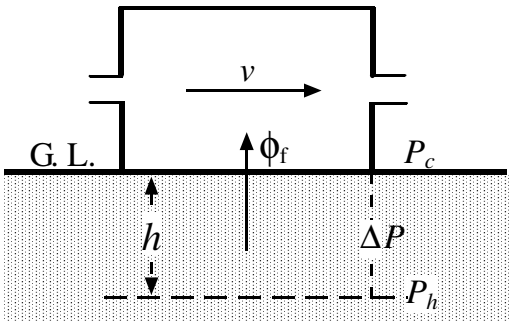

Figure 6.5. Schematic illustration of the additional gas flux (ϕ_f) from the soil to the chamber due to air circulation in a continuously-monitored chamber. For the symbols see the text.

This equation shows that the difference in pressure is proportional to the velocity of air circulating inside the chamber. Furthermore this pressure difference increases as a function of the natural pressure gradient (P_h-P_c) which is fixed by the imposed flux. Moreover, the advective flow ϕ_f of soil gas forced into the chamber by the pressure difference can be expressed using Darcy's equation:

$$\phi_f = \frac{K}{\mu}\frac{\Delta P}{h} = \frac{K}{\mu}\left(P_h - P_c - \frac{1}{2}\rho_a v^2 \right) \Big/ h$$

where k is the soil permeability and μ is the viscosity of the gas sucked out from the soil. Therefore, this equation shows that the amount of additional gas sucked out from the soil into the chamber depends on soil permeability (k), on the pumping flux (which determines the rate of air circulation in the chamber) and on the imposed flux (which regulates the magnitude of the pressure gradient in the soil below the enclosed area). This effect is always present in the system, but it increases as a function of the pumping flux and of the imposed flux. As shown by the data discussed here, the additional advective CO_2 flow is able to cause an overestimation of the measured flux only at high permeability and at high imposed flux (J_{CO_2} > 3000 g m^{-2} day^{-1}), whereas in other experimental conditions this effect is smaller and it is overcome by the other sources of error.

In conclusion, the experimental results discussed here highlight that measurements of soil CO_2 flux effected using the accumulation chamber method are affected by several different types of error. Some of these are causal and are due to the difficulties in assessing the tangent at $t = 0$. Other errors are systematic and depend on the real volume of the system and on an additional advective CO_2 flow from the covered soil matrix induced by air circulation in the chamber. The magnitude and sign of the errors depend on soil permeability, on the imposed flux and on the pumping flow.

6.3 Comparison between the dynamic and the accumulation method

A comparison between the CO_2 flux measurements performed in Vulcano using both the *dynamic method* (DM) (chapter 4) and the *continuously-monitored accumulation chamber method* (CM) has been reported in a recent paper written by Carapezza and Granieri (2004). The flux measurements discussed in this work were performed simultaneously in the same sites, employing both methods, with the aim of investigating their limits and advantages. We will discuss these data here, also taking into consideration the information acquired in this thesis concerning these methods.

The CO_2 flux values measured with the accumulation method (from Carapezza and Granieri 2004) are reported in the second and the third columns of Table 6.3, respectively. As discussed by Carapezza and Granieri (2004), the reported dynamic fluxes were calculated in agreement with equation (4.1) (old calibration) while the accumulation measurements were calculated in accord with equation (6.8). Unfortunately, Carapezza and Granieri (2004) do not state clearly whether or not the probe used on the island of Vulcano to perform flux measurements with the dynamic method was the same as that used during the 1988 experiment (Gurrieri and Valenza, 1988) or if it was a similar probe. Had it been a similar probe, several unknown errors may have affected the flux measurements performed in line with equation (4.1) (pag. 17). Consequently the comparison between the dynamic and accumulation method performed by Carapezza and Granieri (2004) in their paper does not appear to be appropriate. It is also possible that the probe used by Carapezza and Granieri (2004) was the same as that described in Chapter 4 (pag. 17), which has been under experimentation for several years. Therefore, in the fourth column of Table 6.3 we have also reported the flux values measured with the dynamic method and calculated according to equation (4.9) (new calibration).

n.	J_{CO2} **DM**$^{(1)}$ **(g m^{-2} day^{-1})**	J_{CO2} **CM (g m^{-2} day^{-1})**	J_{CO2} **DM**$^{(2)}$ **(g m^{-2} day^{-1})**	***n.***	J_{CO2} **DM**$^{(1)}$ **(g m^{-2} day^{-1})**	J_{CO2} **CM (g m^{-2} day^{-1})**	J_{CO2} **DM**$^{(2)}$ **(g m^{-2} day^{-1})**
2	167	85	44	29	10	4	3
3	610	95	183	30	13	5	4
4	6,135	624	1,588	32	13	3	4
6	55	14	16	33	42	19	10
7	131	21	36	34	13	1	4
8	64	21	16	35	42	32	10
9	48	16	11	36	42	24	12
10	135	33	37	38	64	18	20
12	161	96	46	39	70	29	17
14b	255	47	66	41	10	9	2
15	225	51	60	42	10	8	3
16	691	52	169	44	276	85	85
17	32	15	9	45	19	12	5
19	70	94	17	46	151	85	41
20	51	82	14	47	83	20	23
21	35	18	8	80	13	11	4
22	13	18	4	81	48	35	14
23	19	21	5	83	31	17	9
24	3	4	1	82	51	33	12
26	6	4	2	84	57	19	17
27	19	15	6	85	19	14	5
28	35	15	10	86	295	75	89

Table 6.3. Flux values measured in the surveyed area. J_{CO2} CM = CO_2 flux values measured with accumulation chamber method (from Carapezza and Granieri, 2004); J_{CO2} DM$^{(1)}$ = CO_2 flux values measured with dynamic method (old calibration) (from Carapezza and Granieri, 2004); J_{CO2} DM$^{(2)}$ = CO_2 flux values measured with dynamic method (new calibration).

The comparison between the dynamic and accumulation flux measurements reported here below are to be considered appropriate only if the probe used by Carapezza and Granieri (2004) was the same as that used during the 1988 experiment or that described in Chapter 4.

In Figure 6.6 the accumulation chamber measurements (CM) carried out in the surveyed area, are compared with the dynamic flux values (DM) obtained using both the old (yellow circles) and new calibration (red circles). In both cases (new and old calibration) a reasonable accord is found between the CM and the CM measurements (R = 0.82). Nevertheless, the dynamic values obtained from the old calibration are generally always higher than the corresponding CM values. On the contrary, more comparable values are obtained with the new calibration and moreover, excluding a small number of points, the accumulation measurements are always higher than the corresponding values obtained with the dynamic method.

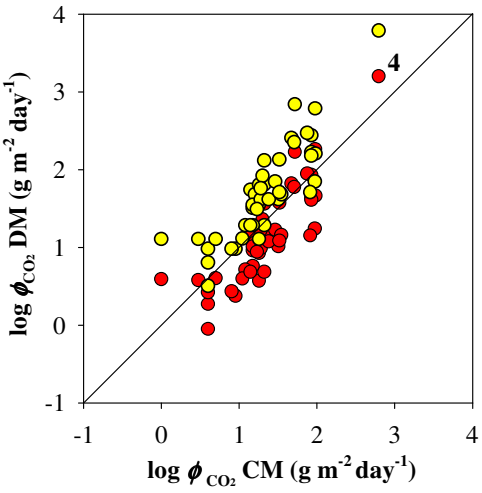

Figure 6.6. Comparison between flux values measured in the same sites with accumulation (CM) and dynamic method (DM). Yellow circles = old calibration; red circles = new calibration.

The highest discrepancy between these two sets of data is found in the most exhalant sector of the surveyed area (point 4, Grotta dei Palizzi). As shown in Table 6.4, the flux values measured with the dynamic method (new calibration) range between 185-1,108 g m^{-2} day^{-1} whereas those measured with the accumulation chamber method range between 155-624 g m^{-2} day^{-1}. Moreover, the same authors reported the results of several measurements of CO_2 concentration sampled at various depths in soils (see Table 6.4).

n.	Soil CO_2 concentration (%)			J_{CO2} CM	J_{CO2} DM$^{(1)}$	J_{CO2} DM$^{(2)}$	J_{CO2} $^{(3)}$
	50 cm	75 cm	100 cm	g m^{-2} day^{-1}	g m^{-2} day^{-1}	g m^{-2} day^{-1}	g m^{-2} day^{-1}
4	22-51	31-68	38-77	155-624	747-4371	185-1108	322-1016

Table 6.4. CO_2 concentration values measured at different depths in soil (from Carapezza and Granieri, 2004). J_{CO2} CM = range of CO_2 fluxes measured with the accumulation chamber method (from Carapezza and Granieri, 2004); J_{CO2} DM$^{(1)}$ = range of CO_2 fluxes measured with the dynamic method (old calibration) (from Carapezza and Granieri, 2004); J_{CO2} DM$^{(2)}$ = range of CO_2 fluxes measured with the dynamic method (new calibration); J_{CO2} $^{(3)}$ = range of CO_2 fluxes calculated using the concentration profile according to the advective–diffusion model (equation 6.9).

To understand which of the two sets of flux measurements is more accurate, we compared the flux range found by these two methods in this site with that calculated by the soil CO_2 concentration profile according to the one-dimensional advection-diffusion model expressed by equation 2.13 (Chapter 2):

$$\varphi_i(z) = -v\left(\frac{C_L}{e^{\frac{v}{D}L} - 1}\right) \tag{6.9}$$

where v is the advective flux, D is the bulk diffusion coefficient of the soil (see definition at pag. 4), L is the thickness of the soil layer and C_L is the CO_2 concentration at L depth (in this equation we have assumed that the CO_2 concentration at the soil-atmosphere surface is equal to 0 and we have used a D value of 0.04 cm^2·sec^{-1} which is reasonable for this soil with k = 61 darcys). The advective flux value v was found by fitting equation (6.9) to experimental mean soil concentration profile (Figure 6.7) measured in the site under investigation by Carapezza and Granieri (2004) (see concentration value reported in Table 6.4).

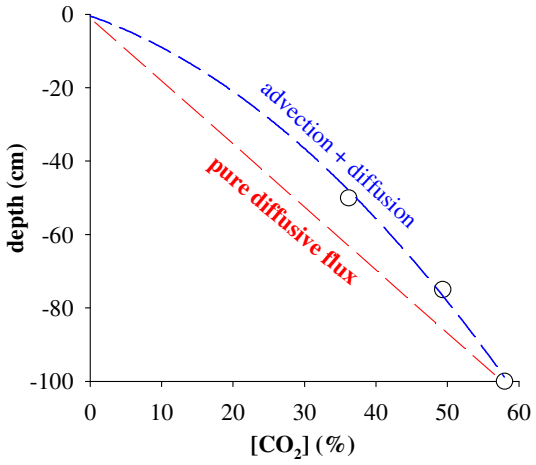

Figure 6.7. Mean soil CO_2 profile (white circles) measured in site 4. Red dashed line indicates pure diffusive CO_2 profile while the blue one indicates advective-diffusive CO_2 profile.

As shown in Table 6.4, the range of flux values obtained using the experimental soil concentration profile according to the advection-diffusion model (322-1016 g m^{-2} day^{-1}) were higher than those of the accumulation chamber measurements (155-624 g m^{-2} day^{-1}). Quite the reverse, this range of fluxes seems to be more in agreement with the dynamic fluxes (185-1108 g m^{-2} day^{-1}) calculated using the new empirical equation (equation (4.9)).

In conclusion, the results shown here suggest that, although significant differences were found in several cases between the absolute flux values measured in the field with the dynamic and accumulation method, a reasonable agreement (R = 0.82) does exist between these pairs of data.

Nevertheless, several other aspects characterize the flux measurements performed with these two methods. The apparatus employed to measure soil CO_2 flux with the dynamic chamber method is more complex and more expensive than that used to measure flux with the dynamic method. In particular, a complex system of levers and motors (Figure 6.8) is used to move the chamber away from the soil area being measured, to ensure that the CO_2 concentration inside the chamber at t = 0 is close to zero. This system is subject to frequent jamming and needs continuous, expensive maintenance.

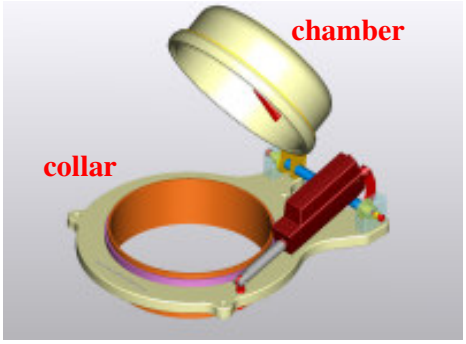

Figure 6.8. Accumulation chamber unit employed in the Continuous Monitoring Station manufactured by the West System S.R.L.

Furthermore, a substantial difference exists between these methods: dynamic flux measurements are taken at a depth of 45 cm in the soil, while the accumulation measurements are taken at the soil-air interface. As shown by Fukuda (1955), the influence of some atmospheric phenomena on soil CO_2 flux, such as the effect of gusts of wind and that induced by atmospheric pressure fluctuations (barometric pumping), decreases with depth. Therefore, accumulation measurements taken at the soil-air interface are generally more dependent on

atmospheric conditions (Hinkle 1990; Klusman 1993) than flux measurements performed with the dynamic method. Often, in the presence of strong gusts of wind, the assessment of the tangent at $t = 0$ when measuring soil CO_2 flux with the accumulation method can be more difficult and therefore the measurements may not, in some cases, be reliable.

Chapter 7

Field Applications

Several field applications of the dynamic method have been reported in literature since 1988 (Badalamenti et al. 1988; Diliberto et al. 2002; De Gregorio et al. 2002; Giammanco et al. 1995, 1998). This method has been principally applied to the monitoring of volcanic activity and to the study of the relationship between soil degassing and tectonics. Since 1988 the method has been officially employed in the discrete monitoring of the volcanic activity of Mt. Etna (Sicily) and Vulcano. Moreover, since 1998 this method has been used to continuously monitor Mt. Etna (Gurrieri and Giudice, 2004).

In this chapter we will discuss the results of some soil CO_2 surveys performed with the dynamic method, in volcanic and seismic areas of Sicily (Italy). The first area is the island of Vulcano, an active volcano which last erupted in 1888-90, and, at present, is characterized by solphataric activity. The second area is the promontory of Capo Calavà (north eastern Sicily), an active seismic area.

7.1 Vulcano Island

7.1.1 influence of the shallow soil permeability on soil degassing

Two surveys of both soil CO_2 flux and soil permeability were performed in Vulcano (Aeolian archipelago, Italy) in April and June 2003. The explored area (Fig. 7.1.) covers about 2.2 square kilometers and is located on the western flank of La Fossa cone, between the isthmus of Vulcanello (to the north) and Grotta dei Palizzi (to the south).

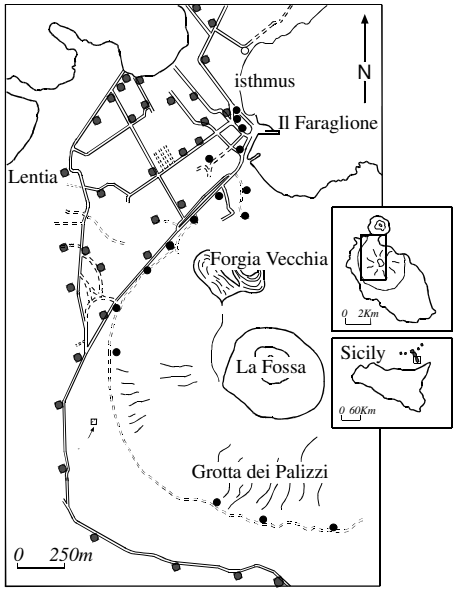

Figure 7.1. Location of the surveyed area in Vulcano. Solid circles indicate the location of the measurement sites.

Soil permeability and flux measurements were performed in the same 48 fixed measurement sites in which soil CO_2 flux measurements are periodically carried out for volcanic surveillance purposes (Diliberto et al., 2002). The permeability was measured *in situ* by the radial advection method described in the previous Chapter. The flux measurements were taken from exactly the same sites as the permeability measurements using the dynamic method discussed in Chapter 4, operating at constant pumping flux of 0.8 l min^{-1}, which represents a good compromise between speed of measurement and influence of soil permeability (see pag. 26). In keeping with this method the exhaled flux was determined introducing into equation (4.9) the dynamic concentration and the permeability values measured in each site of the selected measurement grid. The results of these investigations are reported in Table 7.1. The measured permeability and flux values range between 5 and 74 darcys and 2 and 2823 g m^{-2} day^{-1}, respectively.

The (*a*) and (*b*) maps of the Figure 7.2 show the spatial distribution of soil permeability measured in the surveyed area in April and June 2003, respectively; in general, the most permeable areas are located in the southernmost part of the area (Figure 7.2, Grotta dei Palizzi) under investigation. Other deposits characterized by high permeability (> 60 darcys) are located on the isthmus, the Forgia Vecchia and on the areas of the Il Faraglione, and the Lentia. In general, these soils are essentially composed of pyroclastic debris devoid of any vegetation. The lowest permeability values (5-30 darcys) were found south of the Lentia area where the soils are characterized by a higher degree of cohesion often covered with vegetation.

The Figure 7.2 also reports the flux maps (*c* and *d*) showing the spatial distribution of the CO_2 emissions from the soil. For all field measurements, the highest CO_2 fluxes were located in the areas of Grotta dei Palizzi and Faraglione, while lower fluxes were recorded in the areas to the north of the Grotta dei Palizzi and the area adjacent to the Lentia Complex. This distribution seems to reflect regional tectonic structures in the area. The highest exhaling areas are aligned along a N-S direction, together with the main fumarolic areas of La Fossa crater, the Forgia Vecchia craters, the eastern beach of the isthmus, and the Il Faraglione (Ventura et al., 1999).

Comparing flux and permeability maps it results that high soil CO_2 fluxes were found in areas with low as well as high permeability values. Furthermore as shown in the Figure 7.3, very low numerical correlation was found between the permeability values measured in each period and the corresponding values of soil CO_2 flux.

n.	C_d (ppm) April 2003	C_d (ppm) June 2003	k (darcys) April 2003	k (darcys) June 2003	J_{CO2} (g m^{-2}day^{-1}) April 2003	J_{CO2} (g m^{-2}day^{-1}) June 2003
2	11000	4000	49.4	47.1	200	74
3	7000	1600	33.2	21.1	137	33
4	141960	29920	44.0	60.8	2823	524
6	100	100	24.8	28.7	2	2
7	600	800	25.7	35	12	15
8	350	200	39.7	65.5	7	3
9	1500	800	70.1	71	25	14
10	800	750	24.1	35	16	15
11	1000	700	31.9	28.7	20	14
12	12000	11000	22.0	44.6	249	204
13	77740	34440	44.0	49.9	1476	629
14	300	7900	6.3	27.7	7	159
15	37325	4200	44.0	44.6	698	78
16	1000	700	52.5	65.5	18	12
17	600	400	18.8	28.7	13	8
18	600	450	20.8	23.6	13	9
19	1500	7000	52.5	60.8	27	122
20	1200	1200	49.4	35	22	23
21	1500	1900	41.8	71	28	32
22	700	200	19.7	25.9	15	4
23	1500	1200	44.0	56.7	28	21
24	600	400	25.7	33.6	12	8
26	500	250	16.7	25.1	11	5
27	500	300	17.1	21.1	11	6
28	600	400	20.8	25.1	13	8
29	1100	900	24.8	36.6	22	17
30	600	450	12.5	14.9	13	10
32	300	1200	26.3	22.9	6	25
33	500	600	60.4	73.4	9	10
34	150	100	28.4	19	3	2
35	3200	3200	17.5	60.8	69	56
36	1000	1100	39.7	28.7	19	22
38	400	300	24.1	18.5	8	6
39	1400	1500	63.4	71	24	25
41	2100	2250	60.1	60.8	37	39
42	400	850	60.1	31	7	17
43	600	200	25.7	22.3	12	4
44	100	700	14.2	17.3	2	15
45	1400	800	60.1	40.2	25	15
46	1300	1350	20.8	40.2	27	26
47	500	700	31.9	36.6	10	13
48	23660	68000	60.1	60.8	415	1212
49	1600	8500	18.4	21.1	34	178
80	100	200	16.4	19	2	4
81	500	500	17.1	21.1	11	10
82	1300	1350	49.3	71	24	23
83	650	500	26.6	31	13	10
84	800	350	19.2	26.8	17	7
85	300	400	20.8	56.7	6	7
86	1000	1700	17.9	21.1	21	36
Mean	6949	4171	33.0	39.1	134	76

Table 7.1. C_d, permeability and flux values measured in the surveyed area of Vulcano in April and June 2003; the flux values were obtained according to equation (4.9). The permeability values are shown in the second and third columns of this table.

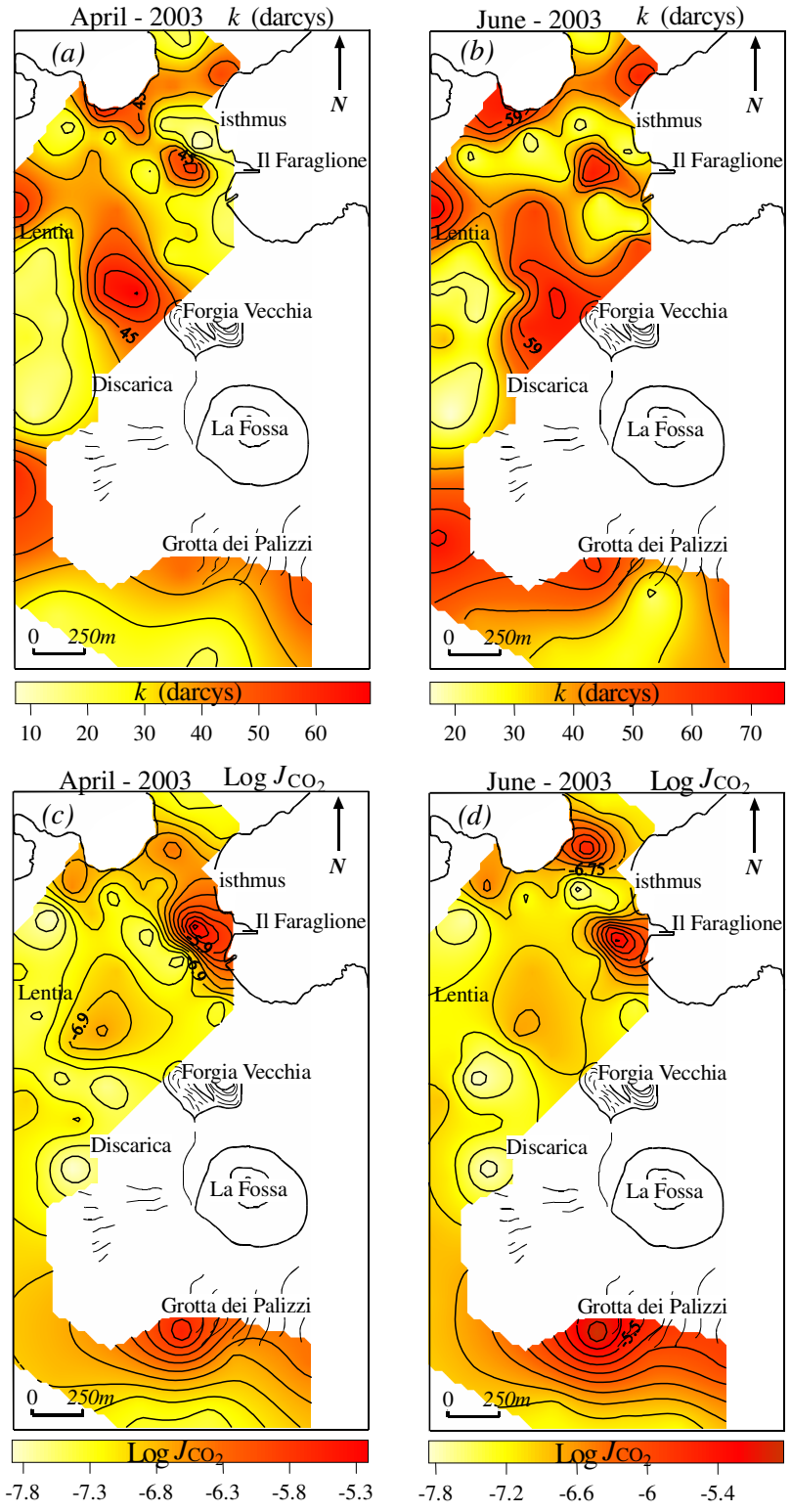

Figure 7.2. Permeability (*a* and *b*) and flux maps (*c* and *d*) of the surveyed area of Vulcano.

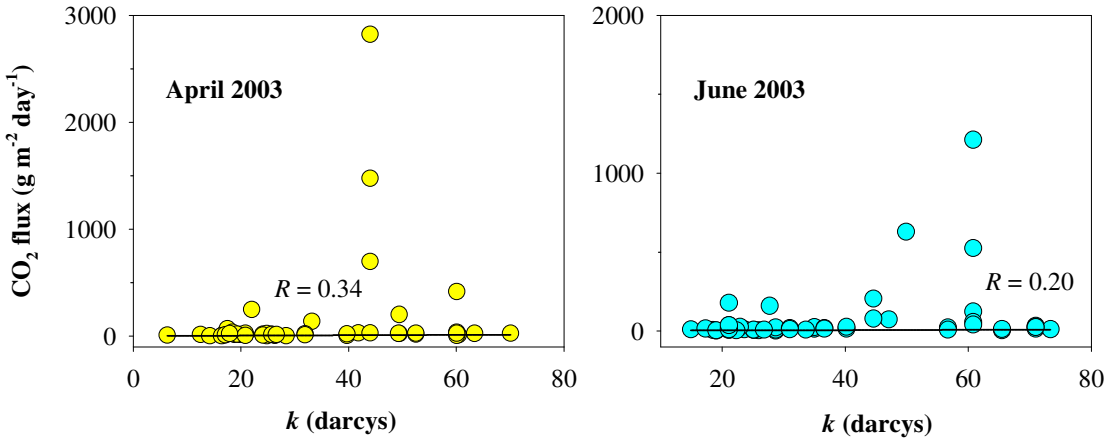

Figure 7.3. Plots of CO_2 flux versus *k,* for each field measurement. A low correlation between measured flux and soil permeability was found.

As indicated by these results, the permeability of the upper soil layers seems to have a secondary influence on the spatial distribution of diffuse soil gas emissions. The permeability of the upper soil could only slightly influence the shape and size of the soil degassing anomalies.

7.1.1. Evaluation of the influence of soil permeability on the flux measurements performed in the field using the dynamic method

In Chapter 4 we have shown that accurate measuring of soil CO_2 flux using the dynamic method can be effected according to equation (4.9), by measuring soil permeability in each measurement site and introducing these values into equation (4.9). Consequently, a new method of measuring *in situ* soil permeability was developed (Chapter 5). In this paragraph we would evaluate the error committed when soil CO_2 flux is calculated for each site using the average permeability value of the surveyed area. To this end, in columns four and five of Table 7.2 we have shown the CO_2 flux values calculated for each site according to equation (4.9) and for a constant permeability equal to the mean value found in the selected area for each permeability survey (32 and 39 darcys for the April and June surveys, respectively). Furthermore, in the last two columns of the same table we have shown the difference (δ), expressed as a percentage, between these values and those (second and third columns) obtained considering each permeability value measured for each site in the surveyed area (fourth and fifth columns of Table 7.1).

n.	J_{CO2} (g m^{-2}day^{-1}) April 2003	J_{CO2} (g m^{-2}day^{-1}) June 2003	J_{CO2} (g m^{-2}day^{-1}) k = 33 darcys April 2003	J_{CO2} (g m^{-2}day^{-1}) k = 39 darcys June 2003	δ (%) April 2003	δ (%) June 2003
2	200	74	215	78	-7	-5
3	137	33	137	31	0	6
4	2823	524	2928	587	-4	-11
6	2	2	2	2	0	0
7	12	15	12	16	0	-6
8	7	3	7	4	0	-29
9	25	14	29	16	-15	-13
10	16	15	16	15	0	0
11	20	14	20	14	0	0
12	249	204	235	215	6	-5
13	1476	629	1545	676	-5	-7
14	7	159	6	155	15	3
15	698	78	733	82	-5	-5
16	18	12	20	14	-11	-15
17	13	8	12	8	8	0
18	13	9	12	9	8	0
19	27	122	29	137	-7	-12
20	22	23	23	23	-4	0
21	28	32	29	37	-4	-14
22	15	4	14	4	7	0
23	28	21	29	23	-4	-9
24	12	8	12	8	0	0
26	11	5	10	5	10	0
27	11	6	10	6	10	0
28	13	8	12	8	8	0
29	22	17	22	18	0	-6
30	13	10	12	9	8	11
32	6	25	6	23	0	8
33	9	10	10	12	-11	-18
34	3	2	3	2	0	0
35	69	56	63	63	9	-12
36	19	22	20	22	-5	0
38	8	6	8	6	0	0
39	24	25	27	29	-12	-15
41	37	39	41	44	-10	-12
42	7	17	8	17	-13	0
43	12	4	12	4	0	0
44	2	15	2	14	0	7
45	25	15	27	16	-8	-6
46	27	26	25	26	8	0
47	10	13	10	14	0	-7
48	415	1212	463	1346	-11	-10
49	34	178	31	166	9	7
80	2	4	2	4	0	0
81	11	10	10	10	10	0
82	24	23	25	26	-4	-12
83	13	10	13	10	0	0
84	17	7	16	7	6	0
85	6	7	6	8	0	-13
86	21	36	20	33	5	9
Mean	134	76	139	82	4	7

Table 7.2. Soil CO_2 flux values measured in the surveyed area in April and June 2003; flux values shown in the second and third columns were obtained by C_d and permeability measurements reported in Table 7.1, according to equation (4.9); flux values shown in the fourth and fifth columns were obtained according to equation (4.9) and for a constant permeability of 33 and 39 darcys (for April and June surveys, respectively). Furthermore in last the two columns of the same table the difference, expressed as a percentage of these values and those shown in the second and third columns, are reported.

As shown in this Table, the δ value results, for all the field measurements, are always lower than 20 %, with a mean value equal to 7 %. This means that the mean error made using the dynamic method, if we do not take into consideration the spatial variability of the soil permeability found in the surveyed area, is on average equal to 7%.

Other important considerations can be made by observing Figure 7.4, where two log-normal probability plots relative to the June survey are shown. In particular, (a) plot refers to the flux values (third column of Table 7.2) obtained using the soil permeability measured in each site while the (b) plot refers to the flux values obtained using a mean permeability value of 39 darcys for each measurement site. Very similar statistical distributions can be recognized for both data sets.

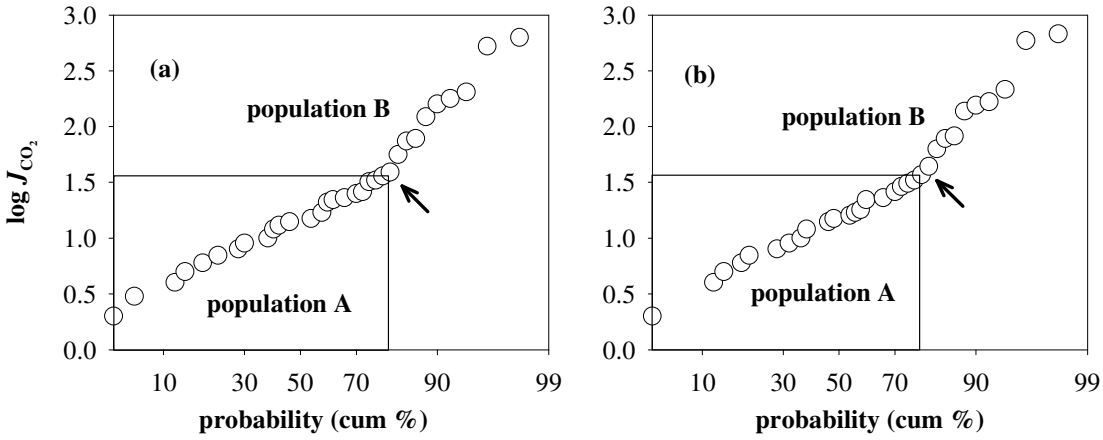

Figure 7.4. Log-normal probability plots of the soil CO_2 fluxes relative to the June survey: (a) plot refers to flux values (third column of Table 4.2) obtained considering the soil permeability measured in each site, while the (b) plot refers to the flux values obtained considering sites a mean permeability value of 39 darcys for each measurement.

As discussed by Sinclair (1974), in a log-normal probability plot, changes in slope are indicative of separate log-normally distributed populations of data. In each plot of Figure 7.4 an inflection point at 72% cumulative percentile can be recognized. These points allow us to distinguish the presence of 72% of the background population in all cases (population A) and 28% of anomalous population (population B).

In Figure 7.5 we have also shown soil CO_2 flux maps (*e*) and (*f*) of the investigated area obtained considering the mean permeability values found in the selected area in the April and June surveys respectively. By comparing these maps with the flux maps (*c* and *d*) reported in Figure 7.2, no significant differences can be seen. Therefore, the results shown here highlight that, when CO_2 flux is measured using the dynamic method as described in Chapter 4 (with

the discussed measurement probe and with a pumping flux of 0.8 l min^{-1}), very small errors are committed if we do not take into consideration the spatial variability of the soil permeability found in the selected area. Furthermore, in all cases these errors are not high enough to cause significant changes either in the statistical or in the spatial distribution of the calculated soil CO_2 fluxes.

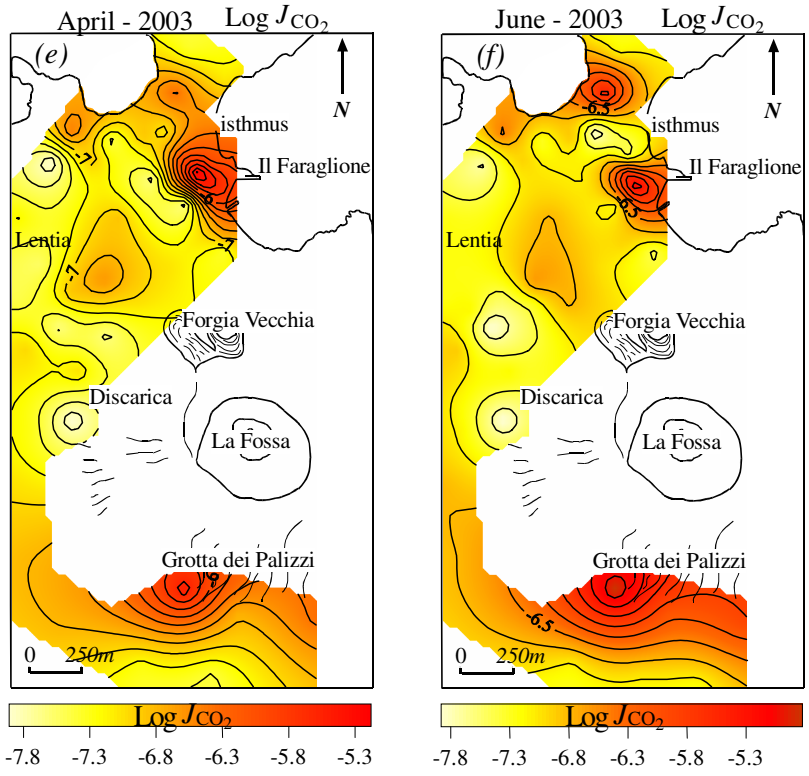

Figure 7.5. Soil CO_2 flux maps obtained with the mean permeability values found in the selected area in the April and June surveys respectively

7.2. Capo Calavà

Over the past years, several studies on diffuse soil degassing carried out in volcanic and geothermal areas have revealed the existence of a strict correlation between the location of soil gas anomalies and the occurrence of active structures (Badalamenti et al., 1988; Baubron et al., 1996; Diliberto et al., 2002; Giammanco et al., 1998; Klusman 1993). These are described as highly permeable channels able to drive deep gases towards the surface. Furthermore, soil degassing can also be used to detect tectonic structures in areas where the lack of sufficient field evidence does not allow them to be identified (Ciotoli et al., 1999).

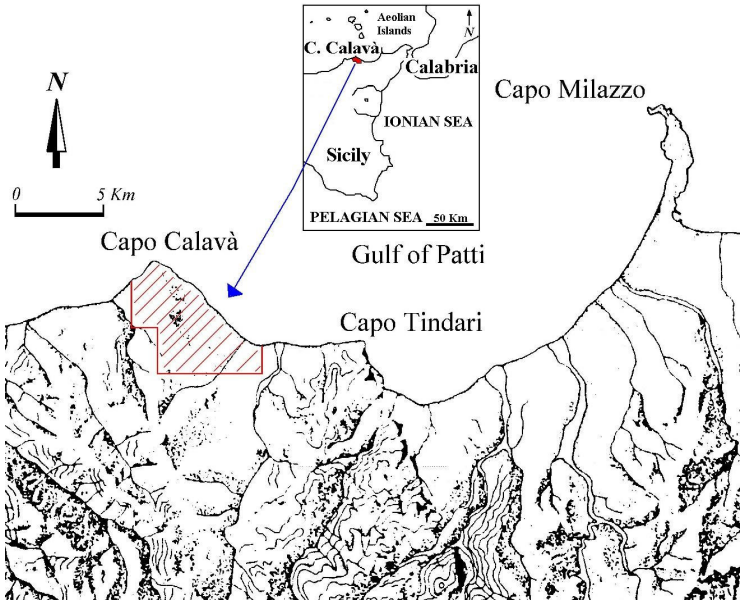

Figure 7.6. Morphological expression of Aeolian-Maltese fault system (modified from Lanzafame et al. 1997). The surveyed area is indicated in red.

The surveyed area is located on the north east coast of Sicily in the Gulf of Patti, close to the Aeolian archipelago (Figure 7.6). As documented by Azzaro et al. (2000) this is an active seismic area related to the presence of faults that are aligned from NNW-SSE to NW-SE. To study the relationships between soil degassing and tectonics, four soil CO_2 flux surveys were performed in this area in October and November 2003 and in February and March 2004. The locations of the measurement sites defined a grid of 430 points (Figure 7.7) covering an area of about 12 square kilometers, that includes the towns of Gioiosa Marea, S. Giorgio, Patti and Sorrentini (on the South) (Figure 7.7). The steep morphology and the wide urbanization of the surveyed area in many cases did not allow for a rigorous uniformity of the measurement grid. The study of the relationships between soil degassing and tectonics was

accomplished by examining the spatial distribution of the measured soil CO_2 fluxes in the investigated area and by comparing it with the tectonic map of the area.

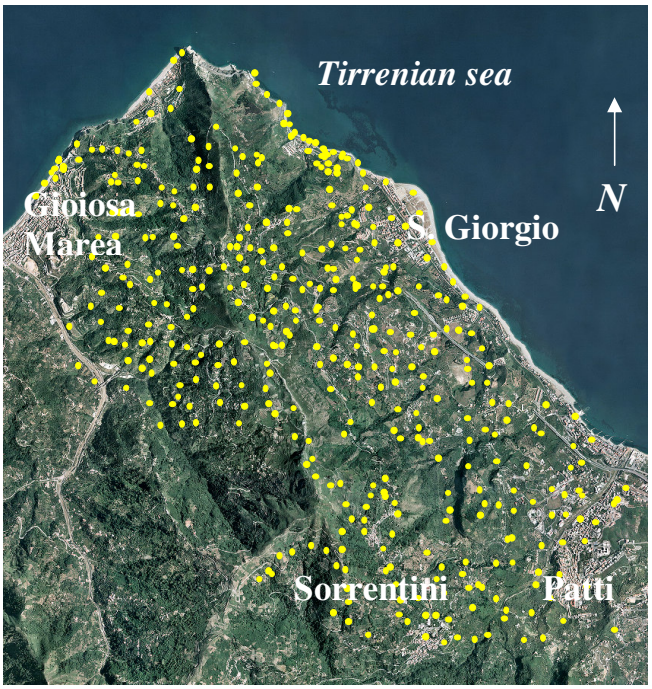

Figura 7.7. Location of measurement sites.

The results of the four field measurements effected in this area are shown in Tables 7.3 and 7.4 (reported at the end of the Chapter). The first two surveys were performed in October and in November 2003, after a long dry period which had affected Sicily since the previous summer, whereas the last two surveys were performed in February and March 2004, during the wettest period. As shown by the results of the C_d measurements repeated in two different periods (Table 7.5), the C_d values obtained in February and March 2004 are sensibly lower than those measured in October and in November 2003.

site	C_d (ppm) (October 2003)	C_d (ppm) (February 2004)
59	2200	300
60	15000	3000
96	48000	4000
97	28000	7000
104	17000	1900
109	15000	15000
119	11000	1000

Table 7.5. Comparison between C_d values obtained in the same sites in two different seasons.

According to the results shown in a previous paper (Camarda et al., submitted), this significant decrease is probably to be referred to the abundant rainfall that fell in Sicily before and during this period.

7.2.1 Results

Figure 7.8 shows the log-normal probability plot of the flux data measured in the area under investigation. As discussed by Sinclair (1974), in this type of plot changes in slope are indicative of separate population of data. In the graph given in Figure 7.8 two inflection points at 20 and 97 cumulative percentile can be recognized. These points allowed us to distinguish the presence of three populations of data with log-normal distribution: a low flux population *A*, representing 20% of the entire data set; an intermediate flux population *B*, and a high flux population *C,* which are respectively 77% and 3% of the entire data set.

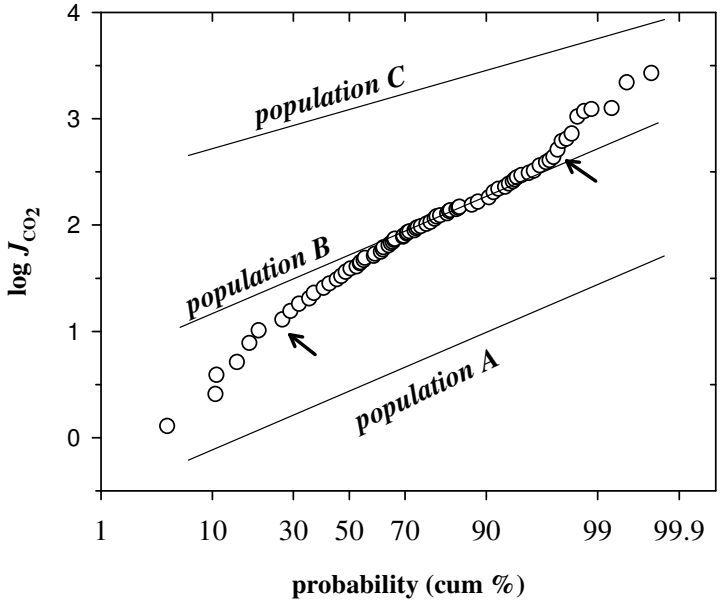

Figure 7.8. Log–normal probability plot of log J_{CO2} measured in the surveyed area. Inflection points (black arrows) indicate the occurrence of three different flux populations in the surveyed area.

The flux values of population *A* range between 1-10 g m^{-2} day^{-1} which are consistent with those typically reported for soil respiration (3.6 - 13.7 g m^{-2} day^{-1}; Monteith et al., 1964; 6 - 11 Brown et al. 1971). On the contrary, higher fluxes ranging between 10 and 360 g m^{-2} day^{-1} defined the second population. These values can be explained as a mixing, in different proportions, of superficial CO_2 produced by biological activity and a deeper CO_2 which

reached the surface through the abundant structural discontinuities recognized in the surveyed area. Flux values higher than 360 g m^{-2} day^{-1} (= $2.1 \cdot 10^{-6}$ $m^3m^{-2}s^{-1}$) up to 11400 g m^{-2} D^{-1} (= $5.4 \cdot 10^{-5}$ $m^3m^{-2}s^{-1}$) characterize the anomalous population directly related to the occurrence of faults.

7.2.2 Relationship between soil degassing and tectonics

As discussed before, the surveyed area is characterized by the occurrence of recent seismic events (Azzaro et al. 2000) related to the presence of faults that are aligned from NNW-SSE to NW-SE. The focal mechanism of the last important earthquake, which occurred in April 1978 (M = 5.5, Barbano et al. 1978), indicated a normal right lateral motion on a plane aligned NNW-SSE. The most recent data (Neri et al., 1991) indicate that in 1985-1989 the seismic activity was concentrated along a NNW-SSE trend. According to Lanzafame and Bousquet (1997) these faults belong to a greater system named "Aeolian Maltese fault system" (Figure 7.9).

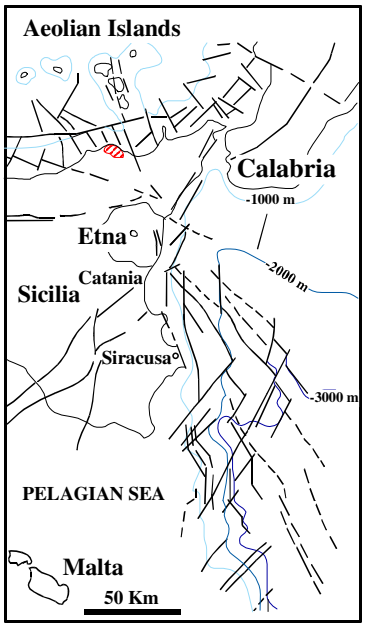

Figure 7.9. The Aeolian-Maltese fault system (modified from Lanzafame et al. 1997). The faults of the Maltese escarpment are from Cesaro et al. (1984), and the faults of the Tyrrhenian margin are from Barone et al. (1982). The surveyed area is indicated in red.

This includes the faults of the Maltese and Hyblean–Maltese submarine escarpment, that traverses north-east Sicily and the southern Tyrrhenian Sea, reaching the Aeolian Islands (Vulcano, Lipari and Salina). The best known of these faults starts at Capo Tindari (Figure 7.6) and extends to the island of Vulcano cutting recent sediments on the sea floor (Ghisetti 1979). The numerous earthquakes which occurred in the past in the ancient village of Gioiosa

Vecchia (see geological map in Figure 7.10 at Pag. 67), located at about 800 m a.s.l., are also ascribed to the activity of these faults. This village was entirely destroyed by the earthquake that occurred in 1783 (Ferla, 1985).

So as to easily visualize the spatial variability of the measured soil CO2 in the surveyed area, a contour plot was made using commercial software (SURFER). The contour was generated from the logarithm values of the flux data expressed in g m-2 day-1 using the kriging algorithm.

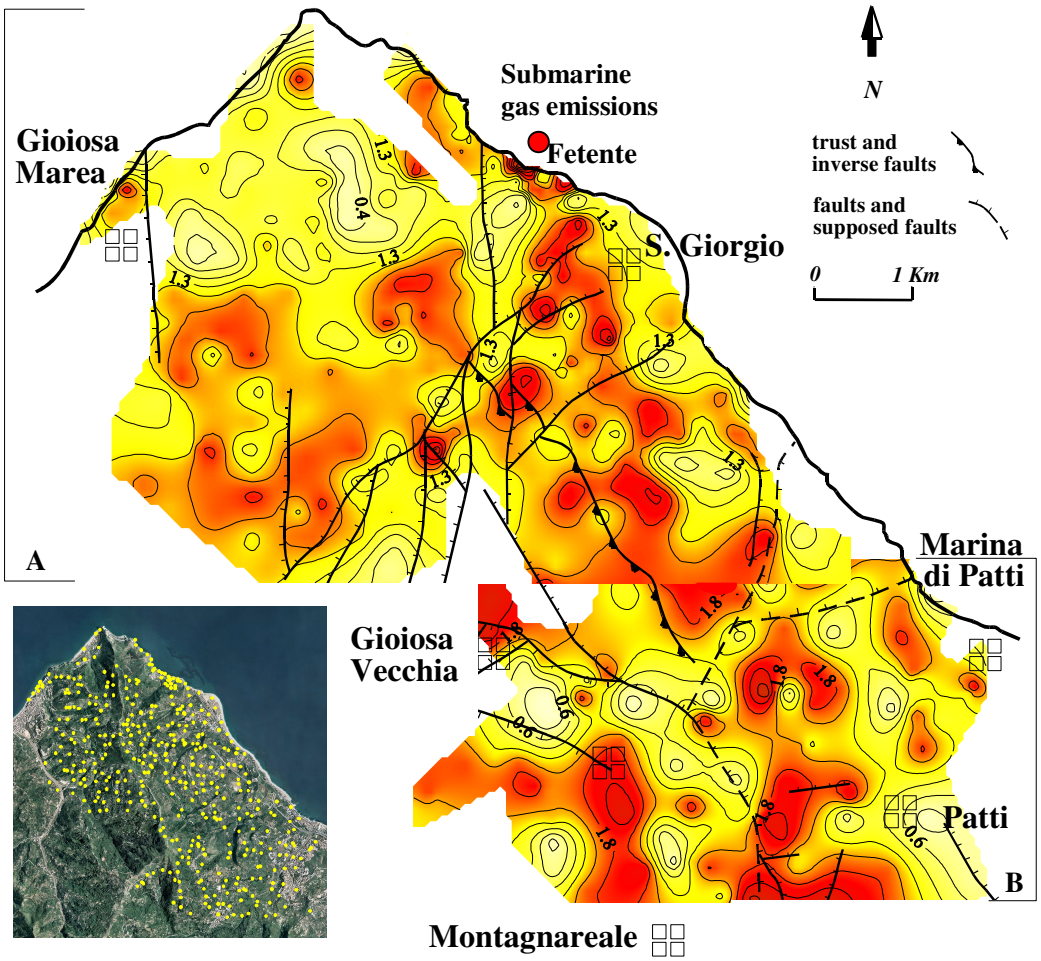

Figure 7.11. Flux map of the investigated area. Map A was obtained by flux measurements performed in October and November 2003**.** Map B was obtained by flux measurements performed in February and March 2004**.**

In particular, the map shown in Figure 7.11 was obtained by combining the contour generated from the data collected in October and November 2003 (map A) and another (map B) generated by the only measurements performed in February and March 2004. We prefer to

distinguish the data collected in the contour elaboration, in order to highlight the smaller flux anomalies found in the last two surveys. In other words, a contour plot generated from the whole data set cannot clearly highlight the smaller but important flux anomalies found in the second data set.

As shown in the map in Figure 7.11, CO_2 flux is characterized by wide spatial variability with differences up to two orders of magnitude within distances of 250 m. Flux anomalies are well aligned along the NNW/SSE direction in the eastern part of the surveyed promontory. These anomalies are likely related to the occurrence of a fault system on the NNW/SSE direction which agrees with the main orientation of the Aeolian Maltese System. To enhance this hypothesis, five CO_2 flux profiles were made across this supposed tectonic structure (Figure 7.12). As shown by profile A-B, the CO_2 fluxes measured along this direction are always higher than the range of soil respiration rate (yellow area), furthermore they change from medium to high anomalous fluxes (orange and red area). These high fluxes suggest that there is an uninterrupted presence of faults that fall along this direction. Quite the opposite, in the profiles that are perpendicular (C-D, E-F and G-H) and transversal (L-M) to this direction, CO_2 fluxes change from the range of soil respiration to medium anomalous fluxes. In these cases, different flux anomalies can be distinguished (positive peaks). This suggests that along these profiles the recognized tectonic structures do not fall along the same direction of the examined profiles. Furthermore, the existence of a fault system striking NNW/SSE is in agreement with geological data (Ferla et al. 1985), which postulate the presence of an echelon fault system along this direction to explain the high apparent thickness (500 m) of the "Verrucano" sequences that outcrop in this area (see geological map in Figure 7.10 at Pag. 69). Furthermore, the recent focal mechanisms suggest that the elevation of the area of Gioiosa Vecchia (Mt. Guardia, 820 m a.s.l.) in respect of the plain of Patti can be explained by invoking normal right lateral motions along these faults.

Other important considerations on the relationship between soil gas anomalies and tectonics can be made by observing Figure 7.12. We can see that although in some cases the recognized flux anomalies are well related to the presence of mapped faults, in several other cases they are found in areas where no known faults are mapped. For example, strong anomalies are shown in the C-D, E-F and G-H profiles, in correspondence with the occurrence of supposed NNW/SSE structures (shown by the pink boxes). Only in the C-D profile is this anomalous area related to a known fault striking NE-SW, while in the other cases no known faults have been found. This suggests that soil flux surveys can highlight the presence of buried structures which are not easily recognized on the basis of the simple superficial features.

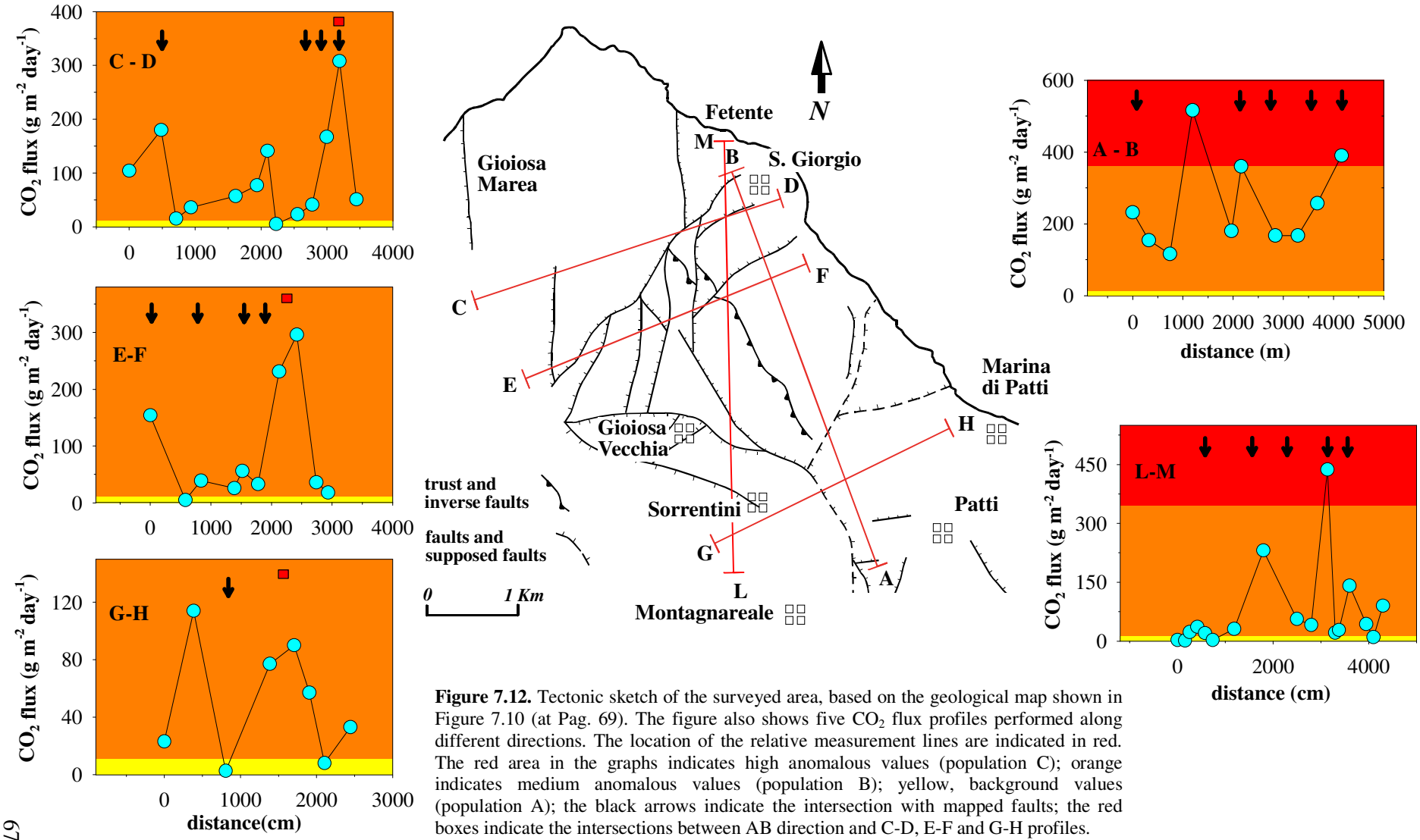

Figure 7.12. Tectonic sketch of the surveyed area, based on the geological map shown in Figure 7.10 (at Pag. 69). The figure also shows five CO_2 flux profiles performed along different directions. The location of the relative measurement lines are indicated in red. The red area in the graphs indicates high anomalous values (population C); orange indicates medium anomalous values (population B); yellow, background values (population A); the black arrows indicate the intersection with mapped faults; the red boxes indicate the intersections between AB direction and C-D, E-F and G-H profiles.

67

Moreover, as shown in Figure 7.12 and in the flux map of Figure 7.11, a good portion of the know structures are not related to the presence of detected anomalies and therefore they are not “degassing" (as defined by Giammanco et al., 1998). These are probably older structures obstructed by the occurrences of mineralizations which have sensibly decreased their permeability. Only the recent active structure subject to a continuous strain maintains a high permeability and it is “degassing”. The main NNW-SSE orientation of the flux anomalies recognized in this area seems to be interrupted sequentially along its extension by a secondary group of anomalies having a NE-SW direction. Although these structures are well known (Ferla, 1985), their evidence on the base of the spatial distribution of soil gas emissions are actually not clear. Furthermore, the high flux anomaly recognized in the south-west sector of the surveyed area does not have a definite structural sense.

In conclusion, the soil flux measurements performed in the investigated area highlight the presence, in the eastern sector, of an important tectonic structure having a NNW-SSE direction. As shown by the comparison of the flux map with the geological map of the surveyed area (Figures 6.5 and 6.6), the recognized NNW-SSE structure is very deep and recent and affects both the Paleozoic metamorphic basement (Unità dell’Aspromonte) and the most recent sediments that outcrop in the area (outcropping close to Marina di Patti). Moreover, the presence of evident submarine gas emissions close to the beach of Fetente shows how this structure extends towards the sea.

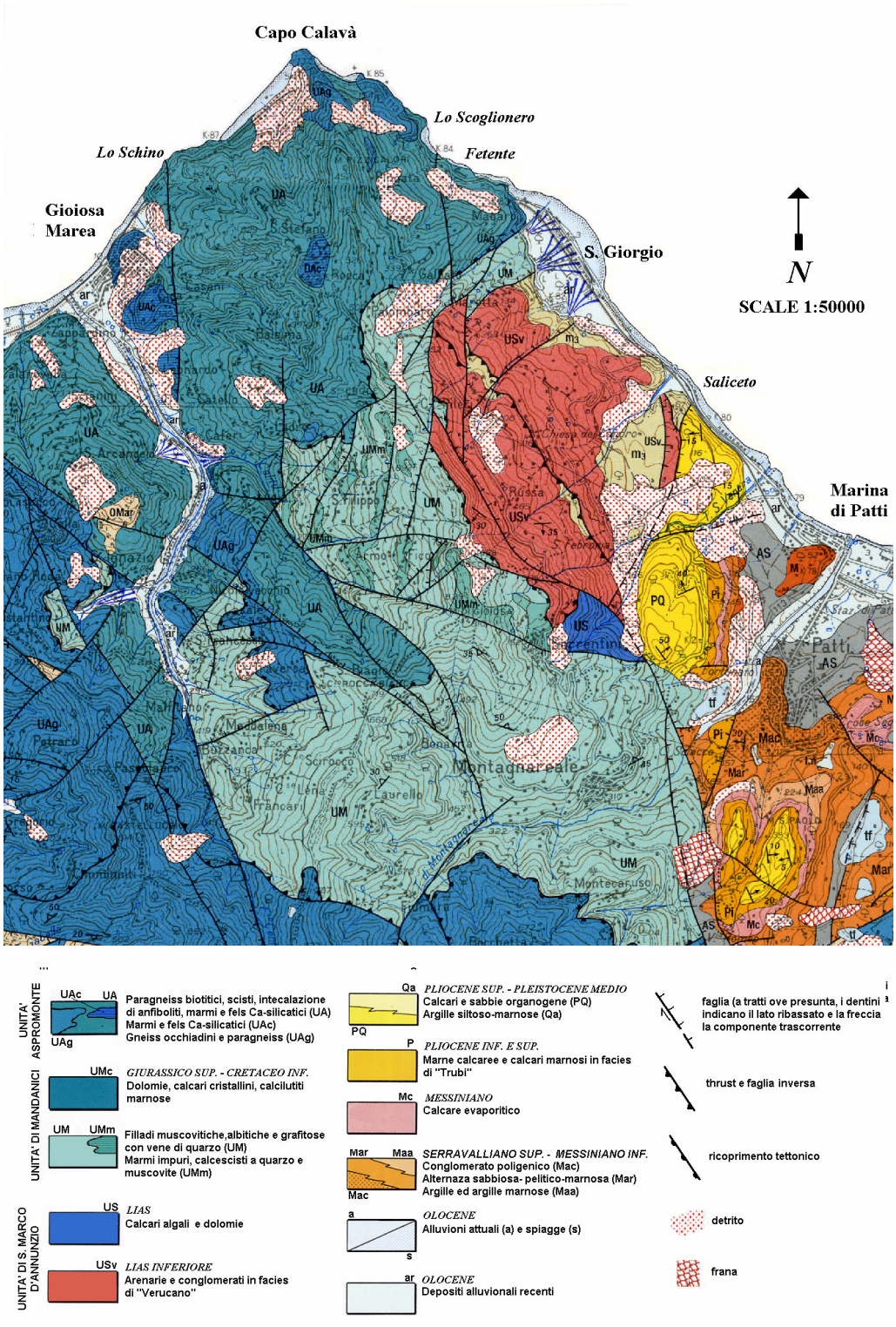

Figure 7.10. Geological map of the surveyed area (modified from Lentini et al. 1999). Several geological contexts can be recognized in the investigated area. This area is situated in the northern sector of the Peloritani Mountains and is characterized by the outcroppings of the Paleozoic crystalline metamorphic basement (Unità dell'Aspromonte). A Triassic sequence in the "Verrucano" facies (conglomerates and arenites) outcrops in a tectonic window in the east sector of the area. More recent terrains (Pleistocene–Olocene) outcrop close to Marina di Patti.

7.2.3 Gas geochemistry

In order to explain the origin of the fluids which are discharged in the surveyed promontory, some soil gas samples were collected in the highest anomalous area. These gases were sampled at a depth of 50 cm through a 5-mm-ID Teflon tube connected to a syringe and then stored in glass flasks. Also, the submarine gases of Fetente were collected and analyzed. The chemical composition of the gases was determined by gas chromatography (Perkin Elmer Mod. 8500 instrument), while the isotopic composition of the carbon was measured by direct injection of CO_2 into the input loop of a Finnigan Mat Delta Plus Mass Spectrometer. The obtained results are shown in Table 7.6.

	sample	date	He (ppm)	O_2 (%)	N_2 (%)	CO (ppm)	CH_4 (pmm)	CO_2 (%)	$\delta^{13}C$ (CO_2)	CO_2 flux (g m^{-2} day^{-1})	CO_2 flux (g m^{-2} day^{-1})
	P66	27/10/03	≤ 5	20.3	79.1	6.26	1.35	0.9	n.d	180	14
	P104	28/10/03	≤ 5	14.2	79.4	0.91	8.47	6.4	-26.9	438	97
	Schino	28/10/03	≤ 5	18.2	79.5	0.5	28.0	2.2	-24.8	1,056	33
	P252	06/11/03	≤ 5	17.9	78.9	2.4	≤ 1	3.3	-22.7	644	50
	P300	17/02/04	6	20.3	78.8	7.0	2.0	1.1	-20.9	180	17
	P297	17/02/04	5	18.6	78.8	10.0	≤ 1	2.6	-22.6	180	39
	P323	18/02/04	6	16.8	78.2	5.0	0.7	5.0	-20.8	309	76
	P327	18/02/04	7	18.7	78.2	7.0	1.0	3.0	-19.0	232	45
	P414	10/03/04	≤ 5	18.9	79.3	2.0	≤ 1	2.1	n.d	77	32
Fetente	**GM 46a**	03/10/03	≤ 5	10.6	47.3	4.1	1.85	42.2	4.2	11,416	
	GM46b	19/02/04	7	5.19	29.2	1.0	1.0	65.9	3.7	14,300	
	Submarine emissions	05/12/03	17.9	0.2	1.2	4.5	6153	97.8	3.6	n.d	

Table 7.6. Chemical and carbon isotopic compositions of the collected gas samples. In the last column the values of CO_2 fluxes are also reported.

As shown in the triangular plot of Figure 7.13, the samples arrange themselves along a line of mixing between atmospheric gases and a CO_2- rich member. The N_2/O_2 ratio in some of the samples is sensibly higher than the atmospheric ratio. This can be explained by invoking a consumption of O_2 throughduring oxidation of the organic matter present in the soil. Moreover, two subsets of samples can be recognized, one rich in CO_2 (*A*) and another, poor in CO_2er one (*B*). The first subset is composed only of submarine gases and soil samples collected in the highest anomalous area (the beach of Fetente).

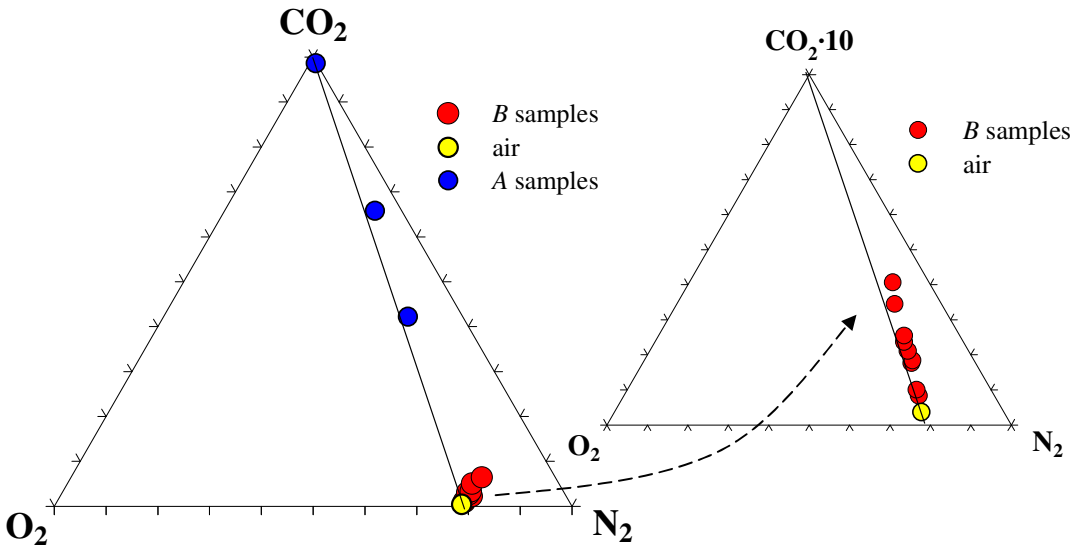

Figure 7.13. CO_2-O_2-N_2 ternary plot of sampled gases. The dotted lines show mixing between air and a CO_2 rich member.

The isotopic signature of the CO_2 of these gases ranges between + 4.2 and + 3.7 ‰ relative to PDB. These high positive values of $\delta^{13}C(CO_2)$ of course allow us to exclude an organic origin of the carbon dioxide present in these gases. However, high positive values of $\delta^{13}C(CO_2)$ like these are very uncommon in literature and are only found in the calcite of carbonatic rocks. Petrological data available for this area indicate the occurrence of different layers of marbles in the metamorphic sequences that outcrop there (Unità di Mandanici and Unità di Aspromonte). Furthermore, these studies have shown that the $\delta^{13}C$ values measured in the carbon of these marbles ranges between +2 and +4.7 ‰ and has a mean value of +4 ‰ (Censi et al. 1982). These results suggest that the gases discharged in the Fetente area may have originated from a hydrothermal system located in the metamorphic basement and fed by deeper gases of mantle origin. In this system the interaction between fluids and marbles could remobilise the heavy carbon contained in these rocks and thereby modify the isotopic composition of the mantle gases (ranging between – 2 and -0.5 ‰ in the Mediterranean area) (Capasso et al., 1997) towards more positive values.

On the contrary, the second subset of data is characterized by lower CO_2 concentrations ranging between 0.9 and 7%, with $\delta^{13}C(CO_2)$ values ranging between -19 and -27 ‰ (see Table 7.6). These negative values of the $\delta^{13}C(CO_2)$ suggest a main organic origin of the carbon dioxide contained in these gases even if, as previously discussed, the high CO_2 flux measured in these sites (which are up to two orders of magnitude, than those typically reported

for soil respiration) suggest a deeper origin. Table 7.6 reports also the CO_2 flux calculated in accord to Fick's first law (equation 2.1) and introducing into it the CO_2 concentration values measured in the soil gases samples (eighth column of Table 7.6). For this calculation a high values of bulk diffusion coefficient (D) equal to $4.5 \cdot 10^{-2}$ cm^2 s^{-1} was utilized (see Table 3.1). As can be deducted by comparing these values with that measured with dynamic method, in each case a high advective component must be considered in order to justify the measured CO_2 flux. Therefore, it is possible that a more complex process than the simple superficial microbiological activity can be invoked to explain the origin of the carbon dioxide contained in these gases. More investigations are needed to clarify this aspect.

site	C_d (ppm)	CO_2 flux (g m^{-2} day^{-1})	site	C_d (ppm)	CO_2 flux (g m^{-2} day^{-1})	site	C_d (ppm)	CO_2 flux (g m^{-2} day^{-1})
1	41000	883	51	2500	37	100	11500	238
2	800	17	52	1700	25	101	1500	32
3	100	2	53	1500	22	102	700	15
4	800	17	54	1000	15	103	28000	594
5	500	11	55	122000	2716	104	17000	357
6	500	11	56	70000	1494	105	800	17
7	100	2	57	500	11	106	4500	95
8	100	2	58	3500	75	107	1600	34
9	150	3	59	2200	48	108	1000	22
10	100	2	60	15000	323	109	5000	107
11	50	1	61	1600	34	109b	15000	323
12	900	19	62	400	8	110	1200	25
13	500	11	63	1700	36	111	2000	42
14	200	4	64	100	2	112	500	11
15	200	4	65	1600	34	113	3000	65
16	700	15	66	6000	127	114	6500	139
17	300	6	66b	7000	149	115	8500	187
18	800	17	67	4500	95	116	1500	32
19	300	6	68	3250	70	117	6000	127
20	600	13	69	7000	149	118	3500	75
21	1000	22	70	2300	49	119	11000	238
22	300	6	71	4700	100	120	3300	70
23	100	2	72	5500	117	121	900	19
24	1400	31	73	1100	24	122	1600	34
25	2500	53	74	14000	306	123	2200	48
26	200	4	75	4200	90	124	2500	53
27	300	6	76	200	4	125	4200	90
28	1100	24	77	4500	95	126	700	15
29	50	1	78	3500	75	127	3000	65
30	50	1	79	800	17	128	3000	65
31	50	1	80	900	19	129	2200	48
32	200	4	81	900	19	130	2000	42
33	600	13	82	1200	25	131	8000	170
34	700	15	83	500	11	132	1300	27
35	100	2	84	1600	34	133	5600	119
36	500	11	85	10000	221	134	1000	22
37	300	6	86	16000	340	135	9000	187
38	400	8	87	24000	509	136	3000	65
39	400	8	88	800	17	137	5200	110
40	1200	25	89	6500	139	138	2600	56
41	400	8	90	12000	255	139	10500	221
42	100	2	91	1400	31	140	1700	36
43	300	6	92	6000	127	141	1400	31
44	50	1	93	6500	139	142	9000	187
45	500	11	94	5500	117	143	1000	22
46	400000	11400	95	1100	24	144	1000	22
47	75000	1154	96	48000	1019	145	3000	65
48	75000	1154	97	3600	76	146	200	4
49	2000	31	98	48000	85	147	1200	25
50	1750	25	99	3600	32	148	85000	1868

Table 7.3. C_d values and relative soil CO_2 fluxes measured in the surveyed area in October and November 2003**.**

site	C_d (ppm)	CO_2 flux (g m^{-2} day^{-1})	site	C_d (ppm)	CO_2 flux (g m^{-2} day^{-1})	site	C_d (ppm)	CO_2 flux (g m^{-2} day^{-1})
149	900	19	199	2000	43	249	5500	117
150	5500	117	200	800	17	250	200	4
151	2400	51	201	4200	89	251	11500	244
152	200	4	202	3800	81	252	25000	533
153	500	11	203	8000	170	253	8000	170
154	3500	75	204	3800	81	254	6500	138
155	2100	45	205	600	13	255	12000	256
156	1600	34	206	2600	55	256	14000	299
157	2200	47	207	4800	102	257	5700	121
158	700	15	208	1300	28	258	12500	267
159	1800	38	209	3600	77	259	1000	21
160	1700	36	210	1500	32	260	7000	149
161	2900	62	211	500	11	261	200	4
162	2700	58	212	700	15	262	5000	106
163	600	13	213	1600	34	263	1100	23
164	6000	128	214	200	4	264	1800	38
165	5000	106	215	100	2	265	3000	64
166	7000	149	216	6000	128	266	2600	55
167	500	11	217	500	11	267	2000	43
168	1000	21	218	1000	21	268	3500	75
169	800	17	219	200	4	269	2200	47
170	6000	128	220	1500	32	270	1000	21
171	3700	79	221	1100	23	271	6500	138
172	4800	102	222	1100	23	272	1600	34
173	8500	182	223	600	13	273	200	4
174	7000	149	224	2000	43	274	9500	202
175	2700	58	225	1200	25	275	2000	43
176	700	15	226	2000	43	276	500	11
177	4000	85	227	600	13	277	100	2
178	500	11	228	200	4	278	500	11
179	2500	53	229	400	9	279	1000	21
180	2500	53	230	500	11	280	200	4
181	7000	149	231	700	15	281	500	11
182	3000	64	232	100	2	282	3250	69
183	3400	72	233	4700	100	283	2000	43
184	1400	30	234	1400	30	284	50	1
185	1300	28	235	1700	36	285	50	1
186	1500	32	236	100	2	286	50	1
187	1400	30	237	800	17	287	50	1
188	5200	111	238	6000	128	288	10000	212
189	3400	72	239	2200	47	289	500	11
190	1800	38	240	600	13	290	1300	28
191	2000	43	241	1000	21			
192	1000	21	242	1600	34			
193	4200	89	243	1100	23			
194	1200	25	244	3500	75			
195	3400	72	245	3100	66			
196	2300	49	246	500	11			
197	1200	25	247	100	2			
198	4500	96	248	100	2			

Table 7.3. C_d values and relative soil CO_2 fluxes measured in the surveyed area in October and November 2003**.**

site	C_d (ppm)	CO_2 flux (g m^{-2} day^{-1})	site	C_d (ppm)	CO_2 flux (g m^{-2} day^{-1})	site	C_d (ppm)	CO_2 flux (g m^{-2} day^{-1})
291	600	13	342	5500	117	393	50	1
292	50	1	343	300	6	394	600	13
293	300	6	344	700	15	395	2000	42
294	3000	65	345	50	1	396	100	2
295	4000	85	346	200	4	397	400	8
296	1500	32	347	300	6	398	50	1
297	7000	149	348	6000	127	399	900	19
298	4000	85	349	6000	127	400	100	25
299	900	19	350	1200	25	401	50	1
300	7000	149	351	12500	272	402	3000	65
301	3200	68	352	1200	25	403	5000	107
302	1800	39	353	800	17	404	100	2
303	1800	39	354	700	15	405	800	17
304	3800	81	355	2800	59	406	400	8
305	500	11	356	600	13	407	100	2
306	500	11	357	800	17	408	300	6
307	2700	58	358	500	11	409	2200	48
308	2800	59	359	500	11	410	1300	27
309	500	11	360	100	2	411	100	2
310	5500	117	361	600	13	412	6000	127
311	100	2	362	100	2	413	20000	424
312	200	4	363	5400	115	414	3000	65
313	500	11	364	8500	187	415	50	1
314	50	1	365	5600	119	416	1200	25
315	4800	102	366	4000	85	417	800	17
316	2200	48	367	1900	41	418	1200	25
317	4800	102	368	50	1	419	2500	53
318	3500	75	369	100	2	420	2000	42
319	500	11	370	3000	65	421	2300	49
320	2500	53	371	1100	24	422	700	15
321	4500	95	372	200	4	423	2200	48
322	500	11	373	4000	85	424	3700	78
323	12000	255	374	300	6	425	1400	31
324	6000	127	375	500	11	426	800	17
325	800	17	376	50	1	427	100	2
326	700	15	377	50	1	428	9500	204
327	9000	187	378	1200	25			
328	400	8	379	100	2			
329	500	11	380	1000	22			
330	1600	34	381	5000	107			
331	4200	90	382	9000	187			
332	2000	42	383	5000	107			
333	400	8	384	3800	81			
334	2100	44	385	5000	107			
335	2500	53	386	1100	24			
336	3200	68	387	1000	22			
337	1300	27	388	5000	107			
338	1900	41	389	3000	65			
339	300	6	390	2000	42			
340	1300	27	391	100	2			
341	400	8	392	4000	85			

Table 7.4. C_d values and relative soil CO_2 fluxes measured in the surveyed area in February and March 2004.

Conclusions

The influence of soil permeability and pumping flux on the soil CO_2 flux measurements performed using the dynamic method (Gurrieri & Valenza, 1988) was clarified by several test performed in this thesis. The data highlights that the measured flux values are strictly influenced by soil permeability because this property regulates the amount of CO_2-rich air that can be sucked out from the soil by the sampling probe. In particular, the laboratory results highlight that, when flux measurements are taken at high pumping flux (4-2 $l \cdot min^{-1}$), the influence of soil permeability is significant. On the other hand, when flux measurements are taken at low pumping flux (0.8 l min^{-1}), smaller differences are observed, especially within the range of fluxes usually measured in active volcanoes and geothermal areas. Starting from these considerations, we choose to employ a pumping flux of 0.8 l min^{-1} in measuring flux with dynamic method and a new empirical equation for performing careful soil CO_2 flux measurements as a function of the soil permeability was deduced. Furthermore, to measure *in situ* soil permeability, a new method based on a physical model of gas radial advection through porous media was developed in this thesis. The new method was coupled with the dynamic method in each measurement site, in order to performe accurate flux measurements according to the new empirical equation. However, we would remark that an absolute estimate of the total CO_2 flux exhaled in an area established by means of field methods such as Gurrieri and Valenza's (1988) method and the accumulation chamber method (Baubron et al., 1990; Tonani and Miele, 1991), included a large degree of uncertainty, because the values obtained depend on the measurement grid adopted (principally location and number of measurements sites) (Diliberto et al., 2002). In contrast, temporal variations in soil CO_2 flux measured in a fixed sampling grid gives little uncertainty and in a volcanic area it can used as an indicator of the evolution of the volcanic activity (Badalamenti et al., 1988; Baubron et al., 1991; Sorey et al., 1998; Diliberto et al; 2002). In particular, for continuous monitoring purposes, a system based on the dynamic method has numerous advantages compared with those based on the accumulation chamber method. As discussed in this thesis, the latter is more complex and expensive than the dynamic method. Furthermore, flux measurements performed using accumulation chamber measurements, which are taken at the surface of the soil, are strongly influenced by atmospheric phenomena (Hinkle 1990; Klusman 1993).

In this thesis we have also discussed the results of several tests performed using the accumulation chamber method. Unlike the dynamic method previously discussed, CO_2 flux

measurements effected using this method are based on a theoretical relationship between soil CO_2 flux and the rate of increase in the concentration of CO_2 inside a continuously-monitored accumulation chamber. The results of our tests, which have been discussed at length in this thesis, have shown that of errors in measuring CO_2 flux with this method do occur. A general underestimation up to – 43% has been observed, especially when operating on low imposed fluxes and on low permeable soils. Furthermore, other tests have shown that the accuracy of the flux measurements performed with this system strongly depends on the pumping rate, which causes errors up to 60% when flux measurements are taken at a low pumping flux (0.2 l min^{-1}). Furthermore, a general overestimation has been found when the measurements are taken at high imposed fluxes and with highly permeable soils. According to Gao and Yates (1998), overestimation is here explained as the result of an additional gas flux from the soil matrix driven by a pressure deficit caused by air flowing into the chamber (Venturi effect). As discussed here, this effect depends on soil permeability, on the imposed flux and on the pumping rate of the system and it can overcome the other sources of error only when flux measurements are taken in highly permeable soils and at high CO_2 fluxes.

The experience acquired during this thesis shows that the difficulties encountered inmeasuring gas fluxes from the soil are principally to be referred to unavoidable errors introduced by perturbing natural soil properties and degassing states by the act of measuring itself. The dynamic method developed in this thesis is based on an empirical relationship obtained under known conditions of disturbance caused to the soil. Therefore flux measurements obtained with this method are characterized by good reliability. On the contrary, the measurements performed by employing the accumulation chamber method show that some errors do occur and that they are mainly to be referred to the inadequacy of the simple physical model at the base of the flux measurements, which does not take into consideration the eventual disturbance caused to the soil by the measurement system. Therefore, several rigorous tests like those described in this thesis are needed to check the reliability of any flux measurement equipment.

Several permeability measurements have been performed using the *in situ* method described in this thesis over a large sector of the island of Vulcano (Aeolian Islands, Italy) the results of which identified a range of values between 6-80 darcys. The permeability values were compared with the soil CO_2 fluxes that had been measured at the same site at the same time using the dynamic method, according to the new empirical equation. A very low correlation between these two parameters was found. This result suggests that the permeability of the upper layers of the soil is not the main factor in determining the spatial

distribution of soil gas emissions. By comparing a flux survey obtained employing the values of permeability measured in each site of the surveyed area with a corresponding survey obtained with a constant value of permeability equal to the mean value found in the area under investigation, very low differences were observed. Moreover, in each case these differences could not have caused any appreciable change in either the statistic or the spatial distribution of the soil CO_2 flux.

The results of the soil CO_2 surveys performed at Capo Calavà (Golfo di Patti, Sicily) indicate the presence of a highly degassing structure that is aligned along the NNW/SSE direction in the eastern sector of the area. This degassing evidence is in accord with the geophysical and geological data available for this area. The examination of the flux maps shows that several mapped faults in this area are not degassing. These are probably old faults sealed by mineralization that has sensibly decreased their permeability. On the other hand, several recognized flux anomalies are not related to the presence of mapped faults, which indicates the presence of some recently buried structures, which cannot be easily recognized on the basis of simple superficial observations. However, these are active structures because they are degassing. In fact only recent, active structures, subject to continuous strain, maintain high permeability and "degassing".

AKNOWLEGEMENTS

I wish to thank:

- FSE and INGV-Pa for economic support
- My tutor, Prof. Mariano Valenza
- Prof. Mario Nuccio, coordinator of PhD Course on Geochemistry
- My co-tutor, Dr. Sergio Gurrieri, responsible of volcanic surveillance of INGV-Pa
- My two reviewers, Prof. Luigi Marini and Dr. B. Mack Kennedy.
- All the staff of the CFTA (University of Palermo).

REFERENCES

Allard, P., Carbonnelle, J., Dajlevic, D., Le Bronec, J., Morel, P., Robe, M. C., Maurenas, J. M., Faivre-Pierret, R., Martin, D., Sabroux, J. C., Zettwoog, P., (1991) - *Eruptive and diffuse emission of CO_2 from Mount Etna.* Nature 351, 387-391.

Anderson, J.M., (1973) - *Carbon dioxide evolution from two temperate deciduous woodland soils.* J. Appl. Ecol. 10, 361-378.

Azzaro, R., Barbano, M.S., Rigano, R., Antichi, B., (2000) – *Contributo alla revisione delle zone sismogenetiche della Sicilia*, in: F. Galadini, C. Meletti & A. Rebez (Ed.), Le ricerche del GNDT nel campo della pericolosità sismica, CNR- GNDT, Roma, 397, 31-38.

Badalamenti, B., Gurrieri, S, Hauser, S., Valenza, M., (1998) - *Ground CO_2 output in the island of Vulcano during the period 1984–1988: gas hazard and volcanic activity surveillance implications.* Rendiconti Società Italiana Mineralogia Petrologia 43, 893–899.

Badalamenti, B., Gurrieri, S., Nuccio, P. M., Valenza, M., (1991) - *Gas hazard on Vulcano island.* Nature 350, 26-27.

Barbano, M.S., Cosentino, M., Lombardo, G., Patanè, G., (1980) – *Isoseismal maps of Calabrian and Sicily eartquakes.* CNR Prog. Fin. Geodin. Publ. 341.

Barone, A., Fabbri, A., Rossi, S., Sartori, R., (1982) – Geological structure and evolution of marine areas adjacent to Calabrian arc. Earth Evol. Sci. 3, 207-221.

Baubron, J.C., Allard, P., Toutain, J.P., (1990) – *Diffuse volcanic emissions of carbon dioxide from Vulcano island, Italy.* Nature 344, 51-53.

Bekku, Y., Koizumi, H., Nakadai, T. Iwaki, H., (1955) – *Measurement of soil respiration using close chamber method; an IRGA technique.* Ecol. Res. 10, 369-373.

Bergfeld, D., Goff, F., Janik, C.J., (2001) - *Elevated carbon dioxide flux at the Dixie Valley geothermal field, Nevada; relations between surface phenomena and the geothermal reservoir.* Chemical Geology 177, 43-66.

Brown, K.W., Rosenberg, N.J., (1971) – *Energy and CO_2 balance of an irrigated sugar beet (Beta vulgaris) field in the Great Plains.* Agron. J. 63: 207 – 213.

Camarda, M., Gurrieri, S., Valenza, M. - *In situ Permeability Measurements Based on Radial Gas Advection Model: Relationships between Soil Permeability and Diffuse CO_2 Degassing in Volcanic Areas.* (Submitted at PAGEOPH).

Carman, P.C., (1956) - *Flow of Gases through Porous Media* (Academic Press, New York, pp. 182).

Capasso, G., Favara, R., Inguaggiato, S., (1997) - *Chemical features and isotopic composition of gaseous manifestations on Vulcano Island, Aeolian Islands, Italy: An interpretative model of fluid circulation.* Geochimica et Cosmochimica Acta 6, 3425-3440.

Carapezza, M.L., Federico, C., (2000) - *The contribution of fluid geochemistry to the volcano monitoring of Stromboli.* J. Volcanol. and Geother. Res. 95, 227-245.

Carapezza, M.L., Granieri D., (2004) – *CO_2 soil flux at Vulcano (Italy): comparison between active and passive methods.* Applied Geochemistry 19, 73-88.

Censi, P., Ferla, P., (1982) - *I marmi dei Monti Peloritani composizione isotopica dell'ossigeno e del carbonio e ricostruzione degli ambienti formazionali.* Rendiconti Società Italiana Mineralogia Petrologia 38 (3), 1101-1117.

Chiodini, G., Cioni, R., Guidi, M., Marini, L., Raco, B., (1998) - *Soil CO_2 flux measurements in volcanic and geothermal areas.* Applied Geochemistry 13, 543–552.

Chiodini G. , Frondini, F., Cardellini, C., Parello, F., Peruzzi, L., (2000) - *Rate of diffuse carbon dioxide earth degassing estimated from carbon balance of regional aquifers: the case of Central Apennine (Italy).* J Geophys. Res., 105, 8423-8434

Chiodini, G., Frondini, F., (2001) – *Carbon dioxide degassing from Albani Hillis volcanic region, Central Italy.* Chemical Geology 177, 67-83.

Chiodini, G., Cardellini, C., Amato, A., Boschi, E., Caliro, S., Frondini, F., Ventura, G., (2004) - *Carbon dioxide Earth degassing and seismogenesis in central and southern Italy.* Geophysical Research Letters 31, L07615.

Cicerone, R.J., Shetter, J.D., (1981) - *Sources of Atmospheric Methane: Measurements in Rice Paddies and Discussion.* Journal Geophysical Research 86, 7203-7209.

Ciotoli, G., Guerra, M., Lombardi, S., Vittori, E., (1998) - *Soil gas survey for tracing seismogenic faults: a case-study in the Fucino basin (Central Italy).* J. Geophys. Res., 103, 23781-23794.

De Gregorio, S., Diliberto, I.S., Giammanco, S., Gurrieri, S., Valenza, M., (2002) – *Tectonic control over large-scale diffuse degassing in eastern Sicily (Italy).* Geofluids 2, 273-284.

Denmead, O.T., (1979) - *Chamber systems for measuring nitrous oxide emissions from soils in the field.* Soil Science Soc. Am. J. 43, 89-95.

Diliberto, I.S., Gurrieri, S., Valenza, M., (2002) – *Relationships between diffuse CO_2 emissions and volcanic activity on the island of Vulcano (Aeolian Island, Italy) during* the period 1984-1994. Bulletin of Volcanology, 64, 219-228.

Etiope, G., Martinelli, G., (2002) - *Migration of carrier and trace gases in the geosphere: an*

overview. Physics of the Earth and Planetary Interiors 129, 185-204.

Evans, D.D., Kirkham, D., (1949) - *Measurement of the air permeability of soil in situ.* Soil. Sci. Soc. Am. Proc. 14, 65-73.

Evans, W.C., Sorey, M.L., Kennedy, B.M., Stonestrom, D.A., Rogie, J.D., Shuster, D.L., (2001) - *High CO_2 emissions through porous media: transport mechanisms and implications for flux measurement and fractionation.* Chemical Geology 177, 15–29.

Fang, C., Moncrieff, J.B., (1998) – *An open-top chamber for measuring soil respiration and influence of pressure difference on CO_2 efflux measurement.* Functional Ecology 12, 319-325.

Fang, C., Moncrieff, J.B., (1999) - *A model for soil CO_2 production and transport 1: Model development*. Agricultural and Forest Meteorology 95, 225-236.

Fang, G., Scott, R.Y., (1998) – Simulations of enclosure chamber methods for measuring gas emissions from soil to the atmosphere. Journal of Geophysical Research 103, 26,127-26,136.

Ferla, P., (1968) - *Il settore di Capo Calavà (Prov. Messina).* Atti Acc. Sc. Let. Arti Palermo, S. IV, 28, 1-184.

Ferla, P., (1970) - *Serie metamorfiche dei Monti Peloritani Occidentali.* Rendiconti Società Italiana Mineralogia Petrologia 28, 125-151.

Ferla, P., (1985) - *Dati preliminari sui prodotti di alterazione lungo direttrici tettoniche a Capo Calavà e Lipari.* Bollottino GNV-CNR, 62 - 70.

Finizola, A., Sortino, F., Lénat, J.F., Valenza, M., (2002) - *Fluid circulation at Stromboli volcano (Aeolian islands, Italy) from self-potential and CO_2 surveys.* Journal of Volcanology and Geothermal Research 116, 1–18.

Finizola, A., Lénat, J.F., Macedo, O., Domingo, R., (2004) - *Fluid circulation and structural discontinuities inside Misti volcano (Peru) inferred from self-potential measurements.* Journal of Volcanology and Geothermal Research 135, 343-360.

Fish, A.N., Koppi A.J., (1994) - *The use of a simple air permeameter as a rapid indicator of functional soil pore space.* Geoderma 63, 255-264.

Fukui, Y., and Doskey, P.V., (1996) - *An Enclosure Technique for measuring non-methane organic compound emissions from grasslands.* Journal of Environmental Quality 25, 601-610.

Fukuda, H., (1955) – *Air and vapor movement in soil due to wind gustiness.* Soil Sci. 79, 249-258.

Gerlach, T.M., Doukas, M.P., McGee, K.A., Kessler, R., (2001) - Soil *efflux and total emission rates of magmatic CO_2 at the Horseshoe Lake tree kill, Mammoth Mountain, California, 1995–1999.* Chemical Geology 177, 101–116.

Ghisetti, F., (1979) – *Relazione tra strutture e fasi trascorrenti e distensive lungo i sistemi Messina – Fiumefreddo, Tindari – Letojanni e Alia – Malvagna (Sicilia nord-orientale):* uno studio microtettonico. Geol. Rom., 18, 23 – 58.

Giammanco, S., Gurrieri, S., Valenza, M., (1995) - *Soil CO_2 degassing on Mt. Etna (Sicily) during the period 1989-1993: discrimination between climatic and volcanic influences.* Bulletin of Volcanology, 57, 52-60.

Giammanco, S., Gurrieri, S., Valenza, M., (1998) – *Anomalous soil CO_2 degassing in relation to faults and eruptive fissure on Mount Etna (Sicily, Italy).* Bulletin of Volcanology, 60, 252 - 259.

Giggenbach, W.F., (1996) - *Chemical composition of volcanic gases. In: Monitoring and Mitigation of Volcano Hazards* (R. Scarpa and R.I. Tilling, Eds.) Springer, 221-256.

Grover, B.L., (1955). – *Simplified Air Permeameters for Soil in Place.* Soil Sci. Soc. Am. Proc. 19, 414-418.

Guerra, M., Lombardi, S., (2000) - *Soil-gas method for tracing neotectonic faults in clay basins: the Pisticci field (Southern Italy).* Tectonophysics 339, 511-522.

Gurrieri, S., Valenza, M., (1988) – *Gas transport in natural porous medium: a method for measuring soil CO_2 flows from the ground in volcanic and geothermal areas.* Rendiconti Società Italiana Mineralogia Petrologia 43, 1151-1158.

Gurrieri, S., Giudice, G., (2004) - The CO_2 soil flux network on Mt. Etna (Italy). Proceedings of the 32nd International Geological Congress, Florence (Italy) "T11.06".

Hernandez P.A., Salazar J.M., Shimoike Y., Mori T., Notsu K., Perez N.M., (2001) -*Diffuse emission of CO_2 from Miyakejima Volcano, Japan*. Chem. Geol., 177, 175-185.

Hinkle, M.E., (1990) – *Factors affecting concentrations of helium and carbon dioxide in soil gases.* In: Geochemistry of gaseous elements and compounds. Theophrastus Publications, Athens, 421-447.

Irwin, W. P., Barnes, I., (1980) - *Tectonic relations of carbon dioxide discharges and earthquakes.* J. Geophys. Res. 85, 3115-3121.

Kanemasu, E.T., Powers, W.L., Sij, J.W., (1974) - *Field chamber measurement of CO_2 flux from soil surface.* Soil Science 118 (4), 233–237.

Kirita, H., (1971) - *Re-examination of the absorption method of measuring soil respiration under field conditions IV. An improved absorption method using a disc of plastic sponge*

as absorbent holder. Japanese Journal of Ecology 21: 119-127 (in Japanese with English abstract).

Klusman, R.W., (1993) - *Soil gas and related methods for natural resource exploration*. Wiley, New York, 1-483.

Kutilek, M., Nielsen, D.R., (1994) - *Soil Hydrology*. GeoEcology Textbook. Catena Verlag. CremlinggenDestedt, Germany.

Lanzafame, G., Bousquet, J.C., (1997) – *The Maltese escarpment and its extension from Mt. Etna to the Aeolian Islands (Sicily): importance and evolution of a lithosphere discontinuity.* Acta Vulcanologica 9 (1/2), 113 – 120.

Lentini, F., Catalano, S., Carbone, S. (2000) - *Carta geologica della Provincia di Messina: scala 1:50.000.* Provincia Regionale di Messina. Assessorato al Territorio, Servizio geologico. Ed. S.E.L.C.A., Firenze, 70 pp.

Loosveldt, H., Lafhaj, Z., Skoczylas, F., (2002) - *Experimental study of gas and liquid permeability of a mortar*, Cement and Concrete Research 32, 1357-1363.

Lunderghard, H., (1927) - *Carbon dioxide evolution of soil and crop growth.* J. Soil Science 23, 417-454.

Marrero, T.R., Mason, E.A., (1972) - *Gaseous diffusion coefficients.* Jour. Phys. Chem. Ref. Data, v. 1, 3-118.

Matthias, A.D., Blackemer, A.M., Bremner, J. M., (1980) – *A simple chamber technique for field measurement of emission of nitrous oxide from soil.* J. Envir. Qual. 9, 252-256.

McCarthy, K.P., Brown, K.W., (1992) - *Soil gas permeability as influenced by soil gas-filled porosity.* Soil. Sci. Soc. Am. J. 56, 997-1003.

Michaels, A.S., Lin, C. S., (1954) - *The permeability of Kaolinite*. Ind. Eng. Chem., 45, 139-1246.

Millington, R.J., Shearer, R.C., (1971) - *Diffusion in aggregate porous media.* Soil Science 111, 372-378.

Moldrup, P., Poulsen, T. G., Schjonning, P., Olesen, T., and Yamaguchi, T., (1998) - *Gas permeability in undisturbed soils: measurement and predictive models.* Soil Science 163, 180-189.

Monteith, J.L., Szeicz, G., Yabuki, K., (1964) - *Crop photosynthesis and the flux of carbon dioxide below the canopy.* J. Appl. Ecol. 1, 321-327.

Moore, T.R., Roulet, N.T., (1991) - *A comparison of dynamic and static chambers for methane emission measurements from subarctic fens.* Atmos. Ocean 29, 102-109.

Nakadai, T., Koizumi, H., Usami, Y., Satoh, M., Oikawa, T., (1993) – *Examination of the methods for measuring soil respiration in cultivated land: Effect of carbon dioxide concentration on soil respiration.* Ecol. Res., 8, 65-71.

Neri, G., Montalto, A., Patanè, D., Privitera, E., (1991) - *Earthquake space-time-magnitude patterns at Aeolian Islands (Southern Italy) and implications for the volcanic surveillance of Vulcano.* Acta Vulcanologica 1, 163-199.

Noorishad, J., Witherspoon, A., (1984/85) - *Can injection tests reveal the potential for fault movements?* Pure Appl. Geophys. 122 608–618.

Norman, J.M., Garcia, R., Verma, S.B., (1992) - *Soil surface CO_2 fluxes and the carbon budget of a grassland.* J. Geophys. Res. 97, 18845-18853.

Rogie, J.D., Kerrick, D.M., Sorey, M.L., Chiodini, G., Galloway, D.L., (2001) – *Dynamics of carbon dioxide emission at Mammoth Mountain Continuous monitoring of diffuse CO_2 degassing, Horseshoe Lake, Mammoth Mountain, California.* Heart and Planetary Science Letters 188, 531-541.

Sahimi, M., (1995) - Flow and Transport in Porous Media and Fractured Rock. (Weinheim; New York; Basel, Chambridge, Tokyo. pp. 223)

Salazar, J.M.L., Pérez, N.M., Hernández, P.A., Soriano, T., Barahona, F., Olmos, R., Cartagena, R., López, D.L., Lima, R.N., Melián, G., Galindo, I., Padrón, E., Sumino, H., Notsu, K., (2002) - *Precursory diffuse carbon dioxide degassing signature related to a 5.1 magnitude earthquake in El Salvador, Central America*. Earth and Planetary Science Letters 205, 81-89.

Scheidegger, A. E., (1974) - *The physics of flow through porous media.* (University of Toronto press. pp. 102).

Sinclair, A.J., (1974) – *Selection of threshold values in geochemical data using probability graphs. J. Geochem. Explor.* 3 (2), 129 - 149.

Spicák, A., Horálek, J., (2001) - *Possible role of fluids in the process of earthquakes swarm generation in the West Bohemia/Vogtland seismoactive region.* Tectonophysics 151-161.

Sugisaki, R., Ido, M., Takeda, H., Isobe, Y., Hayashi, Y., Nakamura, N., Satake, H., Mizutani, Y., (1983). - *Origin of hydrogen and carbon dioxide in fault gases and its relation to fault activity.* J. Geol. 91 (3), 239–258.

Symonds, R.B., Rose, W.I., Bluth, G.J.S., Gerlach, T.M., (1994) - *Volcanic-gas studies: Methods, results, and applications. In, Volatiles in Magmas* (M.R. Carroll and J.R. Holloway, eds.), Reviews in Mineralogy, 30, 1-60.

Taylor, J., (2000) - *Introduzione all'analisi degli errori: lo studio delle incertezze nelle misure fisiche* (Zanichelli).

Toshiya, M., Hernandez, P.A., Salazar, J.M.L., Perez, N.M., Notsu, K., (2001) – *A in situ method for measuring CO2 flux from volcanic-hydrotermal fumaroles.* Chemical Geology 177, 85-99.

Tonani, F., Miele, G., (1991) - *Methods for measuring flow of carbon dioxide through soils in the volcanic setting.* International Conference Active Volcanoes and Risk Mitigation. Napoli. 27 August–1 September 1991.

Ventura, G., Vilardo, G., Molano, G., Pino, N. A., (1999) - *Relationships among crustal structure, Vulcanism and strike-slipe tectonics in the Lipari-Vulcano Volcanic Complex (Aeolian Islands, Southern Tyrrenian Sea, Italy),* Physics of the Earth and Plnetary Interiors 116, 31-52.

Wakita, H., (1996) - *Geochemical challenge to earthquake prediction.* Proc. Natl. Acad. Sci. USA 3781-3786.

Wentworth, C.K., (1922) – *A scale of grade and class terms for clastic sediments.* J. Geol 30, 377-392.

Werner, C., Brantley, S.L., Boomer, K., (2000) - *CO_2 emissions related to the Yellowstone volcanic system 2. Statistical sampling, total degassing, and transport mechanisms.* J. Geophys. Res. 105, 10831-10846.

Witkamp, M., (1966) - *Decomposition of leaf litter in relation to environment, microflora and microbial respiration.* Ecology 47, 194-201.

Witkamp, M., Frank. M.L., (1969) - *Evolution of CO_2 from litter, humus, and subsoil of a pine stand.* Pedobio. 9, 358-365.

Zhao, D., Kanamori, H., Negishi, H., Wiens, D., (1996) - *Tomography of the source area of the 1995 Kobe earthquake: evidence for fluids at the hypocenter?* Science 1891-1894.

Appendix A

Solution of steady state advective-diffusion equation

The general solution of the steady state one-dimensional form of the advective-diffusion equation (see Chapter 2) is:

$$C(z) = A\frac{D}{v}e^{\frac{v}{D}z} + B \tag{A.1}$$

where the A and B constants are calculated as function of the boundary conditions. To show the corretness of this solution we calculed the first and second derivative of this function respect to z and subsequently we esplicite them in steady state advective-diffusion equation (equation A.2):

$$v\frac{\partial C}{\partial z} - D\frac{\partial^2 C}{\partial z^2} = 0 \tag{A.2}$$

$$\frac{\partial C(z)}{\partial z} = Ae^{\frac{v}{D}z} \qquad \text{and} \qquad \frac{\partial^2 C(z)}{\partial z^2} = Ae^{\frac{v}{D}z}\frac{v}{D} \tag{A.3}$$

Replacing the expressions (A.3) in this equation (A.1), we obtain:

$$vAe^{\frac{v}{D}z} - D \cdot Ae^{\frac{v}{D}z}\frac{v}{D} = 0$$

$$\Downarrow$$

$$vAe^{\frac{v}{D}z} - Ae^{\frac{v}{D}z}v = 0$$

$$\Downarrow$$

$$0 = 0$$

which show that equation (A.1) is the solution of equation (A.2).

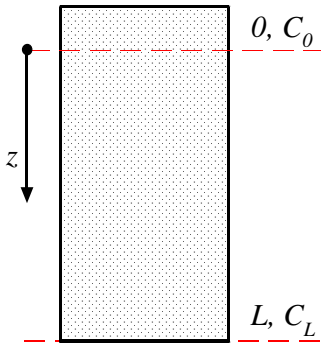

Figure A.1. Sketch of a finite porous medium.

To describe steady state CO_2 concentration as function of depth in a finite porous medium of tikness L (Figure A.1) we imposed the following boundary conditions:

$$C(z=0) = C_0$$

and

$$C(z=L) = C_L$$

wher C_L and C_0 are the concentration of gas at 0 and L depths, respectively. Under these condictions the expression of A and B constants can be easily found:

$$A = \frac{v}{D}(C_L - C_0)\left(e^{\frac{v}{D}z} - 1\right) \qquad \text{and} \qquad B = C_0 - (C_L - C_0)\left(e^{\frac{v}{D}z} - 1\right)$$

Replacing A and B terms in the (A.1) equation (2.10) (see Chapter 2) is obtained:

$$C(z) = C_0 + \frac{(C_L - C_0)}{\left(e^{\frac{v}{D}L} - 1\right)}\left(e^{\frac{v}{D}z} - 1\right) \tag{2.10}$$

As discussed in Chaper 2 this equation shows the change of soil CO_2 concentration as function of depth between two generic sufaces of 0 and L depths respectively.

Appendix B

Experimental data. Table 3.2.

depth (cm)	CO_2 flux (g m^{-2} day^{-1})												
	21849	18487	14621	9747	6722	4202	3529	3025	2352	1849	1210	504	96
101	100	100	100	100	100	100	98.7	97.9	94.6	85.2	72.2	42.7	9.5
96	100	100	100	100	100	99.6	96.6	96.9	91.8	83.8	70.4	40.8	8.6
81	100	100	100	100	99.2	98.2	94.8	96.1	86.6	78.6	65.8	35.8	8.0
67	100	100	100	100	97.6	96.3	94.0	93.7	82.3	73.4	59.0	30.5	6.4
53	100	100	99.5	99.6	94.3	92.8	89.6	89.9	79.2	66.8	51.7	25.1	5.2
38	100	98.9	98.7	97.3	91.2	89.1	83.1	81.8	67.2	55	40.6	18.8	3.8
24	98.6	97.6	97.2	95.6	83.6	74.7	70.7	68.4	55.1	39.3	28.6	11.3	2.8
9	88.3	84.9	81.2	69.6	61.5	44.5	37.7	34.9	25.1	13.1	11.7	3.8	1.2

Tabele 3.2. Steady-state values of soil CO_2 concentration (express as percent) at various depths and for each imposed CO_2 flux. Soil permeability , k = 125 darcys.

Appendix B

Experimental data Table 3.3

depht (cm)	CO_2 flux (g m^{-2} day^{-1})												
	21849	18487	14621	9747	6722	4202	3529	3025	2352	1849	1210	504	96
101	100	100	100	100	100	100	100	100	100	93.3	85.8	62.2	11.2
96	100	100	100	100	100	100	100	100	99.0	92.1	81.3	59.8	10.7
81	100	100	100	100	100	100	100	100	97.6	87.2	75.4	55.0	8.7
67	100	100	100	100	100	99.1	98.3	97.1	95.0	83.7	71.8	41.6	7.6
53	100	100	100	100	99.3	97.7	95.1	93.7	91.1	81.3	64.2	36.0	6.2
38	100	99.3	96.9	99.3	98.1	92.1	93.3	90.9	86.0	68.2	50.2	26.4	4.3
24	100	98.1	94.5	95.7	90.9	88.5	82.2	77.8	59.8	50.2	33.5	14.7	2.7
9	93.3	90.9	87.3	74.2	65.8	59.8	45.5	40.7	37.1	21.5	15.2	5.1	1.3

Tabele 3.3. Steady-state values of soil CO_2 concentration (express as percent) at various depths and for each imposed CO_2 flux. Soil permeability, k = 36 darcys.

Tabele 3.4. Steady-state values of soil CO_2 concentration (express as percent) at various depths and for each imposed CO_2 flux. Soil permeability, k = 6 darcys.

depht (cm)	CO_2 flux (g m^{-2} day^{-1})												
	21849	18487	14621	9747	6722	4202	3529	3025	2352	1849	1210	504	96
101	100	100	100	100	100	100	100	100	100	93.3	85.8	62.2	11.2
96	100	100	100	100	100	100	100	100	99.0	92.1	81.3	59.8	10.7
81	100	100	100	100	100	100	100	100	97.6	86.1	75.4	55.0	8.7
67	100	100	100	100	100	99.1	98.3	97.1	95.0	83.7	71.8	41.6	7.6
53	100	100	100	100	99.3	97.7	95.1	93.7	91.1	81.3	67.0	36.0	6.2
38	100	99.3	96.9	99.3	98.1	92.1	93.3	90.9	86.0	69.4	50.2	26.4	4.3
24	100	98.1	94.5	95.7	90.9	88.5	82.2	77.8	59.8	50.2	33.5	14.7	2.7
9	93.3	90.9	87.3	74.2	65.8	59.8	45.5	40.7	37.1	21.5	15.2	5.1	1.3

depht (cm)	CO_2 flux (g m^{-2} day^{-1})												
	21849	18487	14621	9747	6722	4202	3529	3025	2352	1849	1210	504	96
101	100	100	100	100	100	100	100	100	100	95.7	87.3	62.2	14.4
96	100	100	100	100	100	100	100	100	99.5	94.5	86.1	60.9	14.0
81	100	100	100	100	100	100	99.3	100	98.3	92.1	81.3	54.0	11.6
67	100	100	100	100	100	99.3	98.1	98.1	97.3	88.5	74.4	46.5	9.6
53	100	100	100	100	98.1	98.1	96.9	95.7	93.3	86.1	69.4	41.0	8.2
38	100	100	100	100	95.7	95.7	94.5	93.3	88.5	79.0	60.0	33.5	6.5
24	100	100	96.9	95.3	94.5	88.5	83.7	79.0	71.8	55.0	41.9	19.8	3.8
9	95.7	93.3	88.5	81.3	69.4	57.4	52.6	47.9	43.1	33.5	21.5	8.9	1.4

Tabele 3.5. Steady-state values of soil CO_2 concentration (express as percent) at various depths and for each imposed CO_2 flux. Soil permeability, k = 0.36 darcys.

Appendix C

Solution of mass-balance equation

In this Appendix we will show that the equation (4.3):

$$C_d(t) = \frac{\phi_s}{\phi_p} C_s \left(1 - a \cdot e^{-\frac{\phi_p}{V} t} \right) \tag{4.3}$$

is a general solution of equation:

$$\frac{dC_d(t)}{dt} + \frac{\phi_p}{V} C_d(t) = \frac{\phi_s C_s}{V} \tag{C.1}$$

In order to reach this purpose we calculate the derivative of $C_d(t)$ and successively we substitute equation (4.3) and its derivative into equation (C.1):

$$\frac{\partial C_d(t)}{\partial t} = a \frac{\phi_s}{\phi_p} \frac{\phi_p}{V} C_s e^{-\frac{\phi_p}{V} t} = a \frac{\phi_s}{V} C_s e^{-\frac{\phi_p}{V} t}$$

and performing the substitutions, we obtain:

$$a \frac{\phi_s}{V} C_s e^{-\frac{\phi_p}{V} t} + \frac{\phi_p}{V} \frac{\phi_s}{\phi_p} C_s \left(1 - a \cdot e^{-\frac{\phi_p}{V} t} \right) = \frac{\phi_s C_s}{V}$$

$$\Downarrow$$

$$a \frac{\phi_s}{V} C_s e^{-\frac{\phi_p}{V} t} + \frac{\phi_s}{V} C_s \left(1 - a \cdot e^{-\frac{\phi_p}{V} t} \right) = \frac{\phi_s C_s}{V}$$

$$\Downarrow$$

$$a \frac{\phi_s}{V} C_s e^{-\frac{\phi_p}{V} t} + \frac{\phi_s}{V} C_s - a \frac{\phi_s}{V} C_s e^{-\frac{\phi_p}{V} t} = \frac{\phi_s C_s}{V}$$

$$\Downarrow$$

$$a \frac{\phi_s}{V} e^{-\frac{\phi_p}{V} t} + \frac{\phi_s}{V} - a \frac{\phi_s}{V} e^{-\frac{\phi_p}{V} t} = \frac{\phi_s}{V}$$

As shown by the last equation, the equality was verified and so, we have proved that equation (4.3) is a general solution of equation (C.1).

J_{CO2} (g m^{-2}day^{-1})	C_d (φ_p=4 l·min^{-1})	C_d (φ_p=3 l·min^{-1})	C_d (φ_p=2 l·min^{-1})	C_d (φ_p=1 l·min^{-1})	C_d (φ_p=0.8 l·min^{-1})	C_d (φ_p=0.4 l·min^{-1})	C_s (% vol)
21,849	0.280	0.270	0.273	0.340	0.510	0.720	100
18,487	0.270	0.267	0.260	0.310	0.480	0.640	100
14,621	0.255	0.252	0.250	0.283	0.412	0.566	99.5
9,747	0.244	0.237	0.235	0.260	0.350	0.478	98.8
6,722	0.238	0.226	0.216	0.227	0.310	0.358	95.3
4,202	0.213	0.200	0.184	0.180	0.210	0.312	87.9
3,529	0.195	0.183	0.170	0.170	0.185	0.282	83.4
3,025	0.186	0.174	0.158	0.150	0.175	0.245	80.7
2,352	0.167	0.156	0.144	0.138	0.143	0.165	67.4
1,849	0.138	0.131	0.119	0.109	0.111	0.145	53.7
1,210	0.090	0.080	0.070	0.060	0.066	0.083	39.5
504	0.044	0.040	0.038	0.030	0.028	0.029	17.7
96	0.011	0.009	0.008	0.006	0.006	0.006	3.5

Table 4.1. C_d values express as molar fraction at each imposed flux and for each pumping flux (4, 3, 2, 1, 0.7 e 0.4 l·min^{-1}); in the last column the concentration values of the gas sucked out from the soil (C_s) for each imposed flux are also reported. Experimental data shown in this table refer to the soil sample S_1 (k = 125 darcys).

J_{CO2} (g m^{-2}day^{-1})	C_d (φ_p=4 l·min^{-1})	C_d (φ_p=3 l·min^{-1})	C_d (φ_p=2 l·min^{-1})	C_d (φ_p=1 l·min^{-1})	C_d (φ_p=0.8 l·min^{-1})	C_d (φ_p=0.4 l·min^{-1})	C_s (% vol)
21,849	0.274	0.289	0.335	0.495	0.598	0.752	100
18,487	0.260	0.270	0.300	0.440	0.509	0.655	100
14,621	0.250	0.250	0.272	0.380	0.453	0.561	100
9,747	0.240	0.230	0.240	0.300	0.365	0.466	99.2
6,722	0.215	0.200	0.200	0.237	0.296	0.389	95.8
4,202	0.195	0.185	0.180	0.200	0.230	0.312	89.2
3,529	0.180	0.173	0.167	0.185	0.205	0.251	83.7
3,025	0.167	0.156	0.148	0.157	0.180	0.217	82.4
2,352	0.130	0.120	0.110	0.106	0.115	0.132	69.2
1,849	0.100	0.090	0.081	0.076	0.082	0.094	54.2
1,210	0.078	0.072	0.064	0.057	0.060	0.066	39.8
504	0.041	0.038	0.033	0.028	0.027	0.029	18.0
96	0.007	0.006	0.005	0.004	0.003	0.003	3.7

Table 4.2. C_d values express as molar fraction at each imposed flux and for each pumping flux (4, 3, 2, 1, 0.7 e 0.4 l·min^{-1}); in the last column the concentration values of the gas sucked out from the (C_s) for each imposed flux are also reported. Experimental data shown in this table refer to the soil sample S_2 (k = 36 darcys).

J_{CO2} (g m^{-2}day^{-1})	C_d (φ_p=4 l·min^{-1})	C_d (φ_p=3 l·min^{-1})	C_d (φ_p=2 l·min^{-1})	C_d (φ_p=1 l·min^{-1})	C_d (φ_p=0.8 l·min^{-1})	C_d (φ_p=0.4 l·min^{-1})	C_s (% vol)
21,849	0.226	0.270	0.382	0.642	0.740	0.850	100
18,487	0.200	0.226	0.332	0.516	0.650	0.760	100
14,621	0.174	0.195	0.280	0.400	0.560	0.655	100
9,747	0.142	0.150	0.185	0.310	0.380	0.435	99.6
6,722	0.126	0.132	0.161	0.210	0.260	0.320	98.4
4,202	0.098	0.091	0.100	0.146	0.185	0.280	94.4
3,529	0.089	0.082	0.089	0.126	0.165	0.223	93.4
3,025	0.080	0.072	0.081	0.116	0.140	0.190	90.8
2,352	0.072	0.068	0.070	0.083	0.090	0.102	79.6
1,849	0.057	0.055	0.058	0.065	0.075	0.082	67.1
1,210	0.035	0.031	0.031	0.037	0.045	0.069	48.1
504	0.018	0.016	0.014	0.015	0.018	0.025	24.6
96	0.003	0.002	0.002	0.001	0.001	0.002	4.0

Table 4.3. C_d values express as molar fraction at each imposed flux and for each pumping flux (4, 3, 2, 1, 0.7 e 0.4 l·min^{-1}); in the last column the concentration values of the gas sucked out from the (C_s) for each imposed flux are also reported. Experimental data shown in this table refer to the soil sample S_3 (k = 6 darcys).

J_{CO2} (g m^{-2}day^{-1})	C_d (φ_p=4 l·min^{-1})	C_d (φ_p=3 l·min^{-1})	C_d (φ_p=2 l·min^{-1})	C_d (φ_p=1 l·min^{-1})	C_d (φ_p=0.8 l·min^{-1})	C_d (φ_p=0.4 l·min^{-1})	C_s (% vol)
21,849	0.1820	0.2200	0.3200	0.6000	0.7900	0.8900	100
18,487	0.1550	0.1900	0.2700	0.5100	0.6600	0.8100	100
14,621	0.1280	0.1550	0.2110	0.4200	0.5000	0.6300	100
9,747	0.0840	0.1000	0.1380	0.2600	0.3600	0.4800	100
6,722	0.0640	0.0760	0.1050	0.1870	0.2400	0.3400	98.4
4,202	0.0420	0.0510	0.0700	0.1250	0.1600	0.2400	96.8
3,529	0.0400	0.0470	0.0640	0.1100	0.1500	0.2000	94.3
3,025	0.0370	0.0420	0.0560	0.0960	0.1280	0.1700	91.8
2,352	0.0290	0.0350	0.0470	0.0800	0.1160	0.1400	86.2
1,849	0.0180	0.0200	0.0280	0.0510	0.0700	0.1070	72.4
1,210	0.0075	0.0090	0.0115	0.0200	0.0280	0.0420	57.3
827	0.0052	0.0046	0.0062	0.0105	0.0145	0.0195	38.8
504	0.0037	0.0038	0.0042	0.0064	0.0078	0.0095	30.7
318	0.0015	0.0014	0.0018	0.0029	0.0039	0.0060	17.7
96	0.0004	0.0004	0.0005	0.0007	0.0009	0.0012	5.9

Table 4.4. C_d values express as molar fraction at each imposed flux and for each pumping flux (4, 3, 2, 1, 0.7 e 0.4 l·min^{-1}); in the last column the concentration values of the gas sucked out from the (C_s) for each imposed flux are also reported. Experimental data shown in this table refer to the soil sample S_4 (k = 0.36 darcys).